Introduction to the computational analysis of static properties and dynamics of one-dimensional spin-1/2 systems

Lea F. Santos*
Department of Physics, Yeshiva University, 245 Lexington Ave, New York, New York 10016, USA

These are the notes for the lectures given in the *International Summer School on Exact and Numerical Methods for Low-Dimensional Quantum Structures* that took place at the Izmir Institute of Technology, Turkey, from August 23 to August 31, 2014. This tutorial teaches how to develop computer codes to diagonalize exactly one dimensional spin-1/2 systems. In hands of the eigenvalues and eigenstates, we then: (i) analyze signatures of quantum phase transition, localization, and quantum chaos; (ii) investigate the dynamics of the system by studying the survival probability and the evolution of various few-body observables; (iii) compare the infinite time averages of observables with thermal averages and identify conditions that can lead to the thermalization of isolated quantum systems. Computer programs in *Mathematica* and *Fortran* 90 are provided. They are available at `http://yu.edu/faculty-bios/santos/computer-codes/`. Emphasis are put on pedagogical structures rather than on efficiency. These notes will be frequently updated online, so suggestions and corrections are very welcome.

I. INTRODUCTION

Our goal is to study numerically the properties of many-body quantum systems. In particular, we will deal with one-dimensional (1D) systems of spins-1/2 on a lattice. These are paradigmatic many-body quantum systems. The basic tools you will learn can also be employed to study other equivalent systems.

Our method of analysis will be exact diagonalization. We can deal with larger chain sizes when studying 1D spin-1/2 models than systems with higher spins or with on-site interactions, such as the Bose-Hubbard model, because in contrast to the other cases, only two vectors span the space of a single spin-1/2.

1D spin-1/2 models represent various real physical systems. For example, crystals of apatites studied in solid state nuclear magnetic resonance (NMR) experiments, such as fluorapatite [$Ca_5(PO_4)_3F$], are well approximated by 1D models [1, 2]. Various copper oxides (cuprates), in which anomalous heat transport have been observed, are modeled with spin-1/2 chains, ladders, or two-dimensional lattices [3]. More recently, 1D spin-1/2 systems have also been studied with cold atoms in optical lattices [4–7].

These lectures contain 4 main parts. The first part, covered in Secs. I, II, and III, is essential for what comes next, so you should take your time to master it. These sections teach how to write the Hamiltonian matrix and diagonalize it. They also discuss the symmetries of the systems and the level of delocalization of their eigenstates. The latter depends on the symmetries, basis, and on competing terms of the Hamiltonian. With the eigenvalues and eigenstates, you can study aspects of quantum magnetism, such as quantum phase transitions. We will just mention it in passing. You can also use your results to analyze topics in quantum information. Spin-1/2 models are often used for describing quantum computers and computing measure of entanglement.

The second part of the lectures, corresponding to Secs. IV and V, are about quantum chaos. In 1D, several integrable models exist, but depending on the values of the parameters in the Hamiltonian, the systems may be taken into the chaotic domain. We will study how to characterize the crossover from integrability to chaos and will compare our chaotic spin-1/2 systems with full random matrices. We will deal with spin-1/2 systems without any randomness. However, by including randomness, such as on-site disorder, you could use these models to study Anderson localization and many-body localization.

The third part focuses on the observables. You will learn how to compute their expectation values in Sec. VI and, in Sec. VII, how to use the results to determine whether the considered isolated quantum systems should be able to reach thermal equilibrium or not.

The fourth part, in Sec. VIII and IX, covers the dynamics. We discuss the fidelity decay and the evolution of observables. You can use what you learn in these sections to analyze the Loschmidt echo, the evolution of Shannon entropy, aspect of quantum transport such as ballistic or diffusive motion, and methods of quantum control. For instance, in NMR, various sequences of pulses have been developed to control the dynamics and reduce the effects of decoherence in spin-1/2 systems. Once you know how to evolve the system in time, you can study the effects of such pulses.

There are 20 exercises. Five of them are identified as 'very important exercises'. They are: 1, 2, 3 for the static properties and 17, 20 for the dynamics. Among these, EXERCISES 3 and 20 are the most important. Computer codes are provided

*Electronic address: `lsantos2@yu.edu`

in *Mathematica* and/or *Fortran 90* at `http://yu.edu/faculty-bios/santos/computer-codes/`. Contributions, including more pedagogical codes than the ones available or written in other computer languages, are very welcome.

A. Time-independent Hamiltonians

We will be dealing with time-independent Hamiltonians. In this case, the solutions to Schrödinger equation

$$i\hbar\frac{\partial|\Psi\rangle}{\partial t} = \hat{H}|\Psi\rangle$$

are stationary states

$$|\Psi_\alpha\rangle(t) = |\psi_\alpha\rangle \exp\left(-i\frac{E_\alpha t}{\hbar}\right),$$

where $|\psi_\alpha\rangle$ are solutions of the time-independent Schrödinger equation

$$\hat{H}|\psi_\alpha\rangle = E_\alpha|\psi_\alpha\rangle$$

and α is the quantum number labeling the eigenergies. All static properties can be derived from the eigenvalues E_α and eigenstates $|\psi_\alpha\rangle$.

In a particular (discrete) orthonormal basis $\{|\phi_k\rangle\}$, the vectors $|\psi_\alpha\rangle$ are written as

$$|\psi_\alpha\rangle = \sum_{k=1}^{\mathcal{D}} |\phi_k\rangle\langle\phi_k|\psi_\alpha\rangle,$$

where $\mathcal{D}$ is the dimension of the Hamiltonian matrix. The time-independent Schrödinger equation in the matrix representation becomes

$$\sum_k \langle\phi_{k'}|\hat{H}|\phi_k\rangle\langle\phi_k|\psi_\alpha\rangle = E_\alpha\langle\phi'_k|\psi_\alpha\rangle.$$

Writing the matrix elements $\langle\phi_{k'}|\hat{H}|\phi_k\rangle$ as $H_{k',k}$, the equation for a 3×3 Hamiltonian matrix is

$$\begin{pmatrix} H_{1,1} & H_{1,2} & H_{1,3} \\ H_{2,1} & H_{2,2} & H_{2,3} \\ H_{3,1} & H_{3,2} & H_{3,2} \end{pmatrix} . \begin{pmatrix} \langle\phi_1|\psi_\alpha\rangle \\ \langle\phi_2|\psi_\alpha\rangle \\ \langle\phi_3|\psi_\alpha\rangle \end{pmatrix} = E_\alpha \begin{pmatrix} \langle\phi_1|\psi_\alpha\rangle \\ \langle\phi_2|\psi_\alpha\rangle \\ \langle\phi_3|\psi_\alpha\rangle \end{pmatrix}$$

Our first task when developing the computer codes is therefore to write the matrix elements $\langle\phi_{k'}|\hat{H}|\phi_k\rangle$ and then diagonalize the Hamiltonian matrix.

With the eigenvalues and eigenstates, we can also study the dynamics of the system for a given initial state $|\Psi(0)\rangle = |\text{ini}\rangle$. For this, we need the projections of this state in the eigenstates $C_\alpha^{\text{ini}} = \langle\psi_\alpha|\Psi(0)\rangle$. The evolved state is obtained from

$$|\Psi(t)\rangle = \sum_\alpha C_\alpha^{\text{ini}} \exp(-iE_\alpha t)|\psi_\alpha\rangle. \tag{1}$$

From now on, let us set $\hbar = 1$.

II. ONE-DIMENSIONAL SPIN-1/2 SYSTEMS

A single spin-1/2 is described in terms of spin operators $\hat{S}^{x,y,z} = \hat{\sigma}^{x,y,z}/2$, where

$$\hat{\sigma}^x \equiv \begin{pmatrix} 0 & 1 \\ 1 & 0 \end{pmatrix}, \qquad \hat{\sigma}^y \equiv \begin{pmatrix} 0 & -i \\ i & 0 \end{pmatrix}, \qquad \hat{\sigma}^z \equiv \begin{pmatrix} 1 & 0 \\ 0 & -1 \end{pmatrix}$$

are the Pauli matrices and $\hbar$ has been set to 1. The quantum state of the spin is represented by a two-component vector, known as the spinor. This state is commonly written in terms of basis vectors corresponding to the two eigenstates of $\hat{S}^z$. One eigenstate represents the spin pointing up in the z direction and the other, the spin pointing down. They can be denoted as

$$|\uparrow\rangle = |1\rangle = \begin{pmatrix} 1 \\ 0 \end{pmatrix} \qquad\qquad |\downarrow\rangle = |0\rangle = \begin{pmatrix} 0 \\ 1 \end{pmatrix},$$

$$\hat{S}^z|\uparrow\rangle = +\frac{1}{2}|\uparrow\rangle \qquad \hat{S}^z|\downarrow\rangle = -\frac{1}{2}|\downarrow\rangle.$$

Since the eigenvalue associated with $|\uparrow\rangle$ is +1/2 and that of $|\downarrow\rangle$ is -1/2, we refer to the first as the excitation.

A. Site-basis

The first step when preparing a computer code for any Hamiltonian matrix is to write the basis. For this, let us denote the up-spin with the number '1' and the down-spin with the number '0'. Each different sequence of zeros and ones defines a basis vector. This basis, in which the spin on each site either points up or down in the z direction, is often referred to as computational basis, natural basis, or site-basis. We use the latter term.

The total dimension of the Hilbert space for a spin-1/2 chain with L sites is 2^L. One basis vector has all the spins pointing up; L vectors have all spins pointing up but one; $\binom{L}{2} = \frac{L!}{(L-2)!2!}$ have all spins pointing up but two; $\binom{L}{3}$ have all spins pointing up but three; and so on:

$$2^L = 1 + L + \binom{L}{2} + \binom{L}{3} + \binom{L}{4} + \dots \binom{L}{L-2} + L + 1$$

In *Mathematica*, we can use the command 'IntegerDigits[**number**,2,L]' to get an array of zeros and ones of length L that corresponds to the '**number**' that we chose to write in the binary basis. For example:

$$\text{IntegerDigits[3,2,10]} = 0000000011$$

To get all site-basis vectors for a chain with L sites, we need to create a loop where '**number**' goes from 0 to $2^L - 1$. In *Fortran*, we can use the same idea, that is we generate our basis by converting decimal to binary numbers.

A *Fortran* code is provided below. Careful with it, because the generated arrays do not follow the usual order in the binary sequence. In the code, the first term from the left is 2^0, the second 2^1, the third 2^2, etc, instead of starting from the right. This makes no difference when all basis vectors are required, but in other cases, you may want to have the arrays in the usual form, with 2^0 starting from the right.

```
DO i=1,SizeHilbertSpace
      number=i-1
      Do j=1,ChainSize
            temp=number/2          ! temp = integer
            basis(i,j) = number - 2*temp
            number=temp
      Enddo
ENDDO
```

%%

$\hookrightarrow$ *EXERCISE 1:* Write down only the basis vectors that have a fixed number of up-spins, N_{up}. Use $L = 6$ and $N_{up} = L/2$.

VERY IMPORTANT EXERCISE!

We could, of course, use some if-statement to select these states from the total set we generated above. But instead, let us write a code that generates from the beginning only those specific desired vectors.

In *Mathematica*, we can type one of these basis vectors and then use the command 'Permutations[OneBasisVector]' to get all the others. In *Fortran* there is a subroutine called NEXKSB that does a similar job.

```
! JUST INITIALIZATION:
                        Do ib=1,DimFixedUp
                              Do jb=1,ChainSize
                                    basis(ib,jb)=0
                              enddo
                        enddo
! STARTS HERE
                        ii=1          ! ii = the number of the basis
71                      call NEXKSB(chain,upspins,in,mtc,m2,h)
                        Do jb=1,upspins
                              basis(ii,in(jb))=1
                        Enddo
                        ii=ii+1
                        if(mtc) goto 71
```

Both *Mathematica* and *Fortran* 90 codes are provided in separated files.

%%

B. Ising model

When more than one spin is present, they may interact. In the case of the Ising interaction, the model is characterized by the following Hamiltonian

$$\hat{H} = \sum_{n,m} J^z_{n,m} \hat{S}^z_n \hat{S}^z_m + h \sum_n \hat{S}^z_n, \tag{2}$$

where the spin operator $\hat{S}^z_{n(m)}$ acts only on the spin placed on site n (m). The first term corresponds to the Ising interaction and $J^z_{n,m}$ gives its strength. The second term represents a magnetic field applied on the entire chain. It causes the Zeeman splitting of amplitude h on each site.

Let us assume for the moment that only nearest-neighbor (NN) interaction exists, so $m = n+1$ and that $J^z_{n,n+1}$ is the same for any site n. If we restrict our analysis to a fixed number of up-spins, the second term can be neglected, since it leads simply to the same additional value to all diagonal elements of the Hamiltonian matrix. In this case, we deal with the following simplified Ising Hamiltonian,

$$\hat{H}_{ZZ} = J\Delta \sum_{n=1} \hat{S}^z_n \hat{S}^z_{n+1} \tag{3}$$

Above J sets the energy scale and it is fixed as $J = 1$ in all codes.

The Ising interaction causes a pair of adjacent parallel spins to have different energy from a pair of anti-parallel spins, because

$$J\Delta \hat{S}^z_n \hat{S}^z_{n+1} | \uparrow_n \uparrow_{n+1} \rangle = +\frac{J\Delta}{4} | \uparrow_n \uparrow_{n+1} \rangle, \tag{4}$$

while

$$J\Delta \hat{S}^z_n \hat{S}^z_{n+1} | \uparrow_n \downarrow_{n+1} \rangle = -\frac{J\Delta}{4} | \uparrow_n \downarrow_{n+1} \rangle. \tag{5}$$

We can infer from Eqs. (4) and (5) that the ground state of the Ising model (3) depends on the sign of the interaction strength; it is ferromagnetic, with all spins aligned in the same direction, when $J\Delta < 0$, and it shows an antiferromagnetic arrangement with antiparallel neighboring spins when $J\Delta > 0$.

Depending on the boundary conditions, we refer to the chain as open, when we have open boundary conditions, $\hat{H}_{ZZ} = \hat{H}^{\text{open}}_{ZZ}$ or closed, when we have periodic boundary conditions, $\hat{H}_{ZZ} = \hat{H}^{\text{closed}}_{ZZ}$. In the first case the sum in n in Eq. (3) goes from 1 to $L-1$. A spin on site 1 can only interact with a spin on site 2 and a spin on site L only with a spin on site $L-1$. In the second case, the sum in n goes from 1 to L, the geometry is that of a ring. A spin on site 1 can interact with a spin on site 2 and also with a spin on site L and a spin on site L can interact with site $L-1$ and site 1.

%%
$\hookrightarrow$ *EXERCISE 2:*

VERY IMPORTANT EXERCISE!

(i) Fix the number of up-spins and write down the Hamiltonian matrix for $\hat{H}^{\text{open}}_{ZZ}$ and $\hat{H}^{\text{closed}}_{ZZ}$. Use $L = 6$ and $N_{up} = L/2$. Show as output only the diagonal elements. In *Mathematica*, this can be done symbolically.

```
! JUST INITIALIZATION:
        Do i=1,dimTotal      ! dimTotal = dimension of the Hamiltonian matrix being studied
           Do j=1,dimTotal
              Ham(i,j)=0.0d0
           Enddo
        Enddo
! DIAGONAL ELEMENTS
        Do i=1,dimTotal
           Do j=1,chain-1      ! chain = number of sites in the chain
              Ham(i,i)=Ham(i,i)+(Jz/4.d0)*(-1.0d0)**(basis(i,j)+basis(i,j+1))      ! Jz = JΔ
           enddo
! The line below is for a CLOSED chain. Remove it, if the chain is OPEN.
              Ham(i,i)=Ham(i,i)+(Jz/4.d0)*(-1.0d0)**(basis(i,1)+basis(i,L))
        enddo
```

Both *Mathematica* and *Fortran* 90 codes are provided.

(ii) Find an expression for the diagonal elements in terms of the number of pairs of adjacent parallel spins, N_{pair}.

The off-diagonal elements are all zero and the diagonal elements split into sets of degenerate energies. We refer to each set of degenerate energies as an energy band. The bands are determined by the number of pairs of adjacent parallel spins in the basis vectors. For example, in an open chain with $L=4$, $N_{up}=2$, and $J\Delta>0$, the highest energy, $J\Delta/4$, occurs for the states with two pairs of parallel spins, $|\uparrow\uparrow\downarrow\downarrow\rangle$ and $|\downarrow\downarrow\uparrow\uparrow\rangle$. The band that precedes this one in energy has the states with only one pair of parallel spins, $|\uparrow\downarrow\downarrow\uparrow\rangle$ and $|\downarrow\uparrow\uparrow\downarrow\rangle$, yielding an energy of $-J\Delta/4$. The states of the band with the lowest energy, $-3J\Delta/4$, have no pairs of parallel spins, $|\uparrow\downarrow\uparrow\downarrow\rangle$ and $|\downarrow\uparrow\downarrow\uparrow\rangle$. We see that the energy difference between consecutive bands is $J\Delta/2$, since we move down in energy by breaking a pair, thus adding the factor $J\Delta/4$ one less time and subtracting it one more time. In an open chain, where there are $L-1$ coupling bonds, the general expression for the energy of each band is therefore

$$E_{ZZ}^{\text{open}} = [2N_{pair} - (L-1)]\frac{J\Delta}{4}. \tag{6}$$

In a closed chain, on the other hand, the energy difference between successive bands is $J\Delta$. In this case, there are L bonds and always an even number of antiparallel pairs, because there is no border to absorb any of them. We move down in energy by breaking necessarily two pairs of parallel spins, the factor $J\Delta/4$ thus being added two less times and subtracted two more times. The diagonal energies are then given by

$$E_{ZZ}^{\text{closed}} = (2N_{pair} - L)\frac{J\Delta}{4}. \tag{7}$$

Clearly, the closed chain has fewer bands and therefore more degeneracies than the open one.

%%

C. Heisenberg model

We now add NN couplings in the x and y directions and obtain the Heisenberg model,

$$\hat{H}_{XXZ} = \sum_{n=1}^{L-1}\left[J\left(\hat{S}_n^x\hat{S}_{n+1}^x + \hat{S}_n^y\hat{S}_{n+1}^y\right) + J\Delta\hat{S}_n^z\hat{S}_{n+1}^z\right]. \tag{8}$$

Notice that we are considering open boundary conditions. The parameter Δ has now a clear meaning. It is the ratio between the strength of the Ising interaction and the strength J of the term $\hat{S}_n^x\hat{S}_{n+1}^x + \hat{S}_n^y\hat{S}_{n+1}^y$. It measures the level of anisotropy of the chain. The model is isotropic when $\Delta=1$, in which case it is known as the XXX model, and it is anisotropic when $\Delta\neq 1$, usually referred to as the XXZ model (XYZ also exists when the coupling strengths in the three directions are different).

The first term in Hamiltonian (8) is known as the flip-flop term. By itself, it is often referred to as XX model and can be mapped onto a system of noninteracting spinless fermions, being trivially solvable [8]. The XXZ model can also be solved, by the solution is more involved and done by means of the Bethe ansatz [9].

The flip-flop term interchanges the position of neighboring up and down spins according to

$$J(\hat{S}_n^x\hat{S}_{n+1}^x + \hat{S}_n^y\hat{S}_{n+1}^y)|\uparrow_n\downarrow_{n+1}\rangle = \frac{J}{2}|\downarrow_n\uparrow_{n+1}\rangle.$$

It is also commonly written with raising $\hat{S}^+ = \hat{S}^x + i\hat{S}^y$ and lowering $\hat{S}^- = \hat{S}^x - i\hat{S}^y$ spin operators,

$$\frac{J}{2}(\hat{S}_n^+\hat{S}_{n+1}^- + \hat{S}_{n+1}^+\hat{S}_n^-)|\uparrow_n\downarrow_{n+1}\rangle = \frac{J}{2}|\downarrow_n\uparrow_{n+1}\rangle.$$

The NN flip-flop term couples site-basis vectors that differ only by the orientation of the spins in two adjacent sites. In the site-basis, it constitutes the off-diagonal elements of the Hamiltonian matrix.

Notice that $J(\hat{S}_n^x\hat{S}_{n+1}^x + \hat{S}_n^y\hat{S}_{n+1}^y)|\uparrow_n\uparrow_{n+1}\rangle = 0$ and $J(\hat{S}_n^x\hat{S}_{n+1}^x + \hat{S}_n^y\hat{S}_{n+1}^y)|\downarrow_n\downarrow_{n+1}\rangle = 0$, that is, the XXZ Hamiltonian does not create or annihilate excitations (up-spins), it can only move them along the chain. This is related to a symmetry of the system.

D. Symmetries

Every symmetry of the system is associated with an operator $\hat{O}$ that commutes with the Hamiltonian. As stated in Noether's theorem, this operator represents a constant of motion, that is a physical quantity that is conserved. This is easily seen from the Ehrenfest theorem for a time independent operator, where the expectation value of the operator is related with its commutator with the Hamiltonian,

$$\frac{d\langle\hat{O}\rangle}{dt} = \frac{i}{\hbar}\langle\hat{H}\hat{O} - \hat{O}\hat{H}\rangle.$$

The fact that they commute implies that $\langle\hat{O}\rangle$ does not change in time. For example, invariance of $\hat{H}$ under translation in space leads to conservation of linear momentum, as seen in homogeneous closed chains. In open chains we may find the following symmetries:

$\star\star$ The XXZ Hamiltonian commutes with the total spin in the z direction, $\hat{\mathcal{S}}^z = \sum_{n=1}^{L} \hat{S}_n^z$, that is, $[\hat{H}_{XXZ}, \hat{\mathcal{S}}^z] = 0$. The system is therefore invariant by a rotation around the z-axis, or equivalently, it conserves $\hat{\mathcal{S}}^z$. This means that each eigenstate of $\hat{H}_{XXZ}$ has a fixed number of up-spins, since it has to be also an eigenstate of $\hat{\mathcal{S}}^z$. Each eigenstate is a superposition that involves only site-basis vectors with the same number of up-spins. Example for $L = 4$ and $\mathcal{S}^z = 0$,

$$a_1|1100\rangle + a_2|1010\rangle + a_3|1001\rangle + a_4|0110\rangle + a_5|0101\rangle + a_6|0011\rangle$$

Writing the Hamiltonian matrix of a system with L sites in the site-basis, we see that it is composed of $L+1$ independent blocks (or subspaces), each with a fixed number of up-spins, $N_{up} \in [0, L]$.

$\|1111\rangle$	$\|1110\rangle$	$\|1101\rangle$	$\|1011\rangle$	$\|0111\rangle$	$\|1100\rangle$	$\|1010\rangle$	$\|1001\rangle$	$\|0110\rangle$	$\|0101\rangle$	$\|0011\rangle$	$\|0001\rangle$	$\|0010\rangle$	$\|0100\rangle$	$\|1000\rangle$	$\|0000\rangle$
$\frac{3J\Delta}{4}$	0	0	0	0	0	0	0	0	0	0	0	0	0	0	0
0	$+\frac{J\Delta}{4}$	$\frac{J}{2}$	0	0	0	0	0	0	0	0	0	0	0	0	0
0	$\frac{J}{2}$	$-\frac{J\Delta}{4}$	$\frac{J}{2}$	0	0	0	0	0	0	0	0	0	0	0	0
0	0	$\frac{J}{2}$	$-\frac{J\Delta}{4}$	$\frac{J}{2}$	0	0	0	0	0	0	0	0	0	0	0
0	0	0	$+\frac{J}{2}$	$+\frac{J\Delta}{4}$	0	0	0	0	0	0	0	0	0	0	0
0	0	0	0	0	$+\frac{J\Delta}{4}$	$\frac{J}{2}$	0	0	0	0	0	0	0	0	0
0	0	0	0	0	$\frac{J}{2}$	$-\frac{3J\Delta}{4}$	$\frac{J}{2}$	$\frac{J}{2}$	0	0	0	0	0	0	0
0	0	0	0	0	0	$\frac{J}{2}$	$-\frac{J\Delta}{4}$	0	$\frac{J}{2}$	0	0	0	0	0	0
0	0	0	0	0	0	$\frac{J}{2}$	0	$-\frac{J\Delta}{4}$	$\frac{J}{2}$	0	0	0	0	0	0
0	0	0	0	0	0	0	$\frac{J}{2}$	$\frac{J}{2}$	$-\frac{3J\Delta}{4}$	$\frac{J}{2}$	0	0	0	0	0
0	0	0	0	0	0	0	0	0	$\frac{J}{2}$	$\frac{J\Delta}{4}$	0	0	0	0	0
0	0	0	0	0	0	0	0	0	0	0	$+\frac{J\Delta}{4}$	$\frac{J}{2}$	0	0	0
0	0	0	0	0	0	0	0	0	0	0	$\frac{J}{2}$	$-\frac{J\Delta}{4}$	$\frac{J}{2}$	0	0
0	0	0	0	0	0	0	0	0	0	0	0	$\frac{J}{2}$	$-\frac{J\Delta}{4}$	$\frac{J}{2}$	0
0	0	0	0	0	0	0	0	0	0	0	0	0	$\frac{J}{2}$	$+\frac{J\Delta}{4}$	0
0	0	0	0	0	0	0	0	0	0	0	0	0	0	0	$\frac{3J\Delta}{4}$

We can then write and diagonalize the Hamiltonian matrix for each subspace of dimension $\mathcal{D} = \binom{L}{N_{up}}$ separately. When L is even, the largest sector has $N_{up} = L/2$. In this case, full exact diagonalization can be carried out for $L \leq 14$ [$\mathcal{D} = 3\,432$] with *Mathematica*. For larger systems, we need a high-level computer programming language, such as *Fortran* or *C*$^{++}$. The *Fortran* codes provided here diagonalize, in workstations, matrices with $L = 16, N_{up} = 8, \mathcal{D} = 12\,870$ and $L = 18, N_{up} = 6, \mathcal{D} = 18\,564$. Full exact diagonalizations have been performed for matrices with up to $\mathcal{D} \sim 3 \times 10^4$.

⋆⋆ Hamiltonian (8) is invariant under reflection, which leads to conservation of parity, that is, $\hat{H}_{XXZ}$ commutes with the parity operator

$$\hat{\Pi} = \begin{cases} \hat{\mathcal{P}}_{1,L}\hat{\mathcal{P}}_{2,L-1}\ldots\hat{\mathcal{P}}_{\frac{L}{2},\frac{L+2}{2}} & \text{for } L = \text{even} \\ \hat{\mathcal{P}}_{1,L}\hat{\mathcal{P}}_{2,L-1}\ldots\hat{\mathcal{P}}_{\frac{L-1}{2},\frac{L+3}{2}} & \text{for } L = \text{odd} \end{cases}$$

where $\hat{\mathcal{P}}_{n,m} = (\hat{\sigma}^x_n\hat{\sigma}^x_m + \hat{\sigma}^y_n\hat{\sigma}^y_m + \hat{\sigma}^z_n\hat{\sigma}^z_m + \mathbb{1})/2$ is the permutation operator and $\mathbb{1}$ is the identity operator. $\hat{\mathcal{P}}_{n,m}$ permutes the n^{th} and m^{th} vector spaces. For instance, $\hat{\Pi}|\uparrow\downarrow\downarrow\uparrow\downarrow\rangle = |\downarrow\uparrow\downarrow\downarrow\uparrow\rangle$.

Invariance under reflection may be better understood by imagining a mirror at one edge of the chain. If parity is conserved, the participation of each basis vector in the eigenstate is equal to that of its reflection. For example, suppose we have $L = 4$ and one excitation. The eigenstates $|\psi\rangle$ of $\hat{H}_{XXZ}$, which are also eigenstates of $\hat{\Pi}$, are given by

$$|\psi\rangle = a_1|\uparrow\downarrow\downarrow\downarrow\rangle + a_2|\downarrow\uparrow\downarrow\downarrow\rangle + a_3|\downarrow\downarrow\uparrow\downarrow\rangle + a_4|\downarrow\downarrow\downarrow\uparrow\rangle$$

and the probability amplitudes are either $a_1 = a_4$ and $a_2 = a_3$ for even parity, $\Pi = +1$, or $a_1 = -a_4$ and $a_2 = -a_3$ for odd parity, $\Pi = -1$. [Notice that the hat in $\hat{\Pi}$ indicates the operator and its absence indicates the eigenvalue, $\hat{\Pi}|\psi\rangle = \Pi|\psi\rangle$.]

⋆⋆ If L is even and $N_{up} = L/2$, the XXZ Hamiltonian is also invariant under a global π rotation around the x axis. The operator that realizes this rotation is

$$\hat{R}^x_\pi = \hat{\sigma}^x_1\hat{\sigma}^x_2\ldots\hat{\sigma}^x_L$$

and one can easily verify that $[\hat{H}_{XXZ}, \hat{R}^x_\pi] = 0$. As an example, suppose we have $L = 4$ and $N = 2$. The eigenstate

$$|\psi\rangle = a_1|\uparrow\uparrow\downarrow\downarrow\rangle + a_2|\uparrow\downarrow\uparrow\downarrow\rangle + a_3|\uparrow\downarrow\downarrow\uparrow\rangle + a_4|\downarrow\uparrow\uparrow\downarrow\rangle + a_5|\downarrow\uparrow\downarrow\uparrow\rangle + a_6|\downarrow\downarrow\uparrow\uparrow\rangle,$$

has either $a_1 = a_6$, $a_2 = a_5$, and $a_3 = a_4$, in which case the eigenvalue of $\hat{R}^x_\pi$ is $R^x_\pi = +1$, or $a_1 = -a_6$, $a_2 = -a_5$, and $a_3 = -a_4$, in which case $R^x_\pi = -1$.

⋆⋆ When the system is isotropic, $[\hat{H}_{XXZ}, \hat{\mathcal{S}}^2_T] = 0$, where $\hat{\mathcal{S}}_T = \sum_n \vec{S}_n$ is the total spin.

%%%
↪ *EXERCISE 3:*
VERY IMPORTANT EXERCISE!
(i) Write down the XXZ Hamiltonian matrix with open boundary conditions. Use $L = 6$, $N_{up} = 3$, and $\Delta = 0.4$.

```
! OFF-DIAGONAL ELEMENTS
          Do i = 1, dimTotal-1        ! Select basis vector 'i'
             Do j = i+1, dimTotal       ! to compare it with basis vector 'j'

                tot = 0        ! tot = to count by how many spin states 'i' and 'j' differ
                Do k = 1, chain
                   DifferentSite(k)=0        ! DifferentSite = to identify the sites where the spins differ
                Enddo

                Do k = 1, chain
                   If( basis(i,k).ne.basis(j,k) ) then        ! Check if 'i' and 'j' differ in any site
                      tot = tot + 1        ! If the spin state of basis 'i' and 'j' differ on site 'k', 'tot' increases by 1.
                      DifferentSite(tot)=k        ! Store the site where the states are different
                   Endif
                Enddo

                IF(tot.EQ.2) then        ! If only two sites are different
                   IF((DifferentSite(2) - DifferentSite(1)).EQ.1) then        ! AND if they are neighbors
                      Ham(i,j)=Ham(i,j)+Jxy/2.0d0        ! then there is coupling
                      Ham(j,i)=Ham(i,j)        ! the matrix is symmetric
                   ENDIF
                ENDIF
```

```
        enddo
    enddo
```

(ii) Find all the eigenvalues and corresponding eigenstates.
In *Mathematica*, you can do this with

```
Eigenvalues[Hamiltonian]
Eigenvectors[Hamiltonian]
```

In *Fortran*, you can call the LAPACK library/subroutine

```
CALL DSYEV('V','U',dimTotal,Ham,dimTotal,Eig,WORK,7*dimTotal,INFO)
```

'Ham' will now become the eigenvectors, each column being one, and 'Eig' will be the eigenvalues in increasing order.

(iii) Use the results to write a table with three columns: the first column contains the eigenvalues in increasing order of energy, the second the eigenvalues of $\hat{\Pi}$ of the corresponding eigenstates, and the third the eigenvalues of $\hat{R}^x_\pi$.

Energy	Π	R^x_π	Energy	Π	R^x_π
-0.202384144E+01	–	–	0.248641927E-01	+	+
-0.152529608E+01	+	+	0.521526857E-01	+	–
-0.107293251E+01	–	+	0.337462447E+00	+	+
-0.992344213E+00	–	–	0.410488624E+00	–	–
-0.759139668E+00	+	+	0.601980202E+00	–	–
-0.649384950E+00	+	–	0.622043107E+00	–	+
-0.637126404E+00	+	+	0.797232265E+00	+	–
-0.349110601E+00	–	+	0.852697635E+00	+	+
-0.216906870E+00	–	–	0.115859912E+01	–	–
-0.137975424E+00	–	–	0.150653788E+01	+	+

Both *Mathematica* and *Fortran* 90 codes are provided.
%%%

E. NETLIB

NETLIB: The Netlib repository contains freely available software, documents, and databases of interest to the numerical, scientific computing, and other communities. The repository is maintained by AT&T Bell Laboratories, the University of Tennessee and Oak Ridge National Laboratory, and by colleagues world-wide. The collection is replicated at several sites around the world, automatically synchronized, to provide reliable and network efficient service to the global community.

http://www.netlib.org/

LAPACK provides routines for solving systems of simultaneous linear equations, least-squares solutions of linear systems of equations, eigenvalue problems, and singular value problems. The associated matrix factorizations (LU, Cholesky, QR, SVD, Schur, generalized Schur) are also provided, as are related computations such as reordering of the Schur factorizations and estimating condition numbers. Dense and banded matrices are handled, but not general sparse matrices. In all areas, similar functionality is provided for real and complex matrices, in both single and double precision.

BLAS (Basic Linear Algebra Subprograms) are routines that provide standard building blocks for performing basic vector and matrix operations. The Level 1 BLAS perform scalar, vector and vector-vector operations, the Level 2 BLAS perform matrix-vector operations, and the Level 3 BLAS perform matrix-matrix operations. Because the BLAS are efficient, portable, and widely available, they are commonly used in the development of high quality linear algebra software, LAPACK for example.

When you compile your *Fortran* code, you call those libraries as

```
gfortran -o codeTorun.run codeFortran.f90 -llapack -lblas
```

You run it with
./codeTorun.run &
nohup ./codeTorun.run &

III. COMPETING TERMS IN THE XXZ HAMILTONIAN

The structure of the spectrum and the level of delocalization of the eigenstates depend on which term, Ising or the flip-flop term, dominates the Hamiltonian (8). The competition is also associated with quantum phase transitions in the system.

A. Ising term vs flip-flop term

For an open chain with an even number of sites and $N_{up} = L/2$, the energies of the Ising part of the Hamiltonian form $L - 1$ bands with energies ranging from $-(L-1)J\Delta/4$, when $N_{pair} = 0$, to $(L-3)J\Delta/4$, when $N_{pair} = L-2$. This band structure is symmetric.

In the XXZ model the band structure may or not remain depending on the interplay between the Ising interaction and the flip-flop term [10]. When $\Delta \lesssim 1$, the band structure is lost. This happens because the energy difference between the basis vectors is $\lesssim J$, so the flip-flop term can couple intra- and also inter-band states. In contrast, the band structure is preserved when $\Delta \gg 1$, since states from different bands are too far off-resonance. In this case, the flip-flop term can effectively couple only states belonging to the same band. This intra-band coupling happens in higher order of perturbation theory. Each band acquires a small width, which does not erase the energy gap between them. In this scenario of large Δ, the number of adjacent parallel spins can be seen as some sort of new effective conserved quantity. States with different values of N_{pair} are not effectively coupled.

The competition between the Ising and the flip-flop term of the Hamiltonian is reflected also in the structure of the eigenstates. As the Ising interaction increases, limiting the role of the flip-flop term, the eigenstates become less spread in the site-basis. This can be quantified, for example, with the so-called inverse participation ratio (IPR) [11, 12]. Consider an eigenstate

$$|\psi_\alpha\rangle = \sum_{k=1}^{\mathcal{D}} C_\alpha^{(k)} |\phi_k\rangle \tag{9}$$

written in terms of the orthonormal basis vectors $|\phi_k\rangle$, where $C_\alpha^{(k)} = \langle \phi_k | \psi_\alpha \rangle$. IPR is defined as

$$\text{IPR}_\alpha \equiv \frac{1}{\sum_{k=1}^{\mathcal{D}} |C_\alpha^{(k)}|^4}. \tag{10}$$

This quantity is proportional to the number of basis vectors that contribute to each eigenstate. It is small when the state is localized and large when the state is delocalized in the chosen basis. Thus, IPR must be decrease as Δ increases.

There are other measures of delocalization, such as the Shannon entropy

$$\text{Sh}_\alpha^{(k)} \equiv -\sum_k |C_\alpha^{(k)}|^2 \ln |C_\alpha^{(k)}|^2. \tag{11}$$

%%%

$\hookrightarrow$ *EXERCISE 4:* Make four histograms for $L = 10$, $N_{up} = 5$, and open boundaries: top left for the energies of the Ising model with $\Delta = 0.5$ and right for the energies of the Ising model with $\Delta = 10$. The panels below these two should be the corresponding histograms for the XXZ model with the same values of Δ [left: bin width = 0.2; right: bin width = 1]. Below these four figures, add a panel with the value of IPR obtained in the site-basis and averaged over all the eigenstates of the XXZ model vs Δ. NOTE: do not get too surprised if the results for IPR from *Mathematica* and *Fortran* do not match exactly for $\Delta = 0$ or $\Delta = 0.5$. These are points where there are too many degeneracies. For other values of the anisotropy, the results should coincide.

***Mathematica* and *Fortran* codes are provided.**

%%%

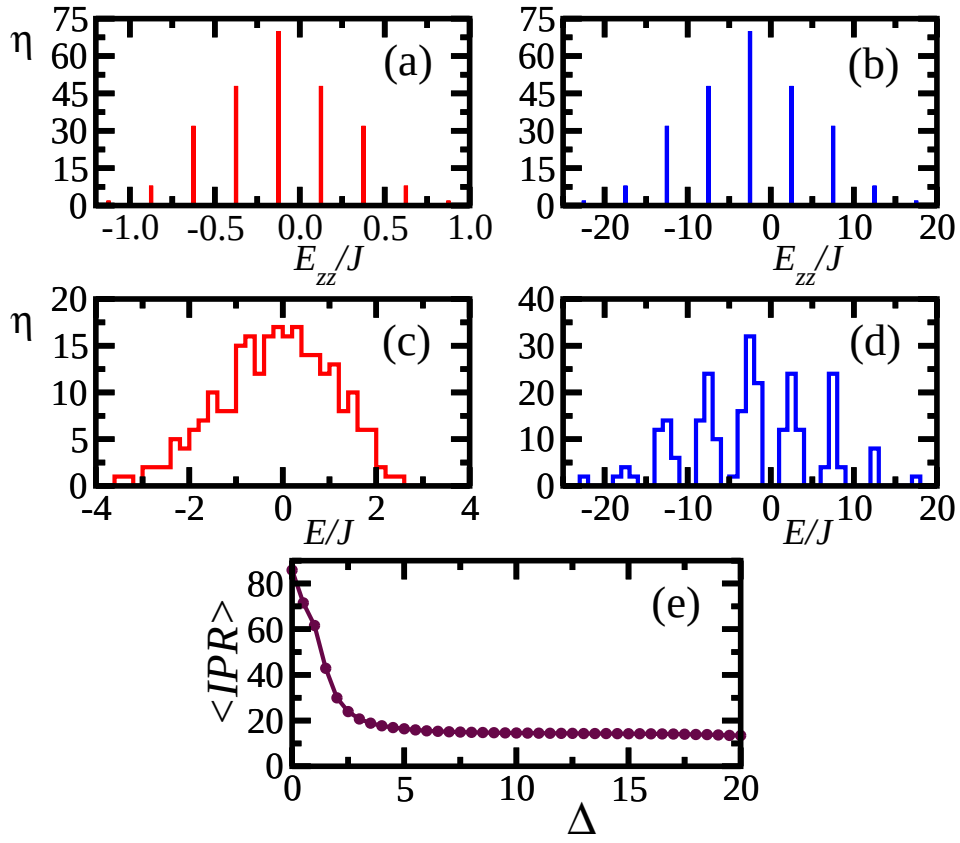

FIG. 1: Competition between the Ising and flip-flop term in the XXZ model

B. Delocalization of eigenstates: basis dependence

Quantities that measure the level of delocalization of the eigenstates depend on the basis. To compute these quantities in a basis other than the site-basis, additional diagonalizations to construct such basis are often necessary.

To change the basis we can either (i) diagonalize the Hamiltonian in the old basis $|\phi_k\rangle$ and then project the eigenstates in the new basis $|\xi_\nu\rangle$ or (ii) first write the Hamiltonian in the new basis and then diagonalize it.

(i) In the first case, we have,

$$|\psi_\alpha\rangle = \sum_{k=1}^{\mathcal{D}} |\phi_k\rangle\langle\phi_k|\psi_\alpha\rangle$$

and we want

$$|\psi_\alpha\rangle = \sum_{\nu=1}^{\mathcal{D}} |\xi_\nu\rangle\langle\xi_\nu|\psi_\alpha\rangle.$$

From the first expression, we get

$$|\psi_\alpha\rangle = \sum_{\nu=1}^{\mathcal{D}}\sum_{k=1}^{\mathcal{D}} |\xi_\nu\rangle\langle\xi_\nu|\phi_k\rangle\langle\phi_k|\psi_\alpha\rangle.$$

In matrix form, assuming that we have three eigenstates, the expression above is written as:

$$\begin{pmatrix} \psi_1^{\text{in }\xi} & \psi_2^{\text{in }\xi} & \psi_3^{\text{in }\xi} \\ \hline \langle\xi_1|\psi_1\rangle & \langle\xi_1|\psi_2\rangle & \langle\xi_1|\psi_3\rangle \\ \langle\xi_2|\psi_1\rangle & \langle\xi_2|\psi_2\rangle & \langle\xi_2|\psi_3\rangle \\ \langle\xi_3|\psi_1\rangle & \langle\xi_3|\psi_2\rangle & \langle\xi_3|\psi_3\rangle \end{pmatrix} = \begin{pmatrix} \xi_1^{\text{in }\phi} & \xi_2^{\text{in }\phi} & \xi_3^{\text{in }\phi} \\ \hline \langle\phi_1|\xi_1\rangle & \langle\phi_1|\xi_2\rangle & \langle\phi_1|\xi_3\rangle \\ \langle\phi_2|\xi_1\rangle & \langle\phi_2|\xi_2\rangle & \langle\phi_2|\xi_3\rangle \\ \langle\phi_3|\xi_1\rangle & \langle\phi_3|\xi_2\rangle & \langle\phi_3|\xi_3\rangle \end{pmatrix}^\dagger \cdot \begin{pmatrix} \psi_1^{\text{in }\phi} & \psi_2^{\text{in }\phi} & \psi_3^{\text{in }\phi} \\ \hline \langle\phi_1|\psi_1\rangle & \langle\phi_1|\psi_2\rangle & \langle\phi_1|\psi_3\rangle \\ \langle\phi_2|\psi_1\rangle & \langle\phi_2|\psi_2\rangle & \langle\phi_2|\psi_3\rangle \\ \langle\phi_3|\psi_1\rangle & \langle\phi_3|\psi_2\rangle & \langle\phi_3|\psi_3\rangle \end{pmatrix}.$$

In short, we play with matrices where the columns are the vectors at hand, so that

$$(\text{Columns are } \psi^{\text{in } \xi}) = (\text{Columns are } \xi^{\text{in } \phi})^{\dagger}.(\text{Columns are } \psi^{\text{in } \phi})$$

Often a diagonalization is involved to get $\xi^{\text{in } \phi}$. Notice that the matrix for these states in the old basis $|\phi\rangle$, that is the first matrix on the right hand side, needs to be (conjugate) transposed, since $\langle \xi_\nu | \phi_k \rangle = \langle \phi_k | \xi_\nu \rangle^{\dagger}$.

If we have $\psi^{\text{in } \xi}$ and want to bring it to $\psi^{\text{in } \phi}$ having available only $\xi^{\text{in } \phi}$, we do

$$\begin{aligned}
(\text{Columns are } \xi^{\text{in } \phi}).(\text{Columns are } \psi^{\text{in } \xi}) &= (\text{Columns are } \xi^{\text{in } \phi}).(\text{Columns are } \xi^{\text{in } \phi})^{\dagger}.(\text{Columns are } \psi^{\text{in } \phi}) \\
(\text{Columns are } \xi^{\text{in } \phi}).(\text{Columns are } \psi^{\text{in } \xi}) &= (\text{Columns are } \psi^{\text{in } \phi})
\end{aligned}$$

(ii) If the second alternative is preferred, we have

$$\begin{pmatrix} \langle \xi_1|H|\xi_1\rangle & \langle \xi_1|H|\xi_2\rangle & \langle \xi_1|H|\xi_3\rangle \\ \langle \xi_2|H|\xi_1\rangle & \langle \xi_2|H|\xi_2\rangle & \langle \xi_2|H|\xi_3\rangle \\ \langle \xi_3|H|\xi_1\rangle & \langle \xi_3|H|\xi_2\rangle & \langle \xi_3|H|\xi_3\rangle \end{pmatrix} = \Xi^{\dagger}. \begin{pmatrix} \langle \phi_1|H|\phi_1\rangle & \langle \phi_1|H|\phi_2\rangle & \langle \phi_1|H|\phi_3\rangle \\ \langle \phi_2|H|\phi_1\rangle & \langle \phi_2|H|\phi_2\rangle & \langle \phi_2|H|\phi_3\rangle \\ \langle \phi_3|H|\phi_1\rangle & \langle \phi_3|H|\phi_2\rangle & \langle \phi_3|H|\phi_3\rangle \end{pmatrix}.\Xi$$

where

$$\Xi = \left(\begin{array}{ccc} \xi_1^{\text{in } \phi} & \xi_2^{\text{in } \phi} & \xi_3^{\text{in } \phi} \\ \hline \langle \phi_1|\xi_1\rangle & \langle \phi_1|\xi_2\rangle & \langle \phi_1|\xi_3\rangle \\ \langle \phi_2|\xi_1\rangle & \langle \phi_2|\xi_2\rangle & \langle \phi_2|\xi_3\rangle \\ \langle \phi_3|\xi_1\rangle & \langle \phi_3|\xi_2\rangle & \langle \phi_3|\xi_3\rangle \end{array} \right).$$

Notice that in Fortran there are libraries from NETLIB to multiply a vector by a matrix [DGEMV] or to multiply two matrices [DGEMM]. They are very efficient for these transformations.

%%

$\hookrightarrow$ *EXERCISE 5:* Make a plot of the value of IPR averaged over all the eigenstates of the XXZ model vs Δ. Show two curves, one for the site-basis (blue) and the other for the basis corresponding to the eigenstates of the XX part of the model (red).

When $\Delta = 0$, IPR in the site-basis reaches the largest values, while in the XX basis, the eigenstates are the basis vectors themselves, so IPR=1. As Δ increases IPR(site-basis) decreases and eventually saturate, while IPR(XX basis) increases.

Both *Mathematica* and *Fortran* 90 codes are provided.

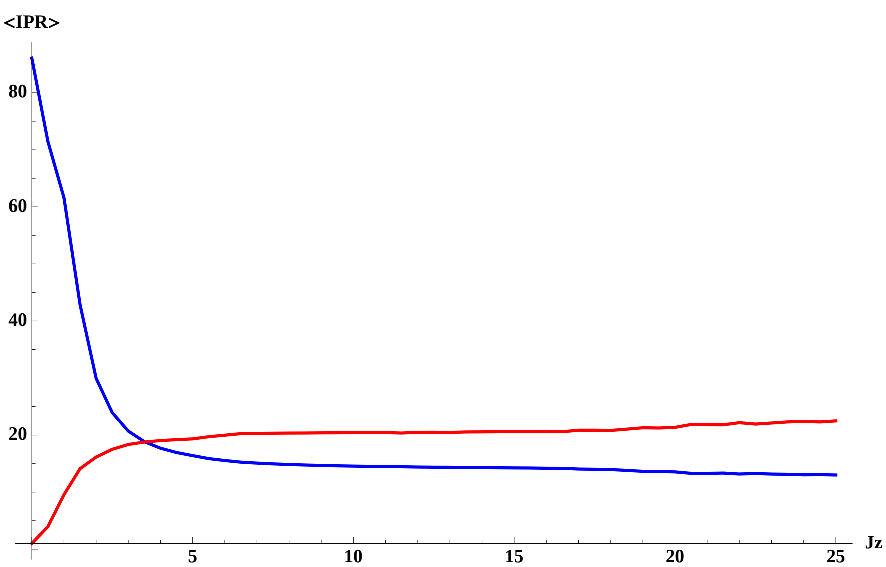

FIG. 2: Level of delocalization dependence on the basis.

%%

C. Quantum phase transition

The 1D XXZ model shows two critical points, one at $\Delta = -1$ and the other at $\Delta = 1$. At $\Delta = -1$ the transition is of first order and at $\Delta = 1$ it is a Berezinskii-Kosterlitz-Thouless transition. For $\Delta < -1$, the chain is in the ferromagnetic Ising phase. The ground state $|GS\rangle$ has either all spins pointing up ($\mathcal{S}^z = +L/2$) or all spins pointing down ($\mathcal{S}^z = -L/2$) in the z direction. For $\Delta > -1$, The ground state has $\mathcal{S}^z = 0$; the total magnetization, $M^z = \mathcal{S}^z$, vanishes. For $-1 < \Delta < 1$, the chain is in the gapless XY phase. For $\Delta > 1$, the chain is in the antiferromagnetic Ising phase (or Néel phase).

Different quantities have been introduced to detect quantum phase transitions. A popular one is the fidelity [13], corresponding to the overlap between the ground state obtained with one value of the parameter of the Hamiltonian related with the transition (Δ is our case) and the ground state obtained by slightly changing the parameter by an amount δ,

$$F(\Delta) = |\langle GS(\Delta)|GS(\Delta+\delta)\rangle|^2 \qquad (12)$$

Generally, since the states are normalized and the change in the parameter is small, the fidelity will be close to one. However, at a transition, the overlap between the states drop significantly and the fidelity is close to zero.

%%
↪ *EXERCISE 6:* Make a plot of the energies of the first five eigenvalues of the *periodic* XXZ model vs Δ for $-1.5 \le \Delta \le +1.5$ in increments of 0.05. Use $L = 6$. As Δ increases, the ground state may change subspace, so diagonalize the whole 2^L Hilbert space. Make a plot also of the total magnetization in the z direction for the ground state for the same values of Δ. The last plot should be for the fidelity (12) vs Δ, in the region $-1.5 < \Delta < 0$. We study the fidelity only up to $\Delta \sim 0$, because this is a region with many degeneracies and special care needs to be taken. ***Mathematica* code is provided.**

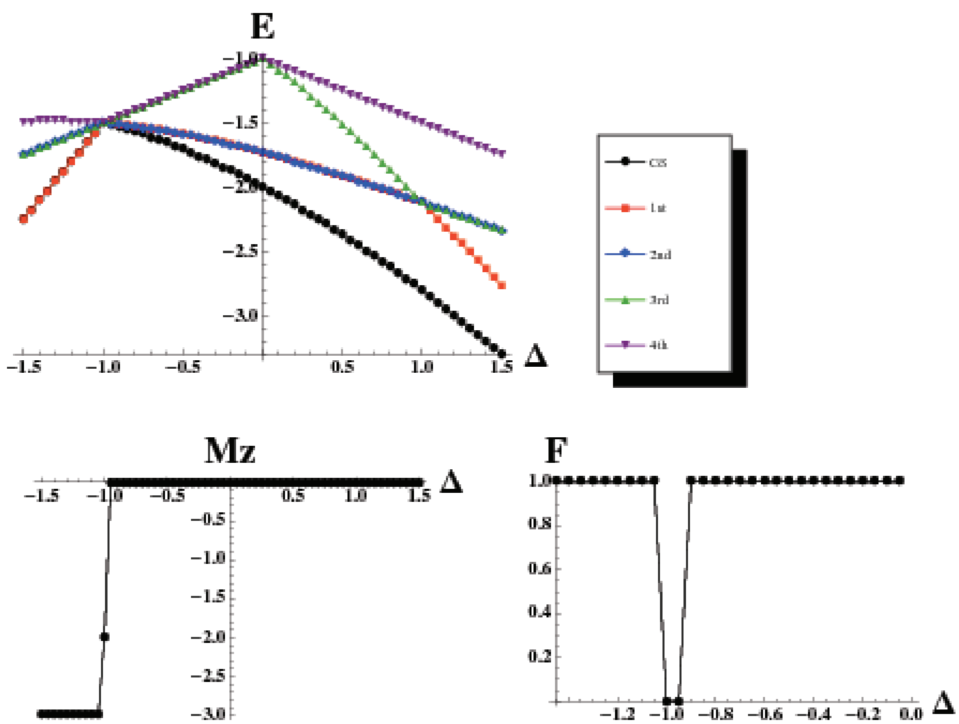

FIG. 3: Eigenvalues, magnetization, and fidelity for the XXZ model

%%

IV. QUANTUM CHAOS

Now that we are well familiar with the XXZ model, we will add terms to the Hamiltonian, for example impurities or couplings between further sites, that will take the system into the chaotic limit. Let us thus start this section with a quick review of quantum chaos.

Classical chaos is related to the extreme sensitivity of the dynamics of a system to its initial conditions, a concept that can be traced back to Poincaré. The main features of classical chaos can be illustrated by a dynamical billiard, which is an idealized billiard table with no friction where a particle reflects elastically from boundaries which can have any shape. The motion of the particle is represented in phase space by a trajectory whose evolution is restricted to a surface of constant energy. Depending on the shape of the boundaries, the system may be chaotic, which means that two trajectories whose initial conditions are very close will diverge exponentially in time. The rate of this separation is characterized by the Lyapunov exponent. The trajectories may also become ergodic, which implies that after a long time the particle will have visited the entire surface of constant energy. Equivalently, we may say that after a long time, the particle is equally likely to be found in any point of the accessible phase space.

For quantum systems the notion of phase-space trajectories loses its meaning, since as stated by the Heisenberg uncertainty principle, we do not have access to precise information about position and momentum at the same time. Nevertheless, because classical physics is a limit of quantum physics, it is natural to search for quantum signatures of classical chaos.

Quantum chaos is a very broad field. The term refers to properties of eigenvalues and eigenstates found in the quantum level that indicate whether the system in the classical level is chaotic or not. The Bohigas-Giannoni-Schmidt conjecture states that any chaotic classical system (K systems in which all parts of the classical phase space show chaotic dynamics) should show the same spectral fluctuations in the quantum limit. Nowadays, the conjecture is overwhelmingly accepted and proofs in the semiclassical limit exist. In fact, the term ”quantum chaos” has even been extended to refer to those properties found in quantum systems without a classical limit.

Quantum chaos is associated spectral fluctuations. So how are they quantified? An important step in the development of the quantum chaos came with the verification that the distribution of the spacings between neighboring energy levels of a quantum billiard depends on the billiard's classical counterpart. If the latter is chaotic, the energy levels are highly correlated and repel each other; if it is regular (integrable), the energy levels are uncorrelated, randomly distributed, and can cross.

Level repulsion had been observed before quantum billiards in studies with full random matrices. Wigner [14] employed these matrices to describe the spectrum of heavy nuclei. His idea was to ignore the details of the interactions of such complex systems and treat them statistically. The matrices are filled with random numbers, their only constraint is to satisfy the symmetries of the system one is trying to describe. The level spacing distributions of these matrices agreed surprisingly well with the data from actual nuclei spectra and showed level repulsion. When level repulsion was later verified in billiards, the connection between quantum chaos and random matrices became established. Level repulsion is one of the main features of what we call quantum chaos. It is seen in various realistic quantum systems, such as atoms in strong magnetic fields and systems of interacting particles (nuclei, atoms, molecules). In these systems, chaos is a cause by the interactions, while in billiards, chaos is a consequence of the boundary conditions.

A. Full random matrices

The distribution $P(s)$ of the spacings, s, of neighboring energy levels of full random matrices is given by the Wigner-Dyson (WD) distribution [15–17]. The form of the Wigner-Dyson distribution depends on the symmetries of the Hamiltonian, but for any case, level repulsion implies that $P(s) \to 0$ when $s \to 0$.

1. Level spacing distributions and symmetries

There are three generic ensembles of random matrices, defined in terms of the symmetry properties of the Hamiltonian:

⋆⋆ *Gaussian Orthogonal Ensemble* (GOE): Time-reversal invariant systems with rotational symmetry. For such systems, the Hamiltonian can be represented by real and symmetric matrices,

$$H_{i,j} = H_{j,i}.$$

The GOE is the most commonly used ensemble of full random matrices. The Bohigas-Giannoni-Schmidt conjecture was originally formulated for the GOE, although it also holds for the two other universality classes discussed below. The GOE is the ensemble that describes nuclear data, the hydrogen atom in a strong magnetic field, microwave stadium billiards, such as Sinai's billiard, and many other experimentally accessible systems, including spin-1/2 models.

The GOE real and symmetric matrix has $\mathcal{D}(\mathcal{D}+1)/2$ independent matrix elements. From its invariance by an orthogonal transformation, we can find the probability density of the matrix elements [18]. The elements are independent random numbers from a Gaussian distribution of mean zero. The diagonal elements have variance

$$\langle H_{i,i}^2 \rangle = 4\sigma^2$$

and the off-diagonal elements

$$\langle H_{i,j}^2 \rangle = 2\sigma^2$$

The GOE matrix can then be constructed in the following way. (i) Generate a $\mathcal{D} \times \mathcal{D}$ matrix whose elements are independent random numbers from a Gaussian distribution of mean zero and standard deviation $\sigma = 1$. (ii) Add this matrix to its transpose to symmetrize it.

From the distribution function for the matrix elements, we can obtain the distribution function for the eigenvalues, and from this one, we derive $P(s)$. The GOE level spacing distribution has the shape,

$$P_{\rm GOE}(s) = \frac{\pi}{2} s \exp\left(-\frac{\pi}{4} s^2\right). \tag{13}$$

⋆⋆ *Gaussian Unitary Ensemble* (GUE): Systems in which time-reversal invariance is violated. For such systems, the Hamiltonian matrices are Hermitian,

$$H_{i,j} = [H^\dagger]_{j,i}.$$

The diagonal elements are real and the off-diagonal elements are complex. Experimentally, time-reversal symmetry can be broken in microwave billiards by changing the reflection properties of the walls. The GUE level spacing distribution is given by

$$P_{\rm GUE}(s) = \frac{32}{\pi^2} s^2 \exp\left(-\frac{4}{\pi} s^2\right). \tag{14}$$

The level repulsion in this case goes as s^2.

⋆⋆ *Gaussian Symplectic Ensemble* (GSE): Time-reversal invariant systems with half-integer spin interaction (such as a spin-orbit interaction) and broken rotational symmetry. The Hamiltonian is invariant under a symplectic transformation [18]. The level spacing distribution is

$$P_{\rm GSE}(s) = \frac{2^{18}}{3^6 \pi^3} s^4 \exp\left(-\frac{64}{9\pi} s^2\right). \tag{15}$$

GAUSSIAN RANDOM NUMBERS: To generate random numbers from a Gaussian distribution in *Mathematica*, use the command

RandomReal[NormalDistribution[0, 1]]

In the first position, enter the mean of the random numbers (0 in our case) and in the second, the standard deviation (1 in our case).

In *Fortran*, we often use a function (available online and in the code for EXERCISE 7) called 'gasdev'. You need to choose an integer value for 'idum', which is the seed for your sequence of random numbers. Every time 'gasdev(idum)' is called, it gives a different random number, although for each 'idum' you get always the same sequence.

2. Density of states

The density of states $\rho(E)$ of full random matrices has a semicircular shape [15–20]

$$\rho(E) = \frac{2}{\pi \mathcal{E}} \sqrt{1 - \left(\frac{E}{\mathcal{E}}\right)^2}, \tag{16}$$

where $2\mathcal{E}$ is the length of the spectrum.

3. Level of delocalization of the eigenstates

The eigenstates $|\psi_\alpha\rangle$ of full random matrices are completely delocalized in any basis $|\phi_k\rangle$. They are random vectors, $|\psi_\alpha\rangle = \sum_k C_\alpha^{(k)} |\phi_k\rangle$, that is $C_\alpha^{(k)}$ are just random number from a Gaussian distribution. Of course, the components also need to satisfy the normalization condition, $\sum_k |C_\alpha^{(k)}|^2 = 1$, so $\overline{C} = 0$ and $\overline{C^2} = 1/\mathcal{D}$. For GOEs, they lead to [11, 12]

$$\text{IPR}_\alpha \sim \frac{\mathcal{D}}{3}. \tag{17}$$

The result above can be obtained by substituting the sum in IPR by an integral. The distribution of the probability amplitudes $C_\alpha^{(k)}$ is given by the Gaussian [12],

$$P(C) = \sqrt{\frac{\mathcal{D}}{2\pi}} \exp\left(-\frac{\mathcal{D}}{2}C^2\right),$$

which guarantees that $\overline{C} = 0$ and $\overline{C^2} = 1/\mathcal{D}$. The latter is obtained by substituting $x = C\sqrt{\mathcal{D}/2}$,

$$\overline{C^2} = \sqrt{\frac{\mathcal{D}}{2\pi}} \int_{-\infty}^{\infty} C^2 \exp\left(-\frac{\mathcal{D}}{2}C^2\right) = \sqrt{\frac{\mathcal{D}}{2\pi}} \int_{-\infty}^{\infty} \frac{2}{\mathcal{D}} x^2 e^{-x^2} \sqrt{\frac{2}{\mathcal{D}}} = \frac{1}{\mathcal{D}}.$$

The sum is approximated by an integral as,

$$\sum_k F(C_k) \to \mathcal{D} \int_{-\infty}^{\infty} F(C) P(C) dC.$$

Thus,

$$\sum_k |C_k|^4 \to \mathcal{D}\sqrt{\frac{\mathcal{D}}{2\pi}} \int_{-\infty}^{\infty} C^4 \exp\left(-\frac{\mathcal{D}}{2}C^2\right) = \mathcal{D}\sqrt{\frac{\mathcal{D}}{2\pi}} \int_{-\infty}^{\infty} \frac{4}{\mathcal{D}^2} x^4 e^{-x^2} \sqrt{\frac{2}{\mathcal{D}}} = \frac{4}{\mathcal{D}\sqrt{\pi}} \frac{3\sqrt{\pi}}{4} = \frac{3}{\mathcal{D}}$$

B. Unfolding the spectrum

As we saw above, very different systems (nuclei, atoms, molecules, etc) show the same level fluctuations. However, to be able to compare these different systems and of different sizes, we need to unfold their spectra. This means that each system's specific mean level density must be removed from the data. It does not make sense to compare local fluctuations from systems with very different average densities. For example, it does not make sense to say that a spectral region with high average density has less repulsion than a spectral region with low average density. Thus, we need to separate the local fluctuations from a systematic global energy dependence of the average density. For this, we rescale the energies, so that the local density of states of the renormalized eigenvalues is 1. Since the density of states is the number of states in an interval of energy, that is, the reciprocal of the mean level spacing, this renormalization procedure ensures also that the mean level spacing becomes unit.

There are different ways to unfold the spectrum. A simple and for our purposes good enough recipe is the following:

(i) Order the spectrum in increasing values of energy.

(ii) Discard some eigenvalues from the edges of the spectrum, where the fluctuations are large. This is arbitrary, you can discard for example 10% of the spectrum.

(ii) Separate the remaining eigenvalues into several small sets of eigenvalues.

(iii) Divide each eigenvalue by the mean level spacing of its particular set. The mean level spacing of the new set of renormalized energies becomes 1.

A possible code for unfolding the spectrum and then making the histogram for the spacings of neighboring levels could go as:

```
! dble(x) = dfloat(x): converts the integer 'x' to double precision real type.
        ⇒ percentage=0.1d0*dfloat(dimTotal)     ! ∼ how much we choose to discard from the edges of the spectrum
        ⇒ half=int(percentage/2.0d0)     ! count eigenvalues not from the ground state Eig(1), but from state Eig(half)
        ⇒ s̄ = (s_1 + s_2 ... + s_{N+1})/N = ((E_2 − E_1) + (E_3 − E_2) ... + (E_{N+1} − E_N))/N = (E_{N+1} − E_1)/N,
        where N is the number of spacings for a selected set of N + 1 eigenvalues.
        ⇒ NspcTot = int( (dfloat(dimTotal)-percentage)/(10.0d0) )     ! total number of sets

  ! FOR THE HISTOGRAM (binS = width of the bin, chosen as 0.1d0)
        Do i=1, NofBINs + 1     ! NofBINs = number of bins in the histogram, chosen as 80
           SPChist(i) = dfloat(i-1)*binS     ! SPChist = the edges of each bin
           Nhist(i)=0.0d0     ! Nhist = number of spacings in each bin (INITIALIZATION)
        Enddo

  ! UNFOLDED SPACINGS (below each set 'j' has 11 eigenvalues and 10 spacings)
        Do j = 1, NspcTot
```

```
        average=(Eig(half+10*j)-Eig(half+10*(j-1)))/(10.0d0)    ! average = s̄
        Do i = 1 + 10*(j-1), 10*j    ! 10*NspcTot = total number of spacing dealt with
           spacing(i)=(Eig(half+i)-Eig(half-1+i))/average
        Enddo
     Enddo

! HISTOGRAM (if a spacing 'k' is inside the bin 'j', Nhist(j) increases by 1)
     Do k = 1, 10*NspcTot
        Do j = 1, NofBINs
           If(spacing(k) >= SPChist(j) .AND. spacing(k) < SPChist(j+1)) then
              Nhist(j) = Nhist(j) + 1.0d0
           Endif
        Enddo
     Enddo

! HISTOGRAM
     normaliza=0.0d0
     Do i=1,NofBINs
        normaliza=normaliza+binS*Nhist(i)
     Enddo

! OUTPUT (the data is written to give a bar plot)
     write(40,130) SPChist(1),0.0d0
     Do i=1,NofBINs
        write(40,130) SPChist(i),Nhist(i)/normaliza
        write(40,130) SPChist(i+1),Nhist(i)/normaliza
     Enddo
```

%%%
$\hookrightarrow$ *EXERCISE 7:* Write a full random matrix of dimension $\mathcal{D} = 3000$ from a GOE. Make plots for
(i) The density of states.
(ii) The values of IPR for all eigenstates. IPR is sometimes also called number of principal components (NPC)].
(iii) The level spacing distribution.
Both *Mathematica* and *Fortran* 90 codes are provided.
%%%

1. When unfolding is not necessary

There are several other quantities the capture level repulsion, such as level number variance and rigidity [16]. Recently, a new one has been introduced that does not require the unfolding of the spectrum [21, 22]. It corresponds to the distribution of the ratios r_n defined as

$$r_n = \frac{\min(s_n, s_{n-1})}{\max(s_n, s_{n-1})}, \tag{18}$$

where $s_n = E_{n+1} - E_n$. It has been shown that the distribution $P(r)$ for a GOE takes the form

$$P_{\rm GOE}(r) = \frac{8}{27}\frac{r + r^2}{(1 + r + r^2)^{5/2}}. \tag{19}$$

For the expressions for other ensembles see Ref [22].

V. REALISTIC INTEGRABLE AND CHAOTIC MODELS WITH TWO-BODY INTERACTIONS

Despite the success of full random matrices in describing spectral statistical properties, it cannot capture the details of real quantum many-body systems. The fact that full random matrices are completely filled with statistically independent elements

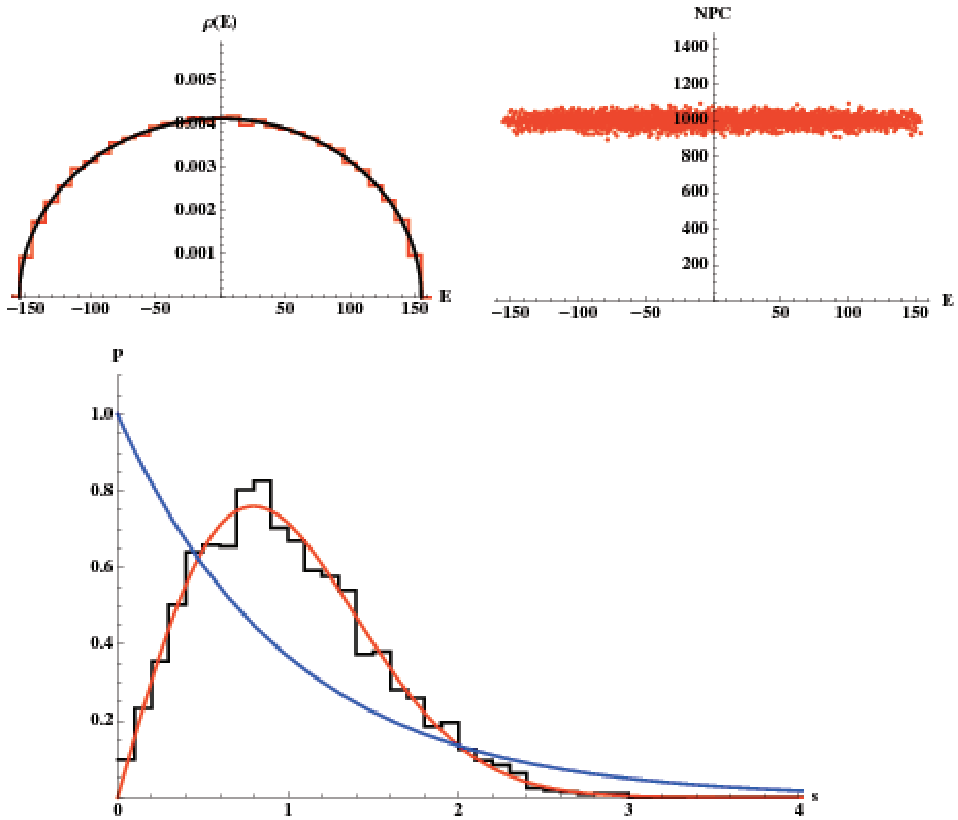

FIG. 4: Properties of the GOE.

implies infinite-range interactions and the simultaneous interaction of many particles. Real systems have few-body (most commonly only two-body) interactions which are usually finite range. A better picture of systems with finite-range interactions is provided by band random matrices, which were also studied by Wigner [23]. Their off-diagonal elements are random and statistically independent, but are non-vanishing only up to a fixed distance from the diagonal. There are also ensembles of random matrices that take into account the restriction to few body interactions, so that only the elements associated with those interactions are nonzero; an example is the two-body-random-ensemble [24, 25] (see reviews in Refs. 26, 27). Other models which describe systems with short-range and few-body interactions do not even include random elements, such as nuclear shell models [12] and quantum interacting systems, such as spin models. All the systems mentioned in this paragraph can lead to level repulsion, but they differ from full random matrices in terms of density of states and level of delocalization of the eigenstates.

A. Integrable spin-1/2 models

The XXZ and XX models (with NN couplings only) are integrable. In integrable systems, since any eigenvalue makes up a symmetry class of its own, the eigenvalues are uncorrelated. The expected level spacing distribution is therefore Poissonian,

$$P_{\mathrm{P}}(s) = e^{-s}. \tag{20}$$

However, deviations from this shape are seen for the XX model due to its the high number of degeneracies. As Δ increases from zero, the excessive degeneracies rapidly fade away and the Poisson is recovered. But, at the special value $\Delta = 1/2$, the form of the distribution departs again from Poisson. This seems to be a special point, where the system develops additional nontrivial symmetries. By changing Δ slightly, for example, by using = 0.48, the Poisson reappears [28].

%%

$\hookrightarrow$ *EXERCISE 8:* Study the level spacing distribution for the spin-1/2 model in Eq. (8) with $L = 18$, 6 spins up, and only the eigenstates with even parity. Consider: $\Delta = 0$ (a); $\Delta = 0.001$ (b); $\Delta = 0.01$ (c); $\Delta = 0.1$ (d); and $\Delta = 0.5$ (e).

Combine the codes provided in EXERCISES 7 and 9.

%%

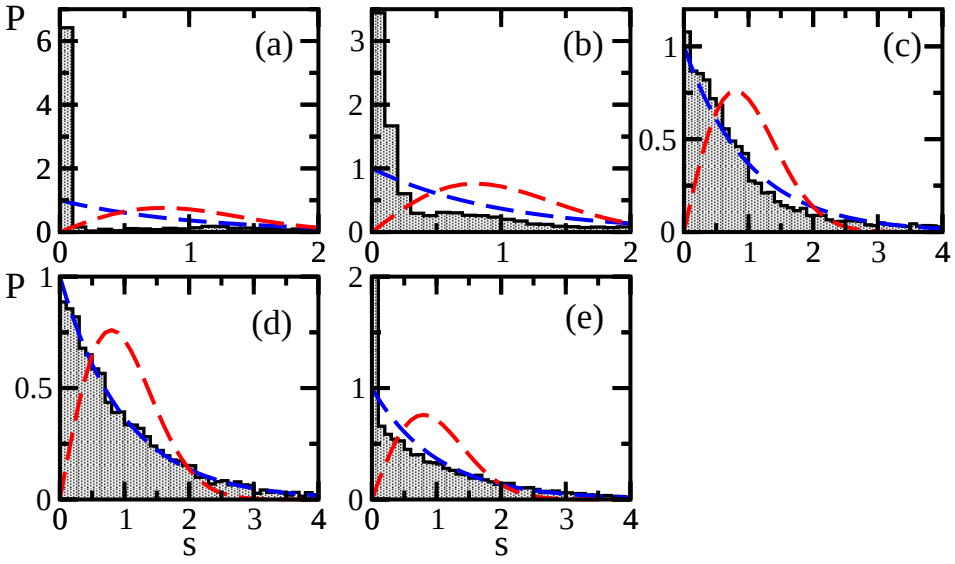

FIG. 5: Level spacing distribution of the XXZ model

B. Chaotic spin-1/2 models

There are many ways to break the integrability of the XXZ model and take it into the chaotic domain. Below we discuss the case where couplings between second neighbors are added and the case where a single impurity is added to the chain. Other ways include couplings between further spins, such as dipolar; randomizing the coupling strengths in the XXZ model, which is closer to the notion of two-body random ensembles; and adding random on-site disorder, which is the path taken in studies of many-body localization.

1. NNN couplings

By considering couplings between next-nearest-neighbors (NNNs) [29], the Hamiltonian for the system with open boundaries becomes

$$\hat{H}_\lambda = \sum_{n=1}^{L-1}\left[J_{xy}\left(\hat{S}_n^x\hat{S}_{n+1}^x+\hat{S}_n^y\hat{S}_{n+1}^y\right)+J_z\hat{S}_n^z\hat{S}_{n+1}^z\right]+\lambda\sum_{n=1}^{L-2}\left[J'_{xy}\left(\hat{S}_n^x\hat{S}_{n+2}^x+\hat{S}_n^y\hat{S}_{n+2}^y\right)+J'_z\hat{S}_n^z\hat{S}_{n+2}^z\right]. \qquad (21)$$

In finite systems, as λ increases, $P(s)$ first acquires an intermediate shape between Poisson and Wigner-Dyson and then eventually reaches the Wigner-Dyson shape.

For sufficiently large λ ($\lambda \gtrsim 0.3$ for $L = 14$ and $\mathcal{S}^z = 0$), there are various scenarios for which chaos can develop, which include:

⋆⋆ Absence of Ising interactions, $J_z = J'_z = 0$;

⋆⋆ Absence of the flip-flop term between next-nearest-neighbors, $J'_{xy} = 0$;

⋆⋆ Absence of Ising interaction between next-nearest-neighbors, $J'_z = 0$;

⋆⋆ Presence of all four terms.

To obtain the level spacing distribution, we first need to separate the eigenvalues according to their symmetry sectors. If we mix eigenvalues from different symmetry sectors, we my not achieve a Wigner-Dyson distribution even if the system is chaotic, because eigenvalues from different subspaces are independent, uncorrelated, so they do not repel each other. From the discussion in Sec. II D, we see that for the system in Eq. (21) we need to take into account parity, spin reversal when $N_{ip} = L/2$ and $\mathcal{S}^z = 0$, and total spin when $J_{xy} = J_z$ and $J'_{xy} = J'_z$.

For closed boundary conditions we would also need to worry about momentum conservation. The more symmetries the system has, the smaller the subspaces become for a given system size, which is not good for statistics. For this reason we often use open boundary conditions and choose parameters to avoid the other symmetries.

%%

$\hookrightarrow$ *EXERCISE 9:* Study the level spacing distribution for the open spin-1/2 model in Eq. (21) with $\lambda = 0.5$ and $J_{xy} = 1$. Consider the following parameters: (a) $L = 14$, 7 spins up and (b)–(e) $L = 15$, 5 spins up.

(a) $J'_{xy} = J_z = J'_z = 1$.

$\hat{H} = \sum_{n=1}^{L-1}\left[\left(\hat{S}^x_n\hat{S}^x_{n+1} + \hat{S}^y_n\hat{S}^y_{n+1}\right) + \hat{S}^z_n\hat{S}^z_{n+1}\right] + 0.5\sum_{n=1}^{L-2}\left[\left(\hat{S}^x_n\hat{S}^x_{n+2} + \hat{S}^y_n\hat{S}^y_{n+2}\right) + \hat{S}^z_n\hat{S}^z_{n+2}\right].$

(b) $J'_{xy} = 1$, $J_z = J'_z = 0.5$.

$\hat{H} = \sum_{n=1}^{L-1}\left[\left(\hat{S}^x_n\hat{S}^x_{n+1} + \hat{S}^y_n\hat{S}^y_{n+1}\right) + 0.5\hat{S}^z_n\hat{S}^z_{n+1}\right] + 0.5\sum_{n=1}^{L-2}\left[\left(\hat{S}^x_n\hat{S}^x_{n+2} + \hat{S}^y_n\hat{S}^y_{n+2}\right) + 0.5\hat{S}^z_n\hat{S}^z_{n+2}\right].$

(c) $J'_{xy} = 1$, $J_z = J'_z = 0$.

$\hat{H} = \sum_{n=1}^{L-1}\left(\hat{S}^x_n\hat{S}^x_{n+1} + \hat{S}^y_n\hat{S}^y_{n+1}\right) + 0.5\sum_{n=1}^{L-2}\left(\hat{S}^x_n\hat{S}^x_{n+2} + \hat{S}^y_n\hat{S}^y_{n+2}\right).$

(d) $J'_{xy} = 0$, $J_z = J'_z = 0.5$.

$\hat{H} = \sum_{n=1}^{L-1}\left[\left(\hat{S}^x_n\hat{S}^x_{n+1} + \hat{S}^y_n\hat{S}^y_{n+1}\right) + 0.5\hat{S}^z_n\hat{S}^z_{n+1}\right] + 0.5\sum_{n=1}^{L-2} 0.5\hat{S}^z_n\hat{S}^z_{n+2}.$

(e) $J'_{xy} = 1$, $J_z = 0.5$, $J'_z = 0$.

$\hat{H} = \sum_{n=1}^{L-1}\left[\left(\hat{S}^x_n\hat{S}^x_{n+1} + \hat{S}^y_n\hat{S}^y_{n+1}\right) + 0.5\hat{S}^z_n\hat{S}^z_{n+1}\right] + 0.5\sum_{n=1}^{L-2}\left(\hat{S}^x_n\hat{S}^x_{n+2} + \hat{S}^y_n\hat{S}^y_{n+2}\right).$

Separate the eigenvalues according to the parity of the corresponding eigenstates. $P(s)$ should be the average of the distributions of the two parity sectors.

***Mathematica* code is provided. The code in *Fortran* 90 gives as output the eigenvalues and their parity. Combine it with the code from EXERCISE 7 to get the level spacing distribution.**

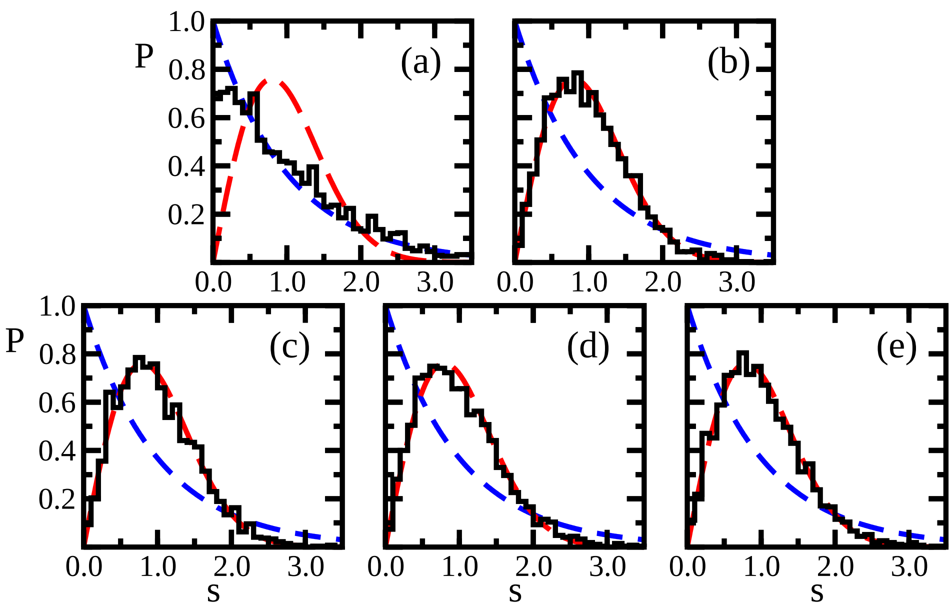

FIG. 6: Level spacing distribution of the spin-1/2 model with NN and NNN couplings.

%%

If you want to study the crossover from integrability to chaos as a chosen parameter (for example λ) increases from zero,

better than looking at the level spacing for each value of the parameter is to use a quantity that can tell how close we are from Poisson or Wigner-Dyson.

The parameter β, used to fit $P(s)$ with the Brody distribution [26],

$$P_B(s) = (\beta+1) b s^{\beta} \exp\left(-b s^{\beta+1}\right), \quad b = \left[\Gamma\left(\frac{\beta+2}{\beta+1}\right)\right]^{\beta+1}, \tag{22}$$

can be used to quantify the level of chaoticity of the system reflected by the spectrum statistics. If $\beta = 1$ the distribution is Poisson and for $\beta = 0$ it is Wigner-Dyson. The value of the parameter leading to the crossover to chaos decrease with the size of the system, suggesting that the onset of chaos in the thermodynamic limit might be achieved with an infinitesimal integrability breaking term [30, 31].

2. *Full random matrices vs chaotic spin-1/2 systems*

If we are careful with the symmetries we do obtain a Wigner-Dyson distribution, just as we did with full random matrices. So where can we see the differences between spin-1/2 models (and system with two-body interactions in general) and full random matrices? For example, in the density of states and in the level of delocalization of the eigenstates. The density of states of Hamiltonians with two-body interactions is Gaussian, independent of the regime (integrable and chaotic) of the system. This is reflected into the eigenstates. The majority of the states are close to the middle of the spectrum, where strong mixing occurs. Thus, the eigenstates reach their highest level of delocalization in the center of the spectrum and are more localized close to the edges.

%%%
$\hookrightarrow$ *EXERCISE 10:* Compare the density of states and the values of IPR for all eigenstates for a full random matrix from a GOE of $\mathcal{D} = 12\,870$ and Hamiltonian (21) with $J_{xy} = J'_{xy} = 1$, $J_z = J'_z = 0.5$, $\lambda = 1$, $L = 16$, and $\mathcal{S}^z = 0$. The IPR for the eigenstates of Hamiltonian (21) should be written in the basis corresponding to the eigenstates of the XXZ model.

Use the codes from EXERCISES 6, 7 and 9.

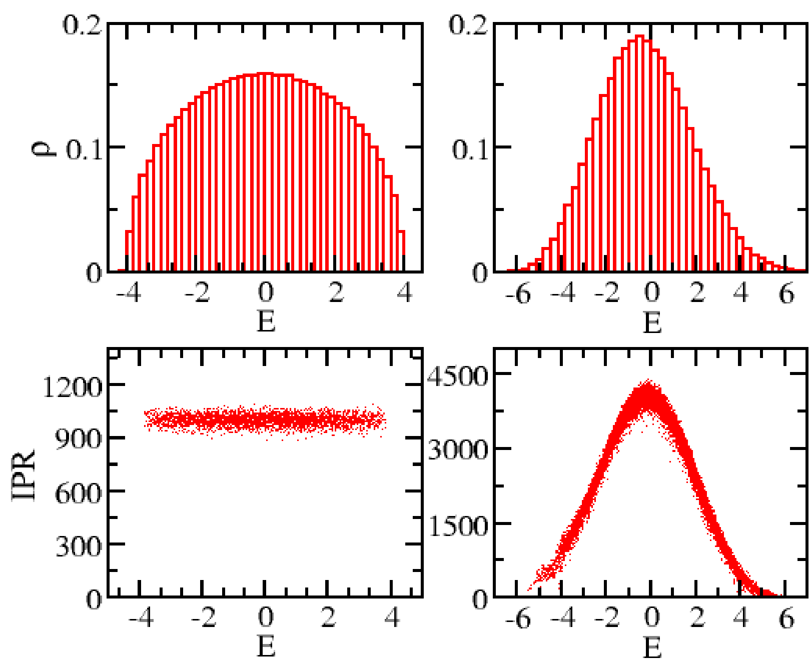

FIG. 7: GOE vs chaotic spin-1/2 model.

%%%

3. *Single impurity*

An impurity (defect) is created by applying a local static magnetic field in the z-direction to a spin on a single site which leads to a Zeeman splitting different from that on the other sites,

$$\hat{H}_{imp} = \varepsilon J \hat{S}_1^z + dJ\hat{S}_{\lfloor L/2 \rfloor}^z + \sum_{n=1}^{L-1} \left[J \left(\hat{S}_n^x \hat{S}_{n+1}^x + \hat{S}_n^y \hat{S}_{n+1}^y \right) + J\Delta \hat{S}_n^z \hat{S}_{n+1}^z \right] \tag{23}$$

The Hamiltonian above contains two impurities. The one on the first site of the chain has amplitude εJ and the one close to the middle of the chain, on site $\lfloor L/2 \rfloor$, is dJ. The defect on the first site breaks trivial symmetries, such as parity, conservation of total spin, and spin reversal, but does not break the integrability of the model [32].

The addition of a single impurity close to the middle of the chain in the presence of NN couplings can bring the system into the chaotic domain [33] provided $d \lesssim 1$ [if the defect becomes too large it effectively splits the system in two independent and integrable chains]. The onset of chaos is caused by the interplay between the Ising interaction and the impurity. In contrast, the addition of d to the XX model does not affect its integrability.

%%%
$\hookrightarrow$ *EXERCISE 11:* Study the level spacing distribution for the spin-1/2 model in Eq. (23) for $J = 1$, $\Delta = 0.5$, $L = 15$, 5 spins up. Consider the two cases: $\varepsilon = 0.5$, $d = 0$ and $\varepsilon = 0$, $d = 0.5$.

Mathematica code is provided. In Fortran, use the codes from EXERCISES 7 and 9.

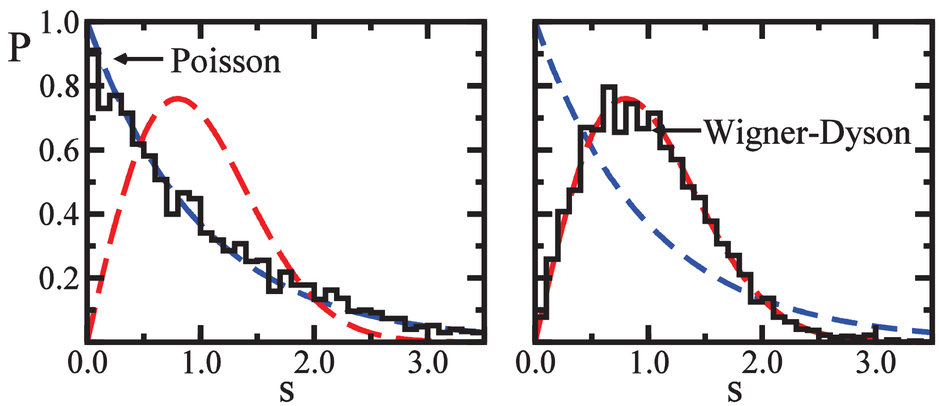

FIG. 8: Level spacing distribution of the XXZ model with and without an impurity.

%%%

4. *NNN model vs impurity model*

Is there any visible difference between the NNN and the impurity models? Yes, in the level of delocalization of the eigenstates, for example. But before we look at the eigenstates, let us compare the Hamiltonian matrices of both models written in the eigenstates of the XXZ model [denoted $|n\rangle$] and verify if differences can already be seen at this level. This choice of the basis corresponding to the mean-field basis, the regular part of the Hamiltonian. Let us fix a small impurity on the first site of value $\varepsilon = 0.1$, so that we do not worry about symmetries.

The details of the matrices are shown in Fig. 9 for $d = 0.9$ and $\lambda = 0.44$. Panel (a) shows the values of the diagonal elements $\langle n|\hat{H}|n\rangle \equiv H_{n,n}$. They are in increasing order. There is a subroutine called MRGRNK that can be used to order the elements.

Figure 9 (b) presents the values of the connectivity M_n of each line n, that is the number of basis vectors directly coupled with each state $|n\rangle$. M_n is comparable for both models. It shows a smooth behavior with n (or equivalently with $H_{n,n}$). It is large in the middle of the spectrum, where the majority of the basis vectors are coupled, and it decreases at the edges. This is related with the level of delocalization of the eigenstates that we saw in EXERCISE 10.

Notice that to count how many off-diagonal elements are non-zero, we use a threshold below which the elements are discarded. This is done because of our numerical procedure. Initially, $\hat{H}$ is written in the site-basis. Subsequently, this basis is transformed

into the eigenstates of the XXZ model, which results in the appearance of many tiny off-diagonal elements not associated with any real coupling. We use as threshold the variance of the absolute value of all off-diagonal elements.

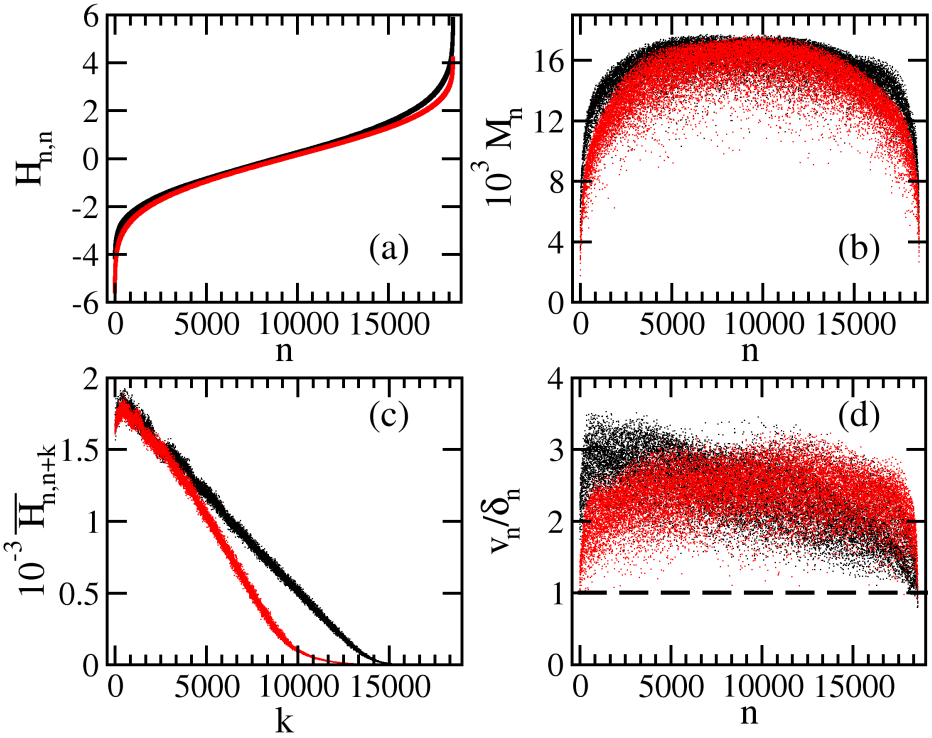

FIG. 9: (Color online) Details of the Hamiltonian matrices of the impurity (light points, $d_F = 0.9$) and NNN (dark points, $\lambda_F = 0.44$) models written in the eigenstates of $\hat{H}_I$; $\Delta = 0.48$, $\varepsilon = 0.1$, $L = 18$. Diagonal elements (a). Connectivity (b). Averages of the absolute values of the off-diagonal elements vs the distance k from the diagonal (c). Ratio of the average coupling strength v_n to the mean level spacing δ_n between directly coupled states in each line n (d).

In Fig. 9 (c), we show the averages of the absolute values of the off-diagonal elements,

$$\overline{H}_{n,n+k} = \frac{\sum_{n=1}^{\mathcal{D}-k} |H_{n,n+k}|}{\mathcal{D}-k}, \tag{24}$$

versus the distance k from the diagonal. They are significantly smaller than the diagonal elements and decay with k. The absence of an abrupt drop implies that both Hamiltonians have long range, although finite interactions in the basis $|n\rangle$.

The similarity between $H_{n,n}$ and M_n holds for both models when $d_F, \lambda_F \lesssim 1$, but differences are visible in the values of the off-diagonal elements. For parameters in the vicinity of those chosen in Fig. 9 (c), $\overline{H}_{n,n+k}$ is comparable for both systems when k is small, but the decay is slower for the NNN model. For the impurity model, we cannot further increase $\overline{H}_{n,n+k}$. By increasing Δ (d_F cannot be much increased, since we are already at the border of splitting the chain), the increase of $\overline{H}_{n,n+k}$ is minor. In contrast, much larger values can be achieved for the NNN model with $\lambda_F \to 1$ (not shown). In this limit, the NNN model must therefore lead to stronger mixing of the basis vectors than the defect case.

To get an idea of how effective the off-diagonal elements are, we compare their average strength

$$v_n = \frac{\sum_{m \neq n} |H_{n,m}|}{M_n}$$

with the mean level spacing δ_n between directly coupled states. The latter is computed as

$$\delta_n = \frac{(H_{m,m})_n^{max} - (H_{m,m})_n^{min}}{M_n},$$

where $(H_{n,m})_n^{max}$ $[(H_{m,m})_n^{min}]$ is the largest (smallest) diagonal element where $H_{n,m} \neq 0$. As seen in Fig. 9 (d), v_n/δ_n is similar for both models for the parameters considered. The ratio can be significantly increased by increasing λ_F, but it is hardly

affected by larger combinations of Δ and d_F (not shown). We can therefore distinguish between two limits: the intermediate perturbation regime, where $v_n/\delta_n \gtrsim 1$, and the strong coupling regime, where v_n/δ_n can reach values significantly greater than 1. The second is only achieved by the NNN model.

We have verified that the values of the parameters leading to $v_n/\delta_n \gtrsim 1$ serve to indicate when the system becomes chaotic, showing Wigner-Dyson distribution and significantly delocalized eigenstates. The onset of chaos may therefore be anticipated by a careful analysis of the Hamiltonian matrices, even before diagonalization. This is a powerful result, although in our case we still had to diagonalize the XXZ Hamiltonian to find our basis vectors.

%%
$\hookrightarrow$ *EXERCISE 12:* Reproduce Fig. 9.
***Fortran* code is provided.**
%%

To quantify the crossover from integrability to chaos, we show in Fig. 10 (left) the level spacing indicator κ defined as

$$\kappa \equiv \frac{\sum_i [\mathcal{P}(s_i) - \mathcal{P}_{WD}(s_i)]}{\sum_i \mathcal{P}_{WD}(s_i)}, \tag{25}$$

where the sums run over the whole spectrum. κ is large close to the integrable domain and it approaches zero in the chaotic regime. This indicator is comparable to the quantity η introduced in Ref. [34] or the parameter β used in the fitting of $\mathcal{P}(s)$ with the Brody distribution shown in Eq.(22).

As the perturbations d_F and λ_F increase, both models become chaotic and show similar values of κ for the same system sizes. If the perturbation is further increased well above 1, the systems eventually reach another integrable point. Notice also that as L increases, not only κ decreases, but also the value of the perturbation leading to small κ. The onset of chaos in the thermodynamic limit might be achieved with an infinitesimally small integrability breaking term [31].

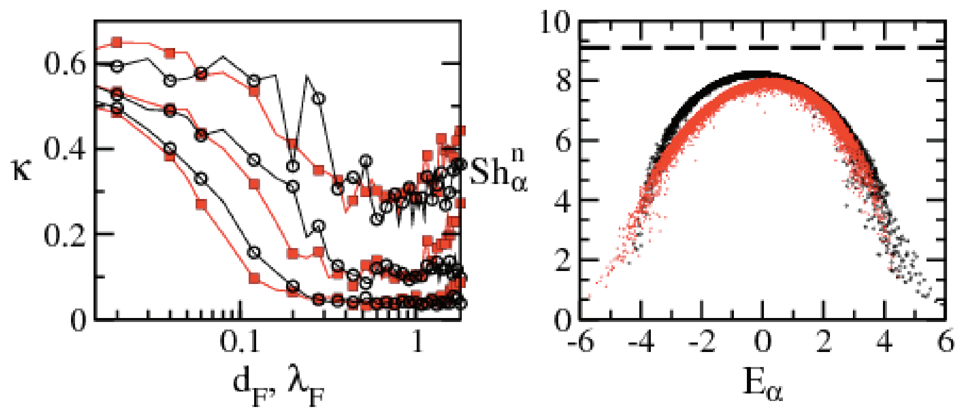

FIG. 10: (Color online) Indicator κ of the integrable-chaos crossover vs the perturbation strength (left) and Shannon entropy for all eigenstates in the basis of $\hat{H}_I$ (right) for the impurity (light color) and the NNN (dark color) models; $\Delta = 0.48$, $d_F = 0.9$, $\lambda_F = 0.44$, $\varepsilon = 0.1$, $L = 18$. Dashed line: GOE result (right).

We also study the structure of the eigenstates $|\psi_\alpha\rangle$ of $\hat{H}$ in the basis $|n\rangle$,

$$|\psi_\alpha\rangle = \sum_n C_\alpha^n |n\rangle,$$

via the Shannon (information) entropy,

$$\text{Sh}_\alpha^n \equiv -\sum_n |C_\alpha^n|^2 \ln |C_\alpha^n|^2, \tag{26}$$

This delocalization measure determines the degree of complexity of the eigenstates. Complete delocalization occurs for full random matrices, where the amplitudes C_α^n are independent random variables. For GOEs, the average over the ensemble leads to $\text{Sh}_{\text{GOE}} \sim \ln(0.48\mathcal{D})$ [11, 12]. For the realistic systems considered here, where the Hamiltonian is sparse and banded, the mixing of the basis vectors is incomplete and $\text{Sh}_\alpha^n < \text{Sh}_{\text{GOE}}$.

Figure 10 (right) compares the Shannon entropy for the defect and NNN models for all eigenvalues E_α. The results are very similar for the parameters considered. They reflect the structure of the matrices in Fig. 9: Sh_α^n is large close to the middle of the spectrum, where $H_{n,n}$ is smaller and M_n is larger, and it decreases as we approach the edges of the spectrum. This behavior mirrors also the density of states, which is Gaussian for systems with few-body interactions [26]. By increasing Δ, hardly any change is noticed on the values of the Shannon entropy for the impurity model, but by increasing λ_F, significantly larger values can be reached for the NNN model. This connects again with the notion of intermediate and strong perturbations discussed in the description of Fig. 9 (d).

VI. OBSERVABLES

The eigenstate expectation values of observables is given by

$$O_{\alpha,\alpha} = \langle\psi_\alpha|\hat{O}|\psi_\alpha\rangle. \tag{27}$$

Observables in the z direction are particularly easy to compute if we have the eigenstates in the site-basis vectors.

The few-body observables commonly studied in spin-1/2 systems include;

• The local magnetization of each site n,

$$\hat{M}_n^z = \hat{S}_n^z. \tag{28}$$

• The spin-spin correlations between sites n and m in the z direction,

$$\hat{C}_{n,m}^{zz} = \hat{S}_n^z \hat{S}_m^z. \tag{29}$$

In the code, for each eigenstate $|\psi_\alpha\rangle = \sum_i A(i,\alpha)|\phi_i\rangle$ in the site-basis vector $|\phi_i\rangle$, we get

$$\langle\psi_\alpha|\hat{C}_{n,m}^{zz}|\psi_\alpha\rangle = \sum_i |A(i,\alpha)|^2(-1)^{basis(i,n)+basis(i,m)}$$

The computation of the interaction energy and the structure factor in the z direction is an extension of $\langle\hat{C}_{n,m}^{zz}\rangle$.

• The interaction energy,

$$\hat{IE} = \sum_{n=1}^{L-1} J_z \hat{S}_n^z \hat{S}_{n+1}^z + \lambda \sum_{n=1}^{L-2} J_z' \hat{S}_n^z \hat{S}_{n+2}^z. \tag{30}$$

• The structure factor in the z direction, defined as the Fourier transform of the spin-spin correlations in z,

$$\hat{S}^{zz}(k) = \frac{1}{L}\sum_{n,m=1}^{L} \hat{S}_n^z \hat{S}_m^z e^{-ik(n-m)} = \frac{1}{4} + \frac{2}{L}\sum_{u=1}^{L-1} \cos(ku) \sum_{v=1}^{L-u} \hat{S}_v^z\, \hat{S}_{v+u}^z, \tag{31}$$

where $k = 2\pi p/L$ stands for momentum and $p = 0, 1, 2 \ldots, L$ is a positive integer.

• The spin-spin correlations between sites n and m in the x direction,

$$\hat{C}_{n,m}^{xx} = \hat{S}_n^x \hat{S}_m^x. \tag{32}$$

An example for a small chain helps understanding how to compute $\langle\hat{C}_{n,m}^{xx}\rangle$. Suppose we have the eigenstate $|\psi_\alpha\rangle = A(1,\alpha)|1100\rangle + A(2,\alpha)|1010\rangle + A(3,\alpha)|1001\rangle + A(4,\alpha)|0110\rangle + A(5,\alpha)|0101\rangle + A(6,\alpha)|0011\rangle$ and we want $\langle\hat{C}_{2,3}^{xx}\rangle$. The operator couples $|1100\rangle$ with $|1010\rangle$ and $|0101\rangle$ with $|0011\rangle$, while $|1001\rangle$ and $|0110\rangle$ do not pair with any state via $\hat{C}_{2,3}^{xx}$. We have

$$\langle\hat{C}_{2,3}^{xx}\rangle = \frac{1}{4}\left[A(1,\alpha)A(2,\alpha)^* + A(2,\alpha)A(1,\alpha)^* + A(5,\alpha)A(6,\alpha)^* + A(6,\alpha)A(5,\alpha)^*\right] = \frac{A(1,\alpha)A(2,\alpha) + A(5,\alpha)A(6,\alpha)}{2}$$

The last equality comes from the fact that the components of the eigenstates are real. To obtain that result, we need to keep track of the pairs of states coupled via $\hat{C}_{2,3}^{xx}$. Let us call the elements of these pairs cxxI and cxxJ and the total number of pairs nxx. Thus

$$\langle\psi_\alpha|\hat{C}_{2,3}^{xx}|\psi_\alpha\rangle = \frac{1}{2}\sum_{q=1}^{\mathrm{nxx}} A(\mathrm{cxxI}(q),\alpha)A(\mathrm{cxxJ}(q),\alpha)$$

In our example, cxxI(1)=1 and cxxJ(1)=2, cxxI(2)=5 and cxxJ(2)=6.

• The kinetic energy,

$$\hat{KE} = \sum_{n=1}^{L-1} J_{xy} \left(\hat{S}^x_n \hat{S}^x_{n+1} + \hat{S}^y_n \hat{S}^y_{n+1} \right) + \lambda \sum_{n=1}^{L-2} J'_{xy} \left(\hat{S}^x_n \hat{S}^x_{n+2} + \hat{S}^y_n \hat{S}^y_{n+2} \right). \tag{33}$$

• The structure factor in the x is the same as Eq. (31), substituting z with x.

• The local spin current, $\hat{I}_{s,n}$, is associated with the conservation of total spin in the z direction and obeys the continuity equation,

$$\frac{\partial \hat{S}^z_n}{\partial t} + div(\hat{I}_{s,n}) = 0.$$

In the bulk,

$$-i[\hat{H}, \hat{S}^z_n] = div(\hat{I}_{s,n}) = (\hat{I}_{s,n} - \hat{I}_{s,n-1}),$$

but in the extremes, since the chain is open, we have

$$-i[\hat{H}, \hat{S}^z_1] = div(\hat{I}_{s,1}) = \hat{I}_{s,1}$$

and

$$-i[\hat{H}, \hat{S}^z_L] = div(\hat{I}_{s,L}) = -\hat{I}_{s,L-1}.$$

From the equations above, we find that the local spin current for a system with NN couplings only, with or without impurity, is given by

$$\hat{I}^{(1)}_{s,n} = J(\hat{S}^x_n \hat{S}^y_{n+1} - \hat{S}^y_n \hat{S}^x_{n+1}), \tag{34}$$

where $1 \leq n \leq L-1$.

In the case of the model with NN and NNN couplings, the local spin current becomes

$$\begin{aligned} \hat{I}^{(2)}_{s,n} &= J(\hat{S}^x_n \hat{S}^y_{n+1} - \hat{S}^y_n \hat{S}^x_{n+1}) \\ &+ \lambda J(\hat{S}^x_n \hat{S}^y_{n+2} - \hat{S}^y_n \hat{S}^x_{n+2} + \hat{S}^x_{n-1} \hat{S}^y_{n+1} - \hat{S}^y_{n-1} \hat{S}^x_{n+1}), \end{aligned} \tag{35}$$

for $2 \leq n \leq L-2$, and at the borders,

$$\hat{I}^{(2)}_{s,1} = J(\hat{S}^x_1 \hat{S}^y_2 - \hat{S}^y_1 \hat{S}^x_2) + \lambda J(\hat{S}^x_1 \hat{S}^y_3 - \hat{S}^y_1 \hat{S}^x_3),$$
$$\hat{I}^{(2)}_{s,L-1} = J(\hat{S}^x_{L-1} \hat{S}^y_L - \hat{S}^y_{L-1} \hat{S}^x_L) + \alpha J(\hat{S}^x_{L-2} \hat{S}^y_L - \hat{S}^y_{L-2} \hat{S}^x_L).$$

Equations (32) and (34) imply that for the XXZ chain a nonzero current gives rise to a static spin configuration where the spins rotate in the XY plane from one site to the next at a rate which increases with the magnitude of the current. However, as is apparent in Eq. (35), this simple relation between the NN spin correlations and the current is lost for NNN couplings.

%%

↪ *EXERCISE 13:* Write a code that computes the eigenstates expectation values of all observables discussed in this section and for all eigenstates $|\psi_\alpha\rangle$ for the spin-1/2 model with NNN couplings. Use $\Delta = 0.48$, $\lambda = 0.44$, $\varepsilon = 0.1$, $L = 18$, 6 up spins.

The *Fortran* code called 'Fortran_Exercise16' can be used for EXERCISES 13, 14, 15, 16.

%%

VII. THERMALIZATION

After an isolated system is taken out of equilibrium it may again equilibrate, but in a probabilistic sense. Equilibration occurs if after a transient time the system remains very close to a steady state for most time and the fluctuations around it decreases with system size. A question that has become very popular recently is whether this new equilibrium can or not be described by a thermodynamic ensemble. If it can, we say that the system thermalized. Thermalization is the subject of this section.

A. Quench Dynamics

We assume that the system starts in an excited eigenstate, $|\Psi(0)\rangle = |\text{ini}\rangle$, of an initial Hamiltonian $\hat{H}_I$, not necessarily a ground state. After an instantaneous perturbation, the state evolves as

$$|\Psi(t)\rangle = e^{-i\hat{H}_{\text{F}}t}|\text{ini}\rangle = \sum_\alpha C_\alpha^{\text{ini}} e^{-iE_\alpha t}|\psi_\alpha\rangle. \tag{36}$$

We use the notation, where E_α and $|\psi_\alpha\rangle$ are the eigenvalues and eigenstates of the final Hamiltonian $\hat{H}_F$, $C_\alpha^{\text{ini}} = \langle\psi_\alpha|\text{ini}\rangle$, and $\mathcal{E}_n$ and $|n\rangle$ are the eigenvalues and eigenstates of the initial Hamiltonian. The subscripts 'I' and 'F' are used for the Hamiltonians and also for their parameters before and after the quench, respectively.

The energy of $|\text{ini}\rangle$ projected on the final Hamiltonian is

$$E_{\text{ini}} = \langle\text{ini}|\hat{H}_F|\text{ini}\rangle = \sum_{\alpha,\beta}\langle\text{ini}|\psi_\alpha\rangle\langle\psi_\alpha|\hat{H}_F|\psi_\beta\rangle\langle\psi_\beta|\text{ini}\rangle = \sum_\alpha |C_\alpha^{\text{ini}}|^2 E_\alpha. \tag{37}$$

Often, the eigenstate of $\hat{H}_I$ that we select to be the initial state is the one for which E_{ini} is closest to the energy

$$E_T = \frac{\sum_\alpha E_\alpha e^{-E_\alpha/k_B T}}{\sum_\alpha e^{-E_\alpha/k_B T}}, \tag{38}$$

fixed by a chosen temperature T. Above, k_B is Boltzmann constant and it is set to 1. This procedure allows for a fair comparison of systems of different sizes and under different parameters.

The energy uncertainty of the initial state is given by

$$\begin{aligned}\sigma_{\text{ini}} &= \sqrt{\langle\text{ini}|\hat{H}_F^2|\text{ini}\rangle - \langle\text{ini}|\hat{H}_F|\text{ini}\rangle^2}\\ &= \sqrt{\sum_{\alpha,\beta}\langle\text{ini}|\psi_\alpha\rangle\langle\psi_\alpha|\hat{H}_F^2|\psi_\beta\rangle\langle\psi_\beta|\text{ini}\rangle - \langle\text{ini}|\hat{H}_F|\text{ini}\rangle^2} = \sqrt{\sum_\alpha |C_\alpha^{\text{ini}}|^2(E_\alpha - E_{\text{ini}})^2}\\ &= \sqrt{\sum_n\langle\text{ini}|\hat{H}_F|n\rangle\langle n|\hat{H}_F|\text{ini}\rangle - \langle\text{ini}|\hat{H}_F|\text{ini}\rangle^2} = \sqrt{\sum_{n\neq\text{ini}} |\langle n|\hat{H}_F|\text{ini}\rangle|^2}.\end{aligned} \tag{39}$$

Notice from the equations above that E_{ini} and σ_{ini} can be obtained *before* the diagonalization of the final Hamiltonian. We only need to write $\hat{H}_{\text{F}}$ in the basis corresponding to the eigenstates of $\hat{H}_{\text{I}}$ and then extract the diagonal element for E_{ini} and sum the square of the off-diagonal elements of the same row to get σ_{ini}. If the initial state is a site-basis vector, this procedure is straightforward, but if it is an eigenstate of the XXZ model, for example, we still need to diagonalize the initial Hamiltonian to get the basis vectors.

We will consider below two kinds of quenches, starting from the XXZ model. In both cases, one defect is placed on the first site with amplitude $\varepsilon = 0.1$ to avoid symmetries.

- Local quench. The perturbation is localized on a single site: $d_{\text{I}} = 0 \to d_{\text{F}} \neq 0$. $\hat{H}_I$ is quenched to the chaotic impurity model with NN couplings only,

$$\hat{H}_F^{\text{local}} = \hat{H}_I + d_F J \hat{S}^z_{\lfloor L/2 \rfloor}.$$

- Global quench. The perturbation affects simultaneously all sites in the chain: $\lambda_{\text{I}} = 0 \to \lambda_{\text{F}} \neq 0$. $\hat{H}_I$ is quenched to the chaotic Hamiltonian with NNN couplings,

$$\hat{H}_F^{\text{global}} = \hat{H}_I + \lambda_F \hat{H}_{\text{NNN}}.$$

%%%

$\hookrightarrow$ *EXERCISE 14:* Write a code for both quenches above and select as initial state the eigenstate of the XXZ model with energy E_{ini} equivalent to temperature T=7.

Get an output file for E_α's and C_α's for $\Delta = 0.48$, $\lambda = 0.44$, $\varepsilon = 0.1$, $L = 18$, 6 up spins.

The *Fortran* code called 'Fortran_Exercise16' can be used for EXERCISES 13, 14, 15, 16.

%%%

B. Eigenstate Thermalization Hypothesis

The dynamics of the expectation value of an observable $\hat{O}$ is computed as

$$\langle \hat{O}(t) \rangle = \langle \Psi(t) | \hat{O} | \Psi(t) \rangle = \sum_{\alpha} |C_{\alpha}^{\text{ini}}|^2 O_{\alpha\alpha} + \sum_{\alpha \neq \beta} C_{\alpha}^{\text{ini}*} C_{\beta}^{\text{ini}} e^{i(E_{\alpha}-E_{\beta})t} O_{\alpha\beta} \ , \tag{40}$$

where $O_{\alpha\beta} = \langle \psi_{\alpha} | \hat{O} | \psi_{\beta} \rangle$ corresponds to the matrix elements of $\hat{O}$ in the energy eigenbasis. In the absence of too many degeneracies, $E_{\alpha} \neq E_{\beta}$ for most states, the off-diagonal elements of $\langle \hat{O}(t) \rangle$ oscillate very fast and cancel out on average, so the infinite time average is given by

$$\overline{O} = \lim_{t \to \infty} \frac{1}{t} \int_0^t d\tau \, \langle \hat{O}(\tau) \rangle = \sum_{\alpha} |C_{\alpha}^{\text{ini}}|^2 O_{\alpha\alpha} \equiv \langle \hat{O} \rangle_{\text{DE}}. \tag{41}$$

Since the steady state average depends only on the diagonal elements of $\hat{O}$, it is commonly referred to as the prediction from the diagonal ensemble (DE).

We can talk about thermalization if the infinite time average of the observables coincide with the thermal (microcanonical) average,

$$O_{\text{ME}} \equiv \frac{1}{\mathcal{N}_{E^{\text{ini}},\delta E}} \sum_{\substack{\alpha \\ |E^{\text{ini}}-E_{\alpha}|<\delta E}} O_{\alpha\alpha}, \tag{42}$$

where $\mathcal{N}_{E^{\text{ini}},\delta E}$ stands for the number of energy eigenstates in the window δE. Actually, coincidence of the two averages can only happen in the thermodynamic limit ($L \to \infty$). In our finite systems, they can only be close. Thus, a condition for thermalization is the proximity of the averages for finite L and their approach as the system size increases.

Obviously, the two averages would be very close if the eigenstate expectation values of the observables, $O_{\alpha\alpha} = \langle \psi_{\alpha} | \hat{O} | \psi_{\alpha} \rangle$, were very close for all eigenstates. Could we have such a scenario? Well, what happens to observables is a reflection of what happens to the eigenstates. The condition above is certainly satisfied when we deal with full random matrices. Since the eigenstates are just random vectors, computing $O_{\alpha\alpha}$ with one eigenstate or another gives very similar results, so $O_{\alpha\alpha}$ can be taken out of the sums. But, as mentioned before, full random matrices do not describe realistic systems, so we need to see what happens to the eigenstates and the eigenstate expectation value of observables in realistic system with few-body interactions.

In real systems, if the values of the observables, $O_{\alpha\alpha}$, do not vary much for eigenstates close in energy inside the microcanonical window, that is they are a smooth function of energy, the result from a single eigenstate agrees with the microcanonical average. Now let us analyze the infinite time average. If the eigenstates $|\psi_{\alpha}\rangle$ contributing the most for the initial state (largest values of $|C_{\alpha}^{\text{ini}}|^2$) are very delocalized and have very similar structure, their $O_{\alpha\alpha}$ will be very similar, so $\sum_{\alpha} |C_{\alpha}^{\text{ini}}|^2 O_{\alpha\alpha} \sim O_{\alpha'\alpha'} \sum_{\alpha} |C_{\alpha}^{\text{ini}}|^2$. This approach, where a single eigenstate can give the value of the average, became known as eigenstate thermalization hypothesis (ETH) [35–37]. It now remains to determine when this condition can be satisfied.

In Fig. 7 of EXERCISE 10, we saw that the values of IPR for the eigenstates of systems with two-body interactions follow a Bell shape, reflecting the Gaussian density of states. For these systems, if the initial state has energy E_{ini} close to the middle of the spectrum, the eigenstates within σ_{ini}, which are the ones leading to the largest values of $|C_{\alpha}^{\text{ini}}|^2$ are very delocalized [31, 38–40]. In particular, when $\hat{H}_F$ is chaotic, the values of IPR_{α} become smooth functions of energy, as seen in Fig. 11 (a) and (c) [and also in Fig. 7 from EXERCISE 10]. This is to be contrasted with the integrable XXZ model, where large fluctuations prevail [Fig. 11 (e)]. The edges of the spectrum, where the eigenstates are more localized, are also problematic, even for chaotic systems. Thus, we anticipate the viability of thermalization in chaotic systems for initial states with E_{ini} away from the edges of the spectrum. Let us now compare this prediction with our numerical results.

The similar structures of the eigenstates in the chaotic domain lead to small fluctuations of $\langle \psi_{\alpha} | \hat{O} | \psi_{\alpha} \rangle$. This is illustrated in Fig. 11 (b) and (d) for the spin-spin correlation in the z direction. We see that for the parameters used, where the structures of $\hat{H}_F^{\text{local}}$ and $\hat{H}_F^{\text{global}}$ are similar (cf. Fig. 9), the sizes of the fluctuations for both models are also comparable. In contrast, for the integrable model, the fluctuations are much larger [Fig. 11 (f)].

But more important than snapshots, we need to see what happens as we increase the system size. In Figs. 12, we analyze the dependence on system size of the fluctuations of the eigenstate expectation values of the structure factor in the z direction. On the right panels we show the results for the extremal of the fluctuations,

$$\Theta S^{zz} \equiv \left| \frac{\max S^{zz} - \min S^{zz}}{S_{\text{ME}}^{zz}} \right| \tag{43}$$

for three system sizes. Above $\max S^{zz}$ ($\min S^{zz}$) stands for the maximum (minimum) value of $\langle \psi_{\alpha} | \hat{S}^{zz} | \psi_{\alpha} \rangle$ obtained in the energy window used to calculate S_{ME}^{zz}. This quantity is more appropriate to test ETH than the standard deviation, which can

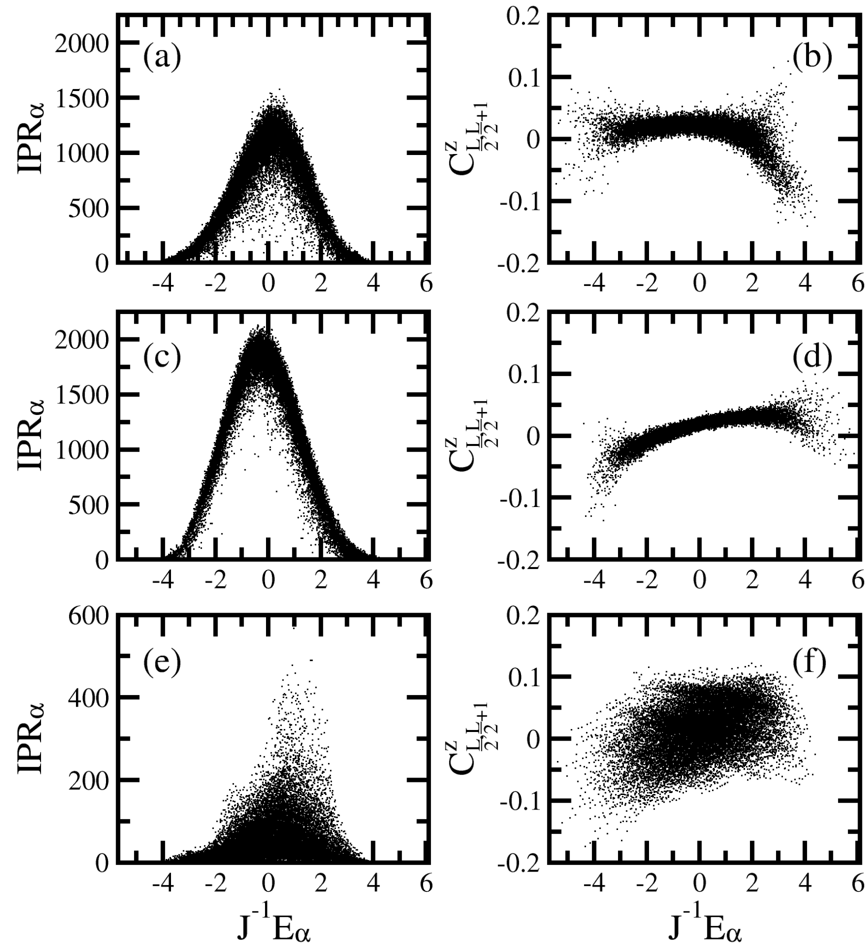

FIG. 11: (Color online) Inverse participation ratio (left) and expectation values of the spin-spin correlation (right) vs E_α for all the eigenstates of the Hamiltonians with $\Delta = 0.48$ and $d_F = 0.9$ (a,b); $\lambda_F = 0.44$ (c,d); and $d_F = \lambda_F = 0$ (e,f). The basis corresponds to the eigenstates of the XXZ model with $\Delta = 0.48$ (a,c) and the eigenstates of the XX model (e). For all cases: $\varepsilon = 0.1$ and $L = 18$.

decrease with L simply because the number of states increases exponentially with L [39]. The values of ΘS^{zz} for the impurity and NNN models are comparable and, away from the edges of the spectrum, they clearly decrease with L. At the edges of the spectrum, where the eigenstates are not much delocalized, it is not clear whether the fluctuations decrease with L. For the XXZ system, ΘS^{zz} is significantly larger and does not seem to decrease with L.

%%
↪ *EXERCISE 15:* Reproduce Figs. 11 and 12.
The *Fortran* code called 'Fortran_Exercise16' can be used for EXERCISES 13, 14, 15, 16.
%%

Above we found indications that thermalization should be possible in the chaotic domain and away from the edges of the spectrum. We now proceed to actually compare the infinite time average and the microcanonical average for different systems sizes and different $E_{\rm ini}$.

Figures 13 and 14 compare the results for the infinite time averages and the microcanonical prediction. We compute the relative difference,

$$\Lambda S^{zz} = \frac{|S^{zz}_{\rm DE} - S^{zz}_{\rm ME}|}{|S^{zz}_{\rm DE}|}, \tag{44}$$

for the structure factor and also the absolute difference,

$$\Lambda_a C^{zz} = \left|C^{zz}_{\rm DE} - C^{zz}_{\rm ME}\right|, \tag{45}$$

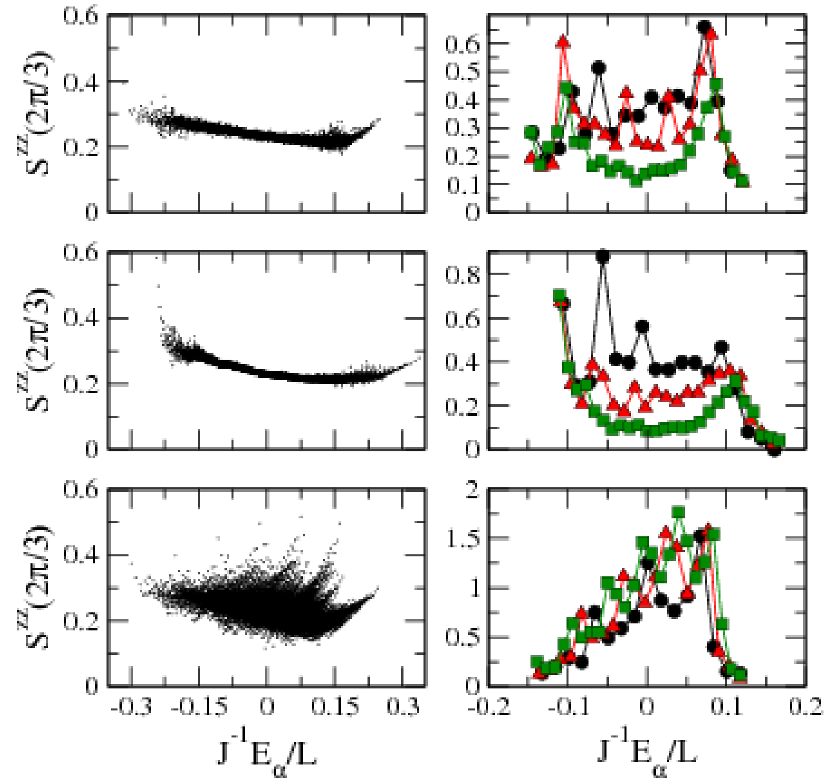

FIG. 12: (Color online) Eigenstate expectation values for $\hat{S}^{zz}(2\pi/3)$ (left) and extremal fluctuations, ΘS^{zz} [Eq. (43)] in windows of energy $[E, E+0.4]$ (right). Final Hamiltonians: impurity (a,b), NNN couplings (c,d), XXZ (e,f). Initial Hamiltonians: XXZ (a,c) and XX (e). $\Delta = 0.48$, $\varepsilon = 0.1$, $d_F = 0.9$, $\lambda_F = 0.44$. Left panels: $L = 18$, $N_{up} = 6$. Right panels: $L = 12$ (circles); $L = 15$ (triangles); $L = 18$ (squares).

for the spin-spin correlation in the z direction for sites in the middle of the chain. We do not compute the ratio for the spin-spin correlation, because the more chaotic the system is the closer to zero C^{zz} becomes.

Figure 13 shows ΛS^{zz} and $\Lambda_a C^{zz}$ for different values of the perturbations for the quenches to the impurity (a,c) and NNN (b,d) Hamiltonians. The relative differences are of similar magnitude for both models and clearly decrease with L.

Figure 14 shows ΛS^{zz} and and $\Lambda_a C^{zz}$ for different values of temperature for quenches to the impurity (a,c) and NNN (b,d) Hamiltonians. In both cases, the agreement between the averages improve as the temperature increases and the energy of $|\text{ini}\rangle$ approaches the middle of the spectrum. The improvement with system size is also evident. The results reinforce the equivalence between the two models for the chosen values of d_F and λ_F. They also corroborate the dependence on the energy of the initial state in the studies of thermalization [41, 42].

%%
$\hookrightarrow$ *EXERCISE 16:* Write a code to select an eigenstate of an initial Hamiltonian according to a chosen temperature [Eq. (38)]. Compute the infinite time averages and the microcanonical averages of the spin-spin correlation and the structure factor. Use your code to reproduce Figs. 13 and 14.

The *Fortran* code called 'Fortran_Exercise16' can be used for EXERCISES 13, 14, 15, 16.
%%

In Ref. [42], we also studied quenches to integrable models, starting from integrable or chaotic models. As the energy of the initial state approached the middle of the spectrum, we saw indications that the infinite time average indeed approaches the microcanonical ensemble. If the initial state is sufficiently close to the middle of the spectrum(where T is infinite), we do see thermal features even when the final Hamiltonian is integrable. The system in this case is already thermalized before the quench, the initial state sampling over most states of the final Hamiltonian, independently of their conserved quantities. What is still not clear is how close to the middle of the spectrum one needs to be to see such thermal features in integrable systems. An open question is also how far from the edges (of gapless systems) we need to be for thermalization to hold in chaotic models.

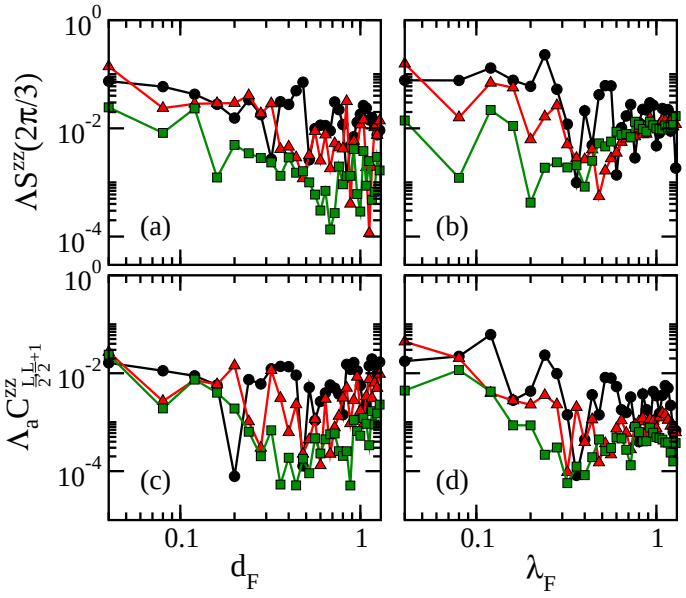

FIG. 13: (Color online) Relative difference for $\hat{S}^{zz}(2\pi/3)$ (a,b) and absolute difference for $C^{zz}_{L/2,L/2+1}$ (c,d) vs d_F (a,c) and λ_F (b,d). Initial state with $T = 7$; $\Delta = 0.48$; $\varepsilon = 0.1$, $L = 12$ (circles); $L = 15$ (triangles); $L = 18$ (squares).

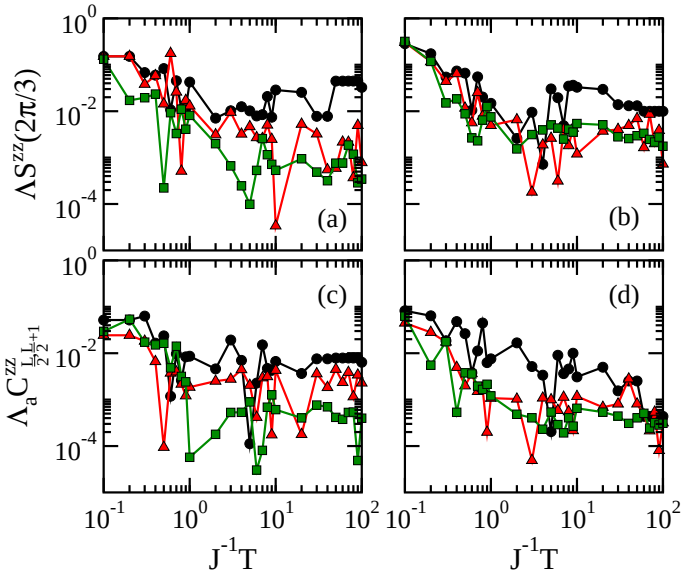

FIG. 14: (Color online) Relative difference for $\hat{S}^{zz}(2\pi/3)$ (a,b) and absolute difference for $C^{zz}_{L/2,L/2+1}$ (c,d) vs temperature; $d_F = 0.9$ (a,c) and $\lambda_F = 0.44$ (b,d); $\Delta = 0.48$; $\varepsilon = 0.1$; $L = 12$ (circles); $L = 15$ (triangles); $L = 18$ (squares).

VIII. DYNAMICS: FIDELITY

So far we have only studied static properties and infinite time averages. We now proceed to the analysis of the actual relaxation process of our isolated systems. As it shall be clear, the relaxation can be very similar for integrable and chaotic models. It does not depend on the regime (integrable or chaotic) of the final Hamiltonian, but on the interplay between the initial state and the final Hamiltonian.

Before studying the evolution of the observables that we discussed before, let us start by analyzing how fast our initial state changes in time after the quench. For that, we will compute the overlap between $|\text{ini}\rangle$ and its corresponding evolved state,

$$F(t) = |\langle \text{ini}|\Psi(t)\rangle|^2 = \left|\langle \text{ini}|e^{-i\hat{H}_F t}|\text{ini}\rangle\right|^2 = \left|\sum_\alpha |C^{\text{ini}}_\alpha|^2 e^{-iE_\alpha t}\right|^2 . \quad (46)$$

This quantity is known as fidelity. Fidelity is the overlap between any two states, it measures how close they are. The fidelity between two evolved states $|\langle\Phi(t)|\Psi(t)\rangle|^2$, where $\Phi(t)$ and $\Psi(t)$ evolve according to slightly different Hamiltonians, is also known as Loschmidt echo and is often studied in NMR experiments, for example. Here, the quantity we refer to as fidelity coincide with the so-called survival probability, non-decay probability, or return probability. It measures the probability for finding the initial state later in time, that is it quantifies the level of stability of the quantum system. From the equation above, one sees that the fidelity is simply the Fourier transform in energy of the components $|C_\alpha^{\text{ini}}|^2$.

The distribution of $|C_\alpha^{\text{ini}}|^2$ in the eigenvalues E_α,

$$P^{\text{ini}}(E) = \sum_\alpha |C_\alpha^{\text{ini}}|^2 \delta(E - E_\alpha) \tag{47}$$

is commonly referred to as local density of states (LDOS) or strength function. When $\mathcal{D}$ is large and the density of states is dense, the sum in Eq. (46) can be substituted by an integral,

$$F(t) \approx \left| \int_{-\infty}^{\infty} P^{\text{ini}}(E) e^{-iEt} dE \right|^2, \tag{48}$$

where $P^{\text{ini}}(E)$ is now the envelope of the LDOS of the initial state. In spectroscopy, $P^{\text{ini}}(E)$ is the spectral line shape and its characteristic function is the time-domain signal.

A. Exponential decay

Very often, the observed fidelity behavior for unstable systems, such as unstable nuclei, is exponential. This implies a Lorentzian (also called Breit-Wigner or Cauchy) LDOS,

$$P_{\text{L}}^{\text{ini}}(E) = \frac{1}{2\pi} \frac{\Gamma_{\text{ini}}}{(E_{\text{ini}} - E)^2 + \Gamma_{\text{ini}}^2/4},$$

$$\Rightarrow F_{\text{L}}(t) = \exp(-\Gamma_{\text{ini}} t), \tag{49}$$

where Γ_{ini} is the full width at half maximum of the distribution. To show that the Fourier transform of the Lorentzian gives the exponential, we solve the integral with residues. Since $E > 0$, we close the contour clockwise in the lower plane adding a negative sign:

$$\int_\infty^\infty \frac{1}{2\pi} \frac{\Gamma_{\text{ini}}}{(E_{\text{ini}} - E)^2 + \Gamma_{\text{ini}}^2/4} e^{-iEt} dE = \frac{\Gamma_{\text{ini}}}{2\pi} \int_\infty^\infty \frac{e^{-iEt}}{[(E_{\text{ini}} - E) + i\Gamma_{\text{ini}}/2][(E_{\text{ini}} - E) - i\Gamma_{\text{ini}}/2]} dE$$
$$= \frac{\Gamma_{\text{ini}}}{2\pi} \oint \frac{\frac{e^{-iEt}}{(E_{\text{ini}} - E) - i\Gamma_{\text{ini}}/2}}{(E_{\text{ini}} - E) + i\Gamma_{\text{ini}}/2]} = \frac{\Gamma_{\text{ini}}}{2\pi} (-2\pi i) \frac{e^{-i(-i\Gamma_{\text{ini}}/2)t}}{-i\Gamma_{\text{ini}}} = \exp(-\Gamma_{\text{ini}} t/2)$$

The Lorentzian and exponential decay can be derived with the Fermi golden rule, valid when the strength g of the perturbation $\hat{V}$ to the initial Hamiltonian, leading to $\hat{H}_F = \hat{H}_I + g\hat{V}$, is not very strong. However, deviations from the exponential behavior do exist. They occur when:

(i) The perturbation is indeed very strong;

(ii) At short times;

(iii) At long times.

Case (i) will be our focus. Case (ii) is trivial to see. Independently of $P^{\text{ini}}(E)$, at very short times, the Taylor expansion of $e^{-iE_\alpha t}$ in Eq. (46) leads to

$$F(t) \approx \left| e^{-iE_{\text{ini}} t} \left[\sum_\alpha |C_\alpha^{\text{ini}}|^2 - i \sum_\alpha |C_\alpha^{\text{ini}}|^2 (E_\alpha - E_{\text{ini}}) t - \frac{1}{2} \sum_\alpha |C_\alpha^{\text{ini}}|^2 (E_\alpha - E_{\text{ini}})^2 t^2 \right] \right|^2 = 1 - \sigma_{\text{ini}}^2 t^2. \tag{50}$$

The decay at $t \to 0$ is therefore necessarily quadratic in time. Clearly, the short-time behavior shown in Eq. (50) cannot be achieved by expanding the exponential expression in Eq. (49). As matter of fact, σ_{ini} is infinite for the Lorentzian function, which forces the energy-time uncertainty relation in systems with exponential fidelity decays to be written in terms of Γ_{ini} instead of σ_{ini} [43]. Case (iii) is a consequence of the existence of a lower bound of the spectrum, even in open systems, where the spectrum is continuous. The cutoff in energy, prevents an exponential result for the Fourier transform $|\int_{E_{\text{min}}}^\infty P^{\text{ini}}(E) e^{-iEt} dE|^2 \Rightarrow \exp(-ct^q)$ with $q < 1$ [44–46].

B. Gaussian decay

In the limit of strong perturbation, the LDOS for isolated systems with two-body interactions becomes Gaussian [12, 42, 47–57], causing the Gaussian fidelity decay,

$$P_{\rm G}^{\rm ini}(E) = \frac{1}{\sqrt{2\pi\sigma_{\rm ini}^2}} \exp\left[-\frac{(E-E_{\rm ini})^2}{2\sigma_{\rm ini}^2}\right],$$

$$\Rightarrow F_{\rm G}(t) = \exp(-\sigma_{\rm ini}^2 t^2), \tag{51}$$

which agrees with Eq. (50) at short times. We have seen several cases, some accessible to experiments in optical lattices, in which the Gaussian behavior of $F(t)$ can hold all the way to saturation [40, 58–60].

To show that the Fourier transform of the Gaussian is Gaussian, we need to complete square:

$$\begin{aligned}
&\int_{-\infty}^{\infty} \frac{1}{\sqrt{2\pi\sigma_{\rm ini}^2}} \exp\left[-\frac{(E-E_{\rm ini})^2}{2\sigma_{\rm ini}^2}\right] e^{-iEt} dE \\
&= \frac{1}{\sqrt{2\pi\sigma_{\rm ini}^2}} \int_{-\infty}^{\infty} \exp\left\{-\frac{1}{2\sigma_{\rm ini}^2}\left[E^2 - 2E(E_{\rm ini} - it\sigma_{\rm ini}^2) + (E_{\rm ini} - it\sigma_{\rm ini}^2)^2\right] + itE_{\rm ini} - t^2\sigma_{\rm ini}^2/2\right\} dE \\
&= \frac{e^{itE_{\rm ini}} e^{-t^2\sigma_{\rm ini}^2/2}}{\sqrt{2\pi\sigma_{\rm ini}^2}} \int_{-\infty}^{\infty} \exp\left[-\frac{x^2}{2\sigma_{\rm ini}^2}\right] dx = \exp(itE_{\rm ini}) \exp(-t^2\sigma_{\rm ini}^2/2) \qquad \text{where} \quad x = E - (E_{\rm ini} - it\sigma_{\rm ini}^2)
\end{aligned}$$

The fact that $P^{\rm ini}(E)$ can become Gaussian is a reflection of the density of states of systems with two-body interactions, which is also Gaussian [24, 26] (see Fig 7 in EXERCISE 10). In such systems, the maximum possible spreading of the LDOS is given by the envelope in Eq. (51), which is known as **energy shell**.

C. Saturation point and temporal fluctuations

Saturation happens because our systems are finite. After a dephasing time, the fidelity

$$F(t) = \sum_{\alpha} |C_\alpha^{\rm ini}|^4 + \sum_{\alpha\neq\beta} |C_\alpha^{\rm ini}|^2 |C_\beta^{\rm ini}|^2 e^{i(E_\alpha - E_\beta)t},$$

saturates. In a system without too many degeneracies the off-diagonal terms at $t \to \infty$ average out, leading to the infinite time average,

$$\overline{F} = \sum_{\alpha} |C_\alpha^{\rm ini}|^4 = {\rm IPR}_{\rm ini}^{-1}. \tag{52}$$

$\overline{F}$ depends only on the level of delocalization of the initial state in the energy eigenbasis, as measured by ${\rm IPR}_{\rm ini}$.

The condition of lack of too many degeneracies is obviously satisfied in chaotic systems, where level repulsion is a main feature. It is also satisfied in integrable systems with interaction. It is true that these systems have some degeneracies, as we seen from the Poisson distribution [cf. Fig.6 (c) (d)], but it also has many non-degeneracies. However, this condition is not satisfied in integrable systems without interaction, such as the XX model. It is evident from the high peak obtained in Fig.6 (a) that an enormous amount of degeneracies are present.

The value of $\overline{F}$ is determined by the interplay between the initial state and the final Hamiltonian. There are cases where the saturation point for chaotic systems is smaller than for integrable models, but there are cases where it is even larger, as shown in Sec. VIII H below. The latter happens when $E_{\rm ini}$ is closer to the edge of the spectrum for the chaotic model than for the integrable one. Moreover if the initial state is a completely delocalized state from a GOE ensemble, then for any final Hamiltonian, $\overline{F}$ is the same; $\overline{F} = 3/\mathcal{D}$.

After saturation, the fidelity simply fluctuates around its infinite time average. The variance of the temporal fluctuations is given by

$$\sigma_F^2 = \overline{|F(t) - \overline{F(t)}|^2} = \sum_{\substack{\alpha\neq\beta \\ \gamma\neq\delta}} |C_\alpha^{\rm ini}|^2 |C_\beta^{\rm ini}|^2 |C_\gamma^{\rm ini}|^2 |C_\delta^{\rm ini}|^2 \overline{e^{i(E_\alpha - E_\beta - E_\gamma + E_\delta)t}}. \tag{53}$$

The terms that do not cancel out are those for which $E_\alpha - E_\beta = E_\gamma - E_\delta$. In the absence of too many spacing degeneracies, $E_\alpha - E_\beta = E_\gamma - E_\delta$ implies that $E_\alpha = E_\gamma$ and $E_\beta = E_\delta$. In this case,

$$\sigma_F^2 = \sum_{\alpha\neq\beta} |C_\alpha^{\rm ini}|^4 |C_\beta^{\rm ini}|^4 = \sum_\alpha |C_\alpha^{\rm ini}|^4 \sum_\beta |C_\beta^{\rm ini}|^4 - \sum_\alpha |C_\alpha^{\rm ini}|^8 = {\rm IPR}_{\rm ini}^{-2} - \sum_\alpha |C_\alpha^{\rm ini}|^8 \sim {\rm IPR}_{\rm ini}^{-2}, \tag{54}$$

We verified numerically that in systems without too many degeneracies, not too many spacing degeneracies are found. One may in fact be a consequence of the other.

Thus, the fluctuations also depend only on the interplay between the initial state and the final Hamiltonian. Since the dimension of the Hamiltonians grows exponentially with systems size, we expect ${\rm IPR}_{\rm ini}$ to grow exponentially with L. This means that the fluctuations after relaxation in systems *with* interaction, be they integrable or chaotic, should decrease exponentially with L; $\sigma_F \propto \exp(-\kappa L)$. The value of the exponent κ depends on ${\rm IPR}_{\rm ini}$ and it should decrease as the energy of the initial state moves away from the middle of the spectrum. Right at the edges, even in gapless systems, it is not clear whether we can still have an exponential growth of the participation of energy eigenbasis.

The scenario is similar for few-body observables, although for them only an upper bound for the temporal fluctuations has been obtained. The variance of the temporal fluctuations of the observable about its equilibrium value corresponds to

$$\sigma_O^2 = \overline{|\langle O(t)\rangle - \overline{\langle O(t)\rangle}|^2} = \sum_{\substack{\alpha\neq\beta\\ \gamma\neq\delta}} C_\alpha^{*\rm ini} C_\beta^{\rm ini} C_\gamma^{*\rm ini} C_\delta^{\rm ini} O_{\alpha\beta} O^\dagger_{\gamma\delta} \overline{e^{i(E_\alpha - E_\beta + E_\gamma - E_\delta)t}} \tag{55}$$

Under the condition of few degenerate spacings, it has been shown that [61, 62]

$$\sigma_O^2 \leq \frac{(O_{\rm max} - O_{\rm min})^2}{{\rm IPR}^{\rm ini}}, \tag{56}$$

where $O_{\rm max(min)}$ is the maximum (minimum) eigenvalue of the operator $\hat{O}$.

In Ref. [28], our numerical results confirm that the exponential decay with L of the time fluctuations of few-body observables after relaxation prevails in systems without excessive degeneracies, be them integrable or chaotic. The coefficient of this decay depends on the level of delocalization of the initial state with respect to the Hamiltonian dictating its evolution.

D. Time to reach the fidelity infinite time average

In what follows, we denote by t_R the time that it takes for the fidelity to first reach $\overline{F}$. When the LDOS is dense and unimodal, the difference between the dephasing time and t_R is small, but when $P^{\rm ini}(E)$ is bimodal, for example, relatively large oscillations can survive for a fairly long time after t_R.

E. Gaussian fidelity decay up to saturation

Typically, for an initial state with $E_{\rm ini}$ close to the middle of the spectrum, as the perturbation increases from zero, the LDOS broadens from a delta function to a Lorentzian shape first, and then it eventually approaches a Gaussian form. The broadening of the LDOS with Δ for a quench from the XX to the XXZ model and with λ for a quench from the XXZ to the NNN model is shown in Fig. 15. For both cases, the distribution is delta-like for a small perturbation, $\Delta = \lambda = 0.2$ (top panels). As the perturbation increases to $\Delta = \lambda = 0.4$ (middle panels), the distribution becomes close to a Lorentzian. Finally, in the limit of strong perturbation, $\Delta = 1.5$ and $\lambda = 1$ (bottom panels), the LDOS becomes Gaussian and approaches the energy shell. Notice that the broadening of LDOS with the perturbation happens in a very similar fashion for both chaotic and also integrable $\hat{H}_F$. The energy shell can also be substantially filled for both regimes provided $E_{\rm ini}$ be close to the middle of the spectrum.

The corresponding fidelity behavior for the LDOS of Fig. 15 are shown in Fig 16. Again, similar results are seen for the quench into the integrable domain and for the quench in the chaotic regime. The associated fidelity decay is independent of the regime of $\hat{H}_F$. When the perturbation is small, $\Delta = \lambda = 0.2$ (top panels), the decay is very slow. At an intermediate value, $\Delta = \lambda = 0.4$ (middle panels), the fidelity decays exponentially (after the short-time quadratic behavior) for both quenches. At strong perturbation (bottom panels), the fidelity behavior is Gaussian. When the initial state fills the energy shell substantially, as in the bottom panels of Fig. 15, the Gaussian decay can persist until saturation, as in the bottom panels of Fig. 16. The saturation point is indicated with the horizontal dashed line.

When the Gaussian behavior holds all the way saturation, the time t_R for $F(t)$ to first reach $\overline{F}$ depends only on the level of delocalization of the initial state and on the width of the energy shell,

$$\exp(-\sigma_{\rm ni}^2 t_R^2) = \overline{F} = {\rm IPR}_{\rm ini}^{-1} \Rightarrow t_R = \frac{\sqrt{\ln({\rm IPR}_{\rm ini})}}{\sigma_{\rm ini}}. \tag{57}$$

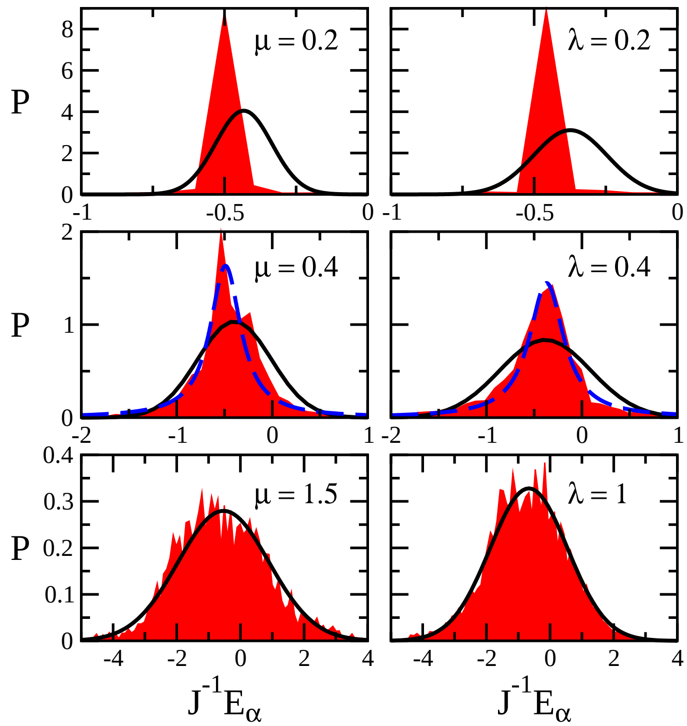

FIG. 15: (Color online) Local density of states. The initial state is an eigenstate of the XX Hamiltonian projected onto the XXZ with $\Delta = 0.2,\ 0.4,\ 1.5$ (left column). The initial state is an eigenstate of the XXZ, $\Delta = 0.5$ projected onto the NNN model with $\lambda = 0.2,\ 0.5,\ 1$ (right column). Numerical distribution: red shaded area; energy shell: black solid curve. The blue dashed curve in the middle panels corresponds to a Lorentzian fitting. The initial states are away from the edge of the spectrum. They are selected for the $E_{\rm ini}$ closest to E_T with $T = 4.4$. Top panels: $E_{\rm ini} = -0.43$, $\sigma_{\rm ini} = 0.10$ (left), $E_{\rm ini} = -0.37$, $\sigma_{\rm ini} = 0.14$ (right). Middle panels: $E_{\rm ini} = -0.39$, $\sigma_{\rm ini} = 0.39$, $\Gamma_{\rm ini} = 0.39$ (left), $E_{\rm ini} = -0.38$, $\sigma_{\rm ini} = 0.48$, $\Gamma_{\rm ini} = 0.44$ (right). $\hat{S}^z_{tot} = -3$, $L = 18$, $D = 18\,564$, $\varepsilon_1 = 0$.

This expression determines the lower bound for the fidelity decay in realistic systems with two-body interactions and unimodal LDOS.

Some remarks:

(i) In the transition region between the Lorentzian and the Gaussian, the LDOS is a convolution of the two, well described by the Voigt distribution, often used in spectroscopy when homogeneous (Lorentzian) and inhomogeneous (Gaussian) broadening exist. In this case, the fidelity decay is Gaussian for some time and then switches to exponential.

(ii) In the limit of strong perturbation, as the energy of the initial state moves away from the center of the spectrum, the Gaussian shape of the LDOS becomes skewed and the rate of the fidelity decay slows down. Close to the edge, where the density of states is small, the fidelity behavior is very slow.

%%

$\hookrightarrow$ *EXERCISE 17:* Reproduce Figs. 15 and 16.

VERY IMPORTANT EXERCISE!

Fortran **code is provided.**

To evolve a state using exact diagonalization, we simply need to write the state in terms of the eigenstates of the final Hamiltonian. In *Fortran*, this can be done as follows

```
! Project the initial state 'INI' on the eigenstates 'VecF' of the final Hamiltonian. This will give the amplitudes 'Calpha'
        call DGEMV('t',dd,dd,1.0d0,VecF,dd,INI,1,0.0d0,Calpha,1)        ! dd is the dimension of the Hamiltonian

! Evolve the vector 'Calpha' with the eigenvalues 'EigF' of the final Hamiltonian. Separate the cosine and sine parts.
        DO tt=tinitial,tfinal        ! tinitial = 0, tfinal = a large integer
           time=dble(itime)*dt        ! dt=0.1d0, dble(x) = dfloat(x)
           auxCos=0.0d0
           auxSin=0.0d0
```

! FIDELITY = $\left|\sum_\alpha |C_\alpha^{\rm ini}|^2 e^{-iE_\alpha t}\right|^2 = \left|\sum_\alpha |C_\alpha^{\rm ini}|^2[\cos(E_\alpha t) - i\sin(E_\alpha t)]\right|^2 = |\text{auxCos} - i\text{auxSin}|^2$

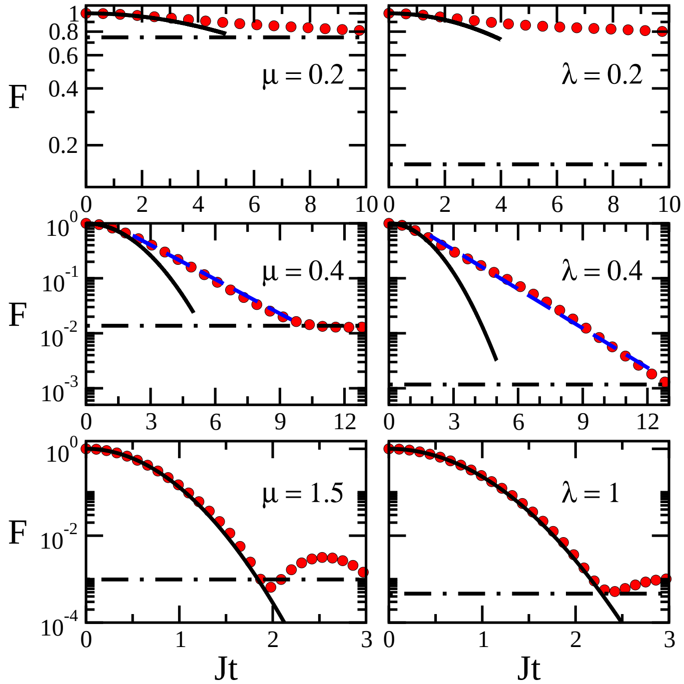

FIG. 16: (Color online) Fidelity decay. Quench XX $\rightarrow$ XXZ (left) and quench XXZ $\rightarrow$ NNN (right). Numerical results: red circles; Gaussian decay: black solid curve; exponential fit in the middle panels: blue dashed line ($\Gamma_{\text{ini}} = -0.48J$ on the left panel and $\Gamma_{\text{ini}} = -0.55J$ on the right panel – not the same values as in Fig. 15); infinite time average of the fidelity: point-dashed horizontal line. Parameters and initial states are the same as in Fig. 15.

```
Do i=1,dimTotal
     auxCos=auxCos+( Calpha(i)**2 )*dcos( time*EigF(i) )
     auxSin=auxSin+( Calpha(i)**2 )*dsin( time*EigF(i) )
Enddo
FIDEL=auxCos**2 + auxSin**2
! Save the values in an output file
ENDDO
%%%%%%%%%%%%%%%%%%%%%%%%%%%%%%%%%%%%%%%%%%%%%%%%%%%%%%%%%%%%%%
```

F. As fast as full random matrices

If the density of states of $\hat{H}_F$ is other than Gaussian, we may find $P^{\text{ini}}(E)$ leading to faster than Gaussian fidelity decays. When $P^{\text{ini}}(E)$ is unimodal, the lower bound for $F(t)$ at long times is achieved when $\hat{H}_F$ is a full random matrix. In this case, the density of states is semicircular, as derived by Wigner [16, 19, 23, 63]. As a result, the LDOS is also semicircular, for an arbitrary initial state [58, 59],

$$P_{\text{SC}}^{\text{ini}}(E) = \frac{1}{\pi\sigma_{\text{ini}}}\sqrt{1-\left(\frac{E}{2\sigma_{\text{ini}}}\right)^2},$$

$$\Rightarrow F_{\text{SC}}(t) = \frac{[\mathcal{J}_1(2\sigma_{\text{ini}}t)]^2}{\sigma_{\text{ini}}^2 t^2}, \qquad (58)$$

where $4\sigma_{\text{ini}}$ is the length of the spectrum and $\mathcal{J}_1$ is the Bessel function of the first kind. Notice that $F_{\text{SC}}(t)$ also agrees with Eq. (50) at short times.

Since full random matrices are not realistic, we studied how to approach it but starting from a spin-1/2 system. Starting with the more realistic XXZ model, we tried to approach a density of states that would resemble the semicircular shape of full random matrices, by gradually adding random couplings between more and more distant pairs of spins and also between more than only two sites. Our Hamiltonian matrix was written in the site-basis, that is product vectors where each site has a spin pointing either

up or down in the z direction. By including only flip-flop terms between distant pairs of spins, $J_{ij}(\hat{S}_i^x\hat{S}_j^x+\hat{S}_i^y\hat{S}_j^y)$ with $j-i\geq 2$ and J_{ij} being random numbers from a Gaussian distribution with variance 1, the shape of the density of states remained Gaussian [Fig. 17 (a)]. We attributed this to sparsity and correlations between the matrix elements. However, the inclusion of hoppings involving four sites and of interactions of the kind $J_{ijk\ldots}\hat{S}_i^z\hat{S}_j^z\hat{S}_k^z\ldots$ did not bring us any closer to a noticeable semicircle. Correlations seemed to be playing a major role.

We then turned our attention back to the XXZ model where only flip-flop terms between any two sites were included, but now substituted the matrix elements corresponding to these couplings with uncorrelated random elements. Quite unexpectedly, because the matrix looked extremely sparse, a density of states very close to semicircular emerged [Fig. 17 (b)]. The justification lies on the basis used. The matrix is sparse in the site-basis, but nearly full in the mean-field basis, that is the basis corresponding to the eigenstates of the regular part (XXZ) of the Hamiltonian. As seen in the plot for the averages of the absolute values of the off-diagonal elements,

$$\overline{H}_{n,n+m}=\frac{\sum_{n=1}^{\mathcal{D}-m}|H_{n,n+m}|}{\mathcal{D}-m}, \qquad \text{[same as Eq.(24)]}$$

versus the distance m from the diagonal [Fig. 17 (c)], the matrix with uncorrelated elements written in the mean-field basis is indeed filled with nonzero elements of similar amplitudes. In contrast, the off-diagonal elements of the Hamiltonian with random flip-flop terms decrease with m. This explains the different shapes of the density of states.

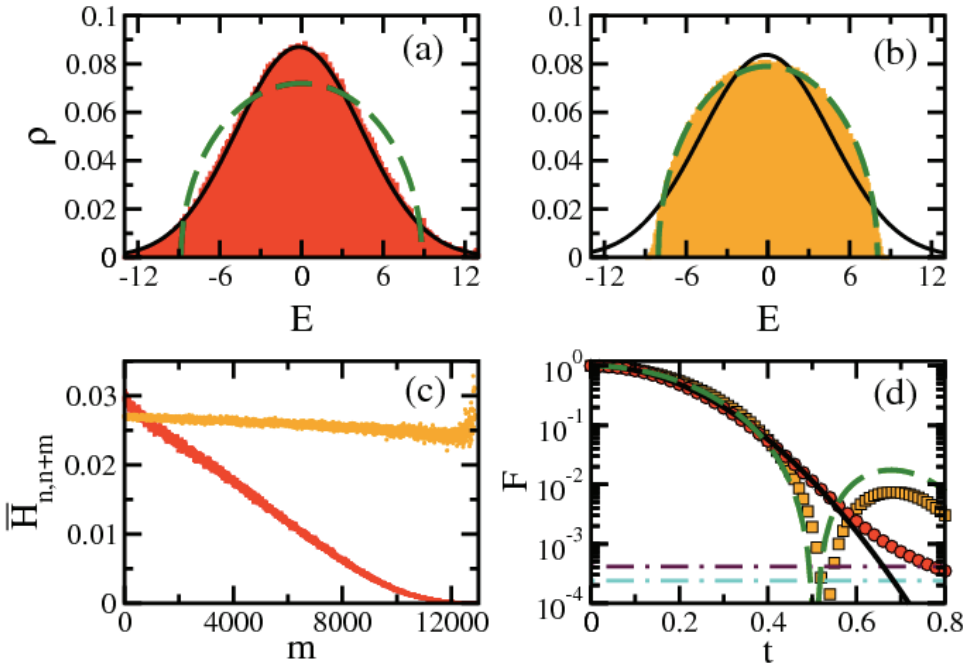

FIG. 17: (Color online) Density of states ρ for the XXZ model with $\Delta_F=0.5$ and added random flip-flop terms between sites i and j, where $j-1\geq 2$ (a), and with those elements replaced with uncorrelated random numbers (b); $\varepsilon=0.1$. Average of the absolute value of the off-diagonal elements vs the distance m from the diagonal (c) for the Hamiltonian from (a) (decaying curve) and from (b) (flat curve). Fidelity decay (d) for system (a) (Gaussian analytical expression is the black solid line; numerical data are the circles; saturation point is the highest horizontal line) and for system (b) (analytical expression is the green dashed line; numerical data are the squares; saturation point is the lowest horizontal line). $\Delta_I=0.5$, $E_{\rm ini}\sim 0$, $\sigma_{\rm ini}=4.42$ (a) and $\sigma_{\rm ini}=4.03$ (b), $L=16$, $\hat{\mathcal{S}}^z=0$, $\mathcal{D}=12\,870$.

The form of the LDOS of initial states close to the middle of the spectrum of $\hat{H}_F$ is similar to that of the density of states (not shown). The corresponding fidelity behaviors are shown in Fig. 17 (d). It is Gaussian up to times close to t_R for the Hamiltonian with random flip-flop terms and it is similar to $F_{\rm SC}(t)$ [Eq. (58)] for the Hamiltonian with uncorrelated elements. The agreement with $F_{\rm SC}(t)$ becomes excellent if uncorrelated random elements replace also matrix elements associated with flip-flop terms involving four sites (not shown).

We saw in the previous subsection that in a system with a Gaussian density of states, the increase of the perturbation strength broadens the local density of states from Lorentzian to Gaussian. Here, we provided a simple recipe to achieve the transition from a Gaussian to a semicircle density of states, which causes the same change in the local density of states. The transition of the shape of the local density of states from Lorentzian to Gaussian and then finally to semicircle was investigated before [64] in the context of band random matrices. An important advantage of our analysis over (band or full) random matrices is to address realistic systems of spins 1/2 that model a very broad range of physical systems.

%%%
$\hookrightarrow$ *EXERCISE 18:*

(i) Consider the quench from a full random matrix to another full random matrix of $\mathcal{D} = 12\,870$. Verify that the numerics for the fidelity decay agrees very well with Eq.(58).

(ii) Reproduce Fig. 17.

%%%

G. Absolute lower bound

A lower bound for the fidelity decay was derived from the energy-time uncertainty relation [43, 65–73],

$$F_{\rm C}(t) \geq \cos^2(\sigma_{\rm ini} t) \tag{59}$$

It can be obtained as follows. The generalized uncertainty relation is given by,

$$\sigma_H \sigma_A \geq \left| \frac{\langle [\hat{H}, \hat{A}] \rangle}{2i} \right| .$$

In the case of a *non-stationary* state $|\Psi(t)\rangle$, where

$$\sigma_A^2 = \langle \Psi(t)|\hat{A}^2|\Psi(t)\rangle - \langle \Psi(t)|\hat{A}|\Psi(t)\rangle^2,$$

we can use Heisenberg equation, $\dfrac{d\hat{A}}{dt} = \dfrac{[\hat{A}, \hat{H}]}{i}$, and deal with the Mandelstam-Tamm uncertainty relation,

$$\sigma_H \sigma_A \geq \frac{1}{2} \left| \frac{d\langle \hat{A} \rangle}{dt} \right| .$$

The uncertainty in energy, σ_H, is the same as $\sigma_{\rm ini}$, since

$$\langle \Psi(t)|\hat{H}_F|\Psi(t)\rangle = \langle {\rm ini}|e^{+i\hat{H}_F t}\hat{H}_F e^{-i\hat{H}_F t}|{\rm ini}\rangle = \langle {\rm ini}|\hat{H}_F|{\rm ini}\rangle$$

If $\hat{A}$ is the projection operator on the initial state, $\hat{A} = |{\rm ini}\rangle\langle{\rm ini}|$, then $\langle \hat{A} \rangle = F(t)$. Since

$$\langle \Psi(t)|\hat{A}^2|\Psi(t)\rangle = \langle \Psi(t)|{\rm ini}\rangle\langle{\rm ini}|{\rm ini}\rangle\langle{\rm ini}|\Psi(t)\rangle = F(t)$$

we have

$$\sigma_A^2 = F(t) - F(t)^2.$$

Thus

$$\sigma_{\rm ini}\sqrt{F(1-F)} \geq \frac{1}{2} \left| \frac{dF}{dt} \right| .$$

A good trick is to write $F(t) = \cos^2 \phi(t)$, so that

$$\sigma_{\rm ini} \cos(\phi)\sin(\phi) \geq \frac{1}{2}\left| -2\cos(\phi)\sin(\phi)\frac{d\phi}{dt} \right| \Rightarrow \left| \frac{d\phi}{dt} \right| \leq \sigma_{\rm ini} \Rightarrow |\phi(t)| \leq \sigma_{\rm ini} t \Rightarrow \left| \arccos\left(\sqrt{F(t)}\right) \right| \leq \sigma_{\rm ini} t.$$

Since the $\arccos$ is a strictly decreasing function,

$$\arccos\left(\sqrt{F(t)}\right) \geq \sigma_{\rm ini} t \Rightarrow \sqrt{F(t)} \geq \cos(\sigma_{\rm ini} t),$$

from where Eq. (59) follows. Notice that the expression above is only valid when the cosine is positive, so $0 \leq t \leq \pi/(2\sigma_{\rm ini})$.

This bound can certainly be reached when $P^{\rm ini}(E)$ is bimodal,

$$P_{\rm C}^{\rm ini}(E) = \frac{\delta(E_1) + \delta(E_2)}{2},$$

$$\Rightarrow F_{\rm C}(t) = \cos^2\left[\frac{(E_2 - E_1)t}{2}\right] . \tag{60}$$

But let us look for a more general picture that does not involve delta functions. To approach the limit $F_{\rm C}(t)$, the LDOS needs to have two separated peaks. This requires the density of states to be bimodal as well.

In Sec. V B 4, we saw that the NNN model and the impurity model are comparable when $\lambda_F \sim 0.5$ and $d_F \lesssim 1$ ($\Delta < 1$). In this case, the Hamiltonian matrix written in the basis of the XXZ model has a very similar structure and the level of delocalization of the eigenstates is approximately the same. As a result, if we look at the LDOS for an initial state away from the edges of the spectrum, we get a Lorentzian for both cases and therefore an exponential decay of the fidelity. We can further increase λ_F to reach the strong perturbation regime, where the LDOS is Gaussian, but this limit can not achieved by the local quench of the magnetic field . If we increase d_F above 1, we effectively break the chain in two. We end up with eigenstates that are superpositions of site-basis vectors that do not have an excitation on the defect site and superpositions that have an excitation on the defect site. The first have lower energy than the latter. If d_F is large, these two sets of states are well separated in energy, which implies a bimodal density of states.

The crossover from a unimodal to a bimodal distribution is carried on also to $P^{\rm ini}(E)$, where $|{\rm ini}\rangle$ is an eigenstate of the XXZ model. When $d_F \gtrsim 1$, the single Lorentzian for $P^{\rm ini}(E)$ starts splitting in two Lorentzians. For the $\mathcal{S}^z = 0$ sector and $E_{\rm ini}$ close to the middle of the spectrum, both equally weighted $P_L(E)$, one centered at E_1 and the other at E_2, have approximately the same width, as shown in Fig. 18 (a). They lead to

$$F_{\rm TL}(t) = \cos^2\left(\frac{E_2 - E_1}{2} t\right) \exp(-\Gamma t), \tag{61}$$

where $E_2 - E_1 \approx d_F$. The expression above matches well the numerical data of the fidelity decay for a fairly long time in Fig. 18 (b). The oscillations after t_R are exponentially suppressed with a rate determined by the width of the Lorentzians.

As d_F further increases, the peaks broaden and approach Gaussians separated in energy by $E_2 - E_1 \approx d_F$. When both peaks have the same width σ,

$$F_{\rm TG}(t) = \cos^2\left(\frac{E_2 - E_1}{2} t\right) \exp(-\sigma^2 t^2). \tag{62}$$

The envelope of the decaying oscillations of the fidelity is now also Gaussian. This scenario is illustrated in Fig. 18 (c), although the widths of the Gaussians there are slightly different. As shown in Fig. 18 (d), the corresponding Fourier transform of the two Gaussians agrees very well with the numerical results for the fidelity decay until very close to the saturation point.

As the energy of the initial state moves towards the edge of the spectrum, $P^{\rm ini}(E)$ becomes, as expected, more asymmetric. Larger contributions to the distribution appear for the peak closer to the border of the spectrum. The fidelity decay becomes slower if compared to states where $E_{\rm ini}$ is closer to the middle of the spectrum. However, for very large d_F, the asymmetry decreases and both peaks approach similar Gaussians again.

From Eqs. (61) and (62), one sees that for $t < \pi/(E_2 - E_1)$, the fidelity decay derived from bimodal distributions can indeed approach the lower bound associated with the energy-time uncertainty relation. This is particularly evident when d_F is large, since in this case $\sigma^2 t^2 < \sigma^2 \pi^2/(E_2 - E_1)^2 \ll 1 \Rightarrow F_{\rm TG}(t) \sim \cos^2(d_F/2t)$.

%%%
$\hookrightarrow$ *EXERCISE 19:* Reproduce Fig. 18.
%%%

The table below summarizes the fidelity behaviors discussed in the subsections of Sec.VIII.A.

H. Experimentally Accessible Initial States

Let us now study the fidelity decay for initial states where each lattice site has a spin either pointing up or pointing down in the z direction, that is site-basis vectors [28, 74–76]:

Sharp domain wall	$\|{\rm DW}\rangle = \|\uparrow\uparrow\uparrow \ldots \downarrow\downarrow\downarrow\rangle$
Pairs of parallel spins	$\|{\rm PS}\rangle = \|\downarrow\uparrow\uparrow\downarrow\downarrow\uparrow\uparrow \ldots\rangle$
Néel state	$\|{\rm NS}\rangle = \|\downarrow\uparrow\downarrow\uparrow \ldots \downarrow\uparrow\downarrow\uparrow\rangle$

These are states that can in principle be prepared experimentally with cold atoms in optical lattices. The proposals for the preparation of domain walls in optical lattices require the application of a magnetic field gradient [77]. The Néel state [4, 78, 79] is similar to the state prepared in [6], where only even sites were initially populated and the evolutions of quasi-local densities, currents, and coherences were experimentally investigated after the quench.

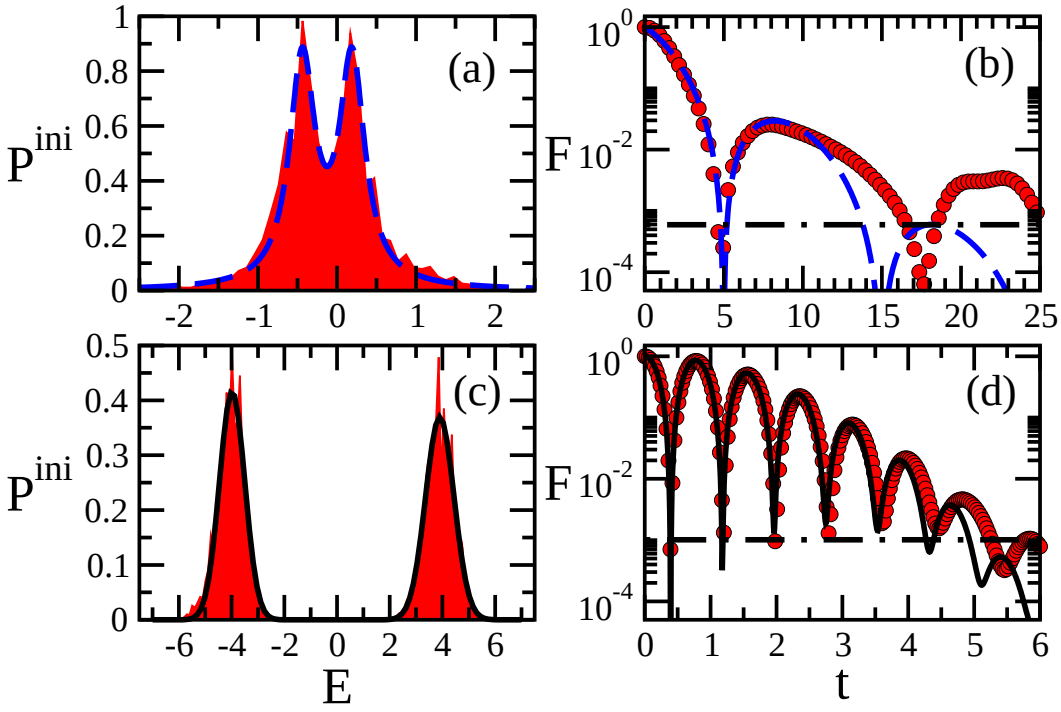

FIG. 18: (Color online) Energy distribution of the initial state (a, c) and corresponding fidelity decay (b, d) for a quench from the XXZ model to the impurity model with $d_F = 1.2$ (a, b) and $d_F = 8.0$ (c, d); $\varepsilon = 0.1$. The initial state is in the middle of the spectrum of $\hat{H}_I$, $\mathcal{E}_{\mathcal{D}/2}$. Panels (a, c): numerical data (shaded red area); two Lorentzians with $E_1 = -0.44$, $E_2 = 0.19$, and $\Gamma_1 = \Gamma_2 = 0.39$ (blue dashed line) (a); two Gaussians with $E_1 = -3.98$, $E_2 = 3.90$, $\sigma_1 = 0.48$, and $\sigma_2 = 0.54$ (black solid line) (c). Panels (b, d): numerical results (circles); Eq. (61) (blue dashed line); Fourier transform of the two Gaussians from (c) (black solid lines). The saturation points are the horizontal lines. $\Delta_I = \Delta_F = 0.48$, $L = 16$, $\hat{\mathcal{S}}^z = 0$, $\mathcal{D} = 12\,870$.

TABLE I: Shape of the LDOS and the corresponding fidelity decay.

LDOS	Fidelity
Breit-Wigner	
$P^{\text{ini}}_{\text{BW}}(E) = \dfrac{1}{2\pi}\dfrac{\Gamma_{\text{ini}}}{(E_{\text{ini}}-E)^2+\Gamma^2_{\text{ini}}/4}$	$F_{\text{BW}}(t) = \exp(-\Gamma_{\text{ini}}t)$
Gaussian	
$P^{\text{ini}}_{\text{G}}(E) = \dfrac{1}{\sqrt{2\pi\sigma^2_{\text{ini}}}}\exp\left[-\dfrac{(E-E_{\text{ini}})^2}{2\sigma^2_{\text{ini}}}\right]$	$F_{\text{G}}(t) = \exp(-\sigma^2_{\text{ini}}t^2)$
Semicircle	
$P^{\text{ini}}_{\text{SC}}(E) = \dfrac{1}{\pi\sigma_{\text{ini}}}\sqrt{1-\left(\dfrac{E}{2\sigma_{\text{ini}}}\right)^2}$	$F_{\text{SC}}(t) = \dfrac{[\mathcal{J}_1(2\sigma_{\text{ini}}t)]^2}{\sigma^2_{\text{ini}}t^2}$
Two Gaussians, $\sigma_1 = \sigma_2 = \sigma$	
$P^{\text{ini}}_{\text{TG}}(E) = \dfrac{1}{2}\dfrac{\exp\left[-\dfrac{(E-E_1)^2}{2\sigma_1^2}\right]}{\sqrt{2\pi\sigma_1^2}} + \dfrac{1}{2}\dfrac{\exp\left[-\dfrac{(E-E_2)^2}{2\sigma_2^2}\right]}{\sqrt{2\pi\sigma_2^2}}$	$F_{\text{TG}}(t) = \exp(-\sigma^2t^2)\cos^2\left[\dfrac{E_2-E_1}{2}t\right]$

We recall that in the context of quench dynamics, the initial state is an eigenstate of $\hat{H}_{\text{I}}$. The eigenstates of the initial Hamiltonian also define the basis in which $\hat{H}_{\text{F}}$ is written. For initial states corresponding to site-basis vectors, $\hat{H}_{\text{I}}$ is the Ising part of the Hamiltonian. In this basis, the diagonal elements of the final Hamiltonian matrix depend on Δ and λ, while the off-diagonal elements depend only on λ, since they come from the flip-flop terms.

For site-basis vectors, it is straightforward to calculate analytically $\langle n|\hat{H}_F|\text{ini}\rangle$ and, from it, the center E_{ini} and the width σ_{ini} of the energy shell. One sees that Eq. (39) reduces to

$$\sigma_{\text{ini}} = \frac{J}{2}\sqrt{M_1 + \lambda^2 M_2}, \tag{63}$$

where the connectivity M_1 (M_2) corresponds to the number of states directly coupled to $|\text{ini}\rangle$ via the NN (NNN) flip-flop term. The values of E_{ini} and σ_{ini} for the three states above are given in Table II.

TABLE II: Energy of $|\text{ini}\rangle$ and width of its LDOS.

	E_{ini}	σ_{ini}
$\|\text{DW}\rangle$	$\frac{J\Delta}{4}[(L-3)+(L-6)\lambda]$	$\frac{J}{2}\sqrt{1+2\lambda^2}$
$\|\text{PS}\rangle$	$-\frac{J\Delta}{4}[1+(L-2)\lambda]$	$\frac{J}{2}\sqrt{\frac{L}{2}+(L-2)\lambda^2}$
$\|\text{NS}\rangle$	$\frac{J\Delta}{4}[-(L-1)+(L-2)\lambda]$	$\frac{J}{2}\sqrt{L-1}$

$|\text{DW}\rangle$, $|\text{PS}\rangle$, and $|\text{NS}\rangle$ are chosen to magnify the effects of the anisotropy and of the NNN couplings. For $|\text{NS}\rangle$, the five Hamiltonians considered lead to the same σ_{ini}, since $M_2 = 0$. For $|\text{PS}\rangle$ and $|\text{DW}\rangle$ only Hamiltonians with the same λ give the same σ_{ini}. The domain wall is directly coupled to only one (three) state(s) when $\hat{H}_F$ is integrable (chaotic), independent of L. It has the smallest σ_{ini} among the states investigated.

Figure 19 displays the LDOS of $|\text{NS}\rangle$ and $|\text{DW}\rangle$ and Fig. 20 for $|\text{PS}\rangle$. As visible, P_α^{ini} depends on both $|\text{ini}\rangle$ and the $\hat{H}_F$ that evolves it.

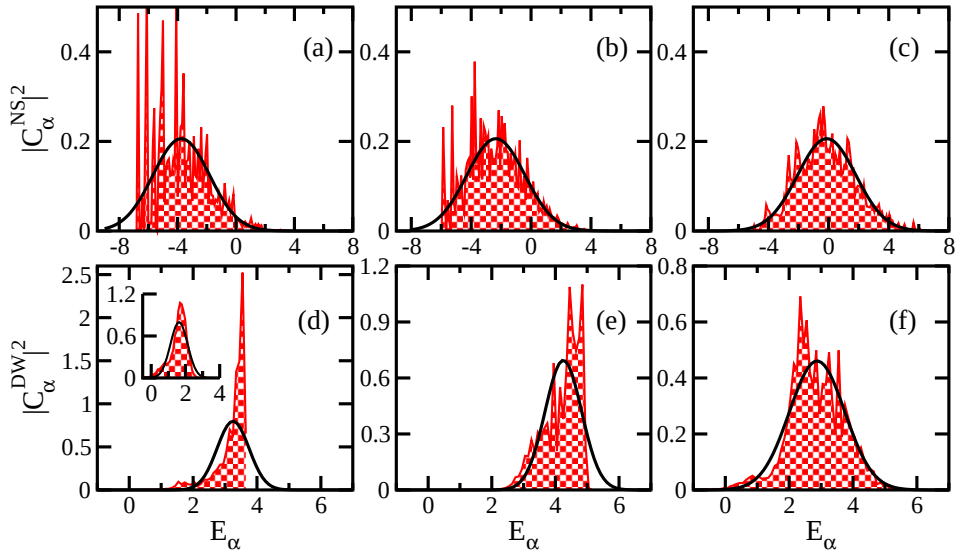

FIG. 19: (Color online) Distribution of $|C_\alpha^{\text{ini}}|^2$ in E_α (*i.e.* LDOS) for $|\text{NS}\rangle$ (top) and $|\text{DW}\rangle$(bottom); $L = 16$. The Hamiltonians are: $\hat{H}_{\Delta=1,\lambda=0}$ (a, d); $\hat{H}_{\Delta=1,\lambda=0.4}$ (b, e); $\hat{H}_{\Delta=0.5,\lambda=1}$ (c, f); and $\hat{H}_{\Delta=0.5,\lambda=0}$ [inset of (d)]. The solid line is the energy shell, $\varepsilon = 0$.

For the Néel state, σ_{ini} is always the same, but the shell gets better filled as λ increases from zero and Δ decreases [Fig. 19 from (a) to (c)], since its energy is brought closer to the middle of the spectrum (cf. Table II), where the density of states is larger.

For $|\text{DW}\rangle$, Δ plays a major role [cf. main panel and inset of Fig. 19 (d)]. At the critical point ($\Delta = 1$) or above it, this state approaches the right edge of the spectrum. In this region, $|\text{DW}\rangle$ and the few states directly coupled to it are more localized. As a result, in addition to the narrow energy shell, the latter is also poorly filled. $|\text{DW}\rangle$ should therefore decay very slowly when $\Delta \sim 1$ and it should freeze for $\Delta \gg 1$.

For $|\text{PS}\rangle$, the worst filling actually occurs for the *chaotic* model, $\Delta = 1$ and $\lambda = 1$, since this combination pushes the distribution to the edge of the spectrum (cf. Table II). This means that the saturation point is larger for this chaotic isotropic model than for the integrable ones.

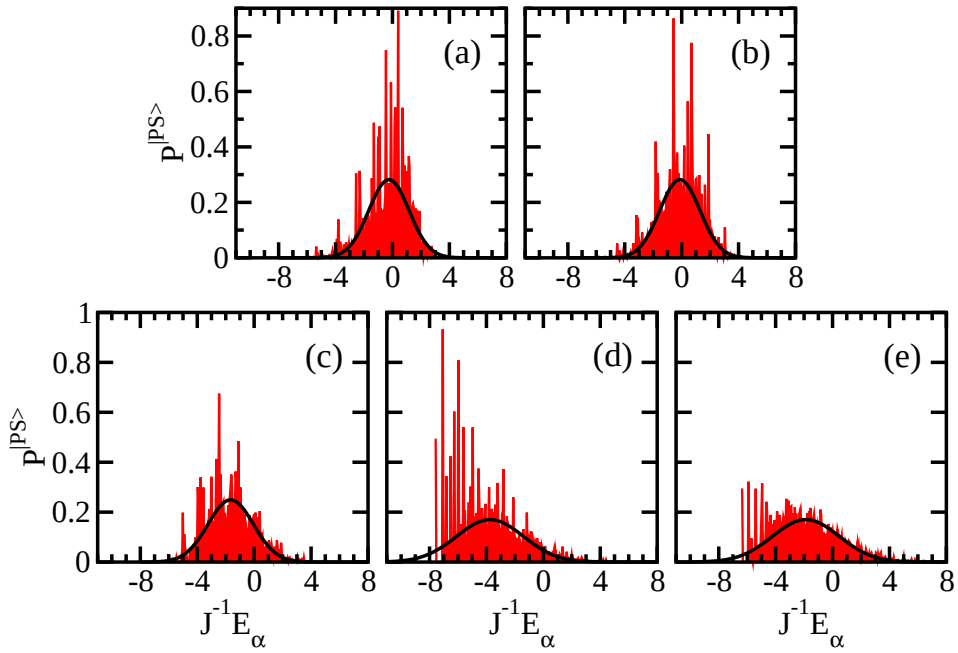

FIG. 20: (Color online) LDOS for $|\mathrm{PS}\rangle$. The final Hamiltonians are: (a) $\hat{H}_{\Delta=1,\lambda=0}$; (b) $\hat{H}_{\Delta=0.5,\lambda=0}$; (c) $\hat{H}_{\Delta=1,\lambda=0.4}$; (d) $\hat{H}_{\Delta=1,\lambda=1}$ and (e) $\hat{H}_{\Delta=0.5,\lambda=1}$. The solid line is the energy shell: Gaussian centered at E_{ini} of width σ_{ini} (see Tables II, **??**); bin size = 0.05 J; $L = 16$.

The fidelity decay reflects the results of the LDOS of $|\mathrm{ini}\rangle$, as illustrated in Fig. 21. Overall, when the energy shell is well filled, the decay is Gaussian and this behavior may persist until saturation, as seen for the Néel state. In contrast, poor filling causes a mixture of Gaussian and exponential behavior, as shown for $|\mathrm{DW}\rangle$ and $|\mathrm{PS}\rangle$.

The fidelity decays slowly for $|\mathrm{DW}\rangle$, due to its low connectivity and narrow LDOS. At short time the behavior is Gaussian and equal for systems with the same λ (same $\sigma_{|\mathrm{DW}\rangle}$), but soon the curves for isotropic and anisotropic systems diverge, the first being slower than the latter, as expected from the filling of the shell. It is close to this point of separation that the exponential behavior takes over, although it does not remain until saturation. This state has a complicated dynamics at long times before saturation.

The fidelity decay for $|\mathrm{PS}\rangle$ shares common features with $|\mathrm{DW}\rangle$: at short time it is Gaussian and equal for Hamiltonians with the same λ, later it switches to an exponential behavior. However, contrary to $|\mathrm{DW}\rangle$, the exponential decay of $|\mathrm{PS}\rangle$ persists until close to equilibration. Furthermore, according to Table II, the fidelity decay rate increases with L for $|\mathrm{PS}\rangle$, whereas $\sigma_{|\mathrm{DW}\rangle}$ does not depend on the system size.

For the Néel state, where $\sigma_{|\mathrm{NS}\rangle}$ is dissociated from Δ and λ, the curves for $F(t)$ fall on top of each other for the five Hamiltonians considered in the figure. The decay is Gaussian until saturation. The Néel state emphasizes the role of the interplay between initial state and Hamiltonian. It is impressive to find integrable and chaotic, isotropic and anisotropic systems, all leading to the same dynamics. The difference appears only at the saturation point. The infinite-time average value decreases monotonically from $\Delta = 1$ to $\Delta = 0.5$ and from $\lambda = 0$ to $\lambda = 1$.

An advantage of using site-basis vectors as initial states is the access that they give to exact analytical expressions for E_{ini} and σ_{ini}. In general, one needs exact full diagonalization to find these values, which limits the system sizes that can be studied. For the dynamics, on the other hand, there are alternative methods, such as Krylov subspace techniques or density matrix renormalization group, that can deal with larger L. Having access to σ_{ini} without the need to resort to exact diagonalization allows us to compare the analytical expression in Eq. (51) with numerical results for $F(t)$ for $L > 16$. In the bottom right panel of Fig. 21, we use EXPOKIT [80, 81] and confirm the Gaussian fidelity decay for the Néel state up to saturation also for $L = 24$.

EXPOKIT is a software package based on Krylov subspace projection methods. Instead of diagonalizing the complete system Hamiltonian, the package computes directly the action of the matrix exponential $e^{-i\hat{H}_{\mathrm{F}}t}$ on a vector of interest. You can download the package at:

`http://www.maths.uq.edu.au/expokit/`

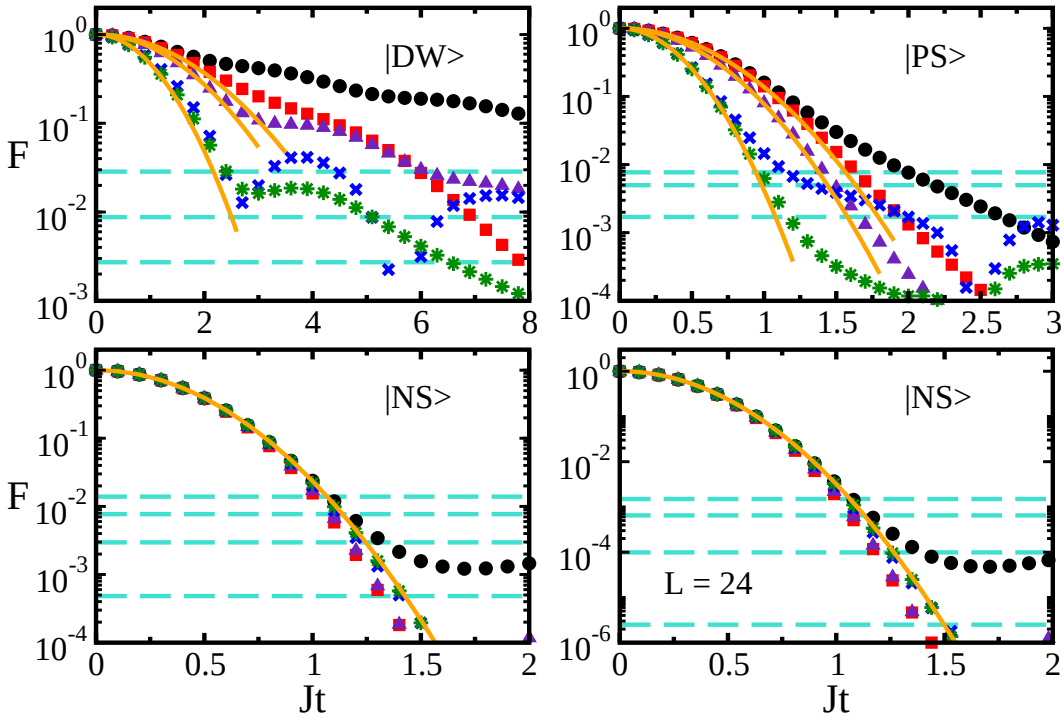

FIG. 21: (Color online) Fidelity decay for the Hamiltonians: $\hat{H}_{\Delta=1,\lambda=0}$ (circle), $\hat{H}_{\Delta=0.5,\lambda=0}$ (square), $\hat{H}_{\Delta=1,\lambda=0.4}$ (triangle), $\hat{H}_{\Delta=1,\lambda=1}$ (cross) and $\hat{H}_{\Delta=0.5,\lambda=1}$ (star). The initial states are indicated; $L = 16$ unless indicated otherwise. Solid curves correspond to the analytical Gaussian expression in Eq. (51). The dashed horizontal lines give the saturation value $\mathrm{IPR}_{\mathrm{ini}}^{-1}$ (see Table **??**). For $|\mathrm{DW}\rangle$ from top to bottom: $\hat{H}_{\Delta=1,\lambda=0}$ (other isotropic cases are very close); $\hat{H}_{\Delta=0.5,\lambda=0}$; $\hat{H}_{\Delta=0.5,\lambda=1}$. For $|\mathrm{PS}\rangle$ from top to bottom: $\hat{H}_{\Delta=1,\lambda=1}$; $\hat{H}_{\Delta=1,\lambda=0}$ ($\hat{H}_{\Delta=0.5,\lambda=0}$ is very close); $\hat{H}_{\Delta=0.5,\lambda=1}$ ($\hat{H}_{\Delta=1,\lambda=0.4}$ is very close). For $|\mathrm{NS}\rangle$, both system sizes, from top to bottom: $\hat{H}_{\Delta=1,\lambda=0}$; $\hat{H}_{\Delta=0.5,\lambda=0}$; $\hat{H}_{\Delta=1,\lambda=0.4}$; $\hat{H}_{\Delta=0.5,\lambda=1}$ ($\hat{H}_{\Delta=1,\lambda=1}$ is very close). For $L = 24$, the saturation values are obtained from an infinite time average with $Jt \in [1000, 2000]$. All saturation values are larger than the one reached by a state evolved under GOE full random matrices, where $\mathrm{IPR}_{\mathrm{ini}}^{-1} \approx 3/\mathcal{D}$; $\varepsilon = 0.1$.

IX. DYNAMICS: FEW-BODY OBSERVABLES

The analysis of the evolution of few-body observables is, of course, more involved than the study of the fidelity decay. It depends on the overlaps between the evolved $|\mathrm{ini}\rangle$ and on the details of the observables $\hat{O}$. However, a simple general picture, valid at short times, can be constructed for observables that commute with $\hat{H}_I$. In this case, the fidelity, and therefore σ_{ini}, plays an important role in the dynamics of O.

The evolution of the observables is given by

$$\begin{aligned} O(t) &= F(t)O(0) \\ &+ \sum_{n\neq \mathrm{ini}} \langle \mathrm{ini}|e^{i\hat{H}_F t}|\mathrm{ini}\rangle O_{\mathrm{ini},n}\langle n|e^{-i\hat{H}_F t}|\mathrm{ini}\rangle + \sum_{n\neq \mathrm{ini}} \langle \mathrm{ini}|e^{i\hat{H}_F t}|n\rangle O_{n,\mathrm{ini}}\langle \mathrm{ini}|e^{-i\hat{H}_F t}|\mathrm{ini}\rangle \\ &+ \sum_{n,m\neq \mathrm{ini}} \langle \mathrm{ini}|e^{i\hat{H}_F t}|n\rangle O_{n,m}\langle m|e^{-i\hat{H}_F t}|\mathrm{ini}\rangle, \end{aligned} \tag{64}$$

where $O_{n,m} = \langle n|\hat{O}|m\rangle$ and $|n\rangle$ are the eigenstates of $\hat{H}_I$. When $[\hat{H}_I, \hat{O}] = 0$, since $|\mathrm{ini}\rangle$ is one of the eigenstates of $\hat{H}_I$, $O_{\mathrm{ini},n} = 0$ for $|n\rangle \neq |\mathrm{ini}\rangle$ and the second line in Eq. (64) cancels.

Finding the second term on the right hand side in

$$O(t) = F(t)O(0) + \sum_{n,m\neq \mathrm{ini}} \langle \mathrm{ini}|e^{i\hat{H}_F t}|n\rangle O_{n,m}\langle m|e^{-i\hat{H}_F t}|\mathrm{ini}\rangle \tag{65}$$

is still not trivial. However, we see at least that for observables that commute with the initial Hamiltonian, the short time

dynamics is necessarily quadratic in time,

$$O(t) \approx \left(1-\sigma_{\rm ini}^2 t^2\right) O(0) + t^2 \sum_{n\neq {\rm ini}} |\langle n|\hat{H}_F|{\rm ini}\rangle|^2 O_{n,n}. \tag{66}$$

Moreover, for initial states corresponding to site-basis vectors, where $\hat{H}_I$ is the Ising part of the Hamiltonian, it is straightforward to compute $\langle n|\hat{H}_F|{\rm ini}\rangle$ and $\sigma_{\rm ini}$. Both do not depend on the anisotropy parameter. For the Néel state, not even λ is important, and completely different Hamiltonians (integrable and chaotic, isotropic and anisotropic) lead to a very similar initial relaxation of the observables. Computing $O_{n,n}$ for site-basis vectors $|n\rangle$ is also simple. Notice that because of $\langle n|\hat{H}_F|{\rm ini}\rangle$, the only states $|n\rangle$ that we consider are the ones directly coupled with $|{\rm ini}\rangle$.

For the site-basis vectors initial states, there are several experimentally relevant observables that commute with $\hat{H}_I$, such as the local magnetization, potential energy, spin-spin correlation in the z direction, and structure factor in the z direction.

Let us consider as an example, an initial state corresponding to the Néel state and let us compute $\hat{C}^{zz}_{2,3}$. There are $L-1$ states directly coupled with $|{\rm NS}\rangle$ via the NN flip-flop term. For all of them $\langle n|\hat{H}_F|{\rm ini}\rangle = J/2$. As we saw before, $\sigma^2_{\rm ini} = J^2(L-1)/4$. Among the states directly coupled, all of them have a pair of antiparallel spins on sites 2,3, just like the Néel state, except two of them. For one, the excitation left the pair, $|0100110101\ldots\rangle$ and for the other, an additional excitation was included in the pair, $|00110101\ldots\rangle$. As a result $\sum_{n\neq{\rm ini}} |\langle n|\hat{H}_F|{\rm ini}\rangle|^2 O_{n,n} = (J^2/4) C^{z,|{\rm NS}\rangle}_{2,3}(0)[(L-3)-2]$. We then obtain $C^{zz,|{\rm NS}\rangle}_{2,3} \approx C^{z,|{\rm NS}\rangle}_{2,3}(0)[(1-(Jt/2)^2(L-1)+(Jt/2)^2(L-5)] = C^{z,|{\rm NS}\rangle}_{2,3}(0)[1-J^2t^2]$.

The analytical results at short times for the spin-spin correlation in the z direction between sites $L/2$ and $L/2+1$ and the site-basis vectors studied in Fig. 19 are:

$$C^{z,|{\rm DW}\rangle}_{\frac{L}{2},\frac{L}{2}+1}(t) = C^{z,|{\rm DW}\rangle}_{\frac{L}{2},\frac{L}{2}+1}(0)\left[1-\frac{J^2\lambda^2t^2}{2}\right], \tag{67}$$

$$C^{z,|{\rm PS}\rangle}_{\frac{L}{2},\frac{L}{2}+1}(t) = C^{z,|{\rm PS}\rangle}_{\frac{L}{2},\frac{L}{2}+1}(0)\left[1-J^2t^2(1+2\lambda^2)\right], \tag{68}$$

$$C^{z,|{\rm NS}\rangle}_{\frac{L}{2},\frac{L}{2}+1}(t) = C^{z,|{\rm NS}\rangle}_{\frac{L}{2},\frac{L}{2}+1}(0)\left[1-J^2t^2\right]. \tag{69}$$

The expression for $|{\rm PS}\rangle$ above holds for ${\rm mod}(L,4)=0$, when the spins on sites $L/2, L/2+1$ are parallel. When ${\rm mod}(L,4)\neq 0$, and the two middle spins are anti-parallel, the expression changes to $C^{z,|{\rm PS}\rangle}_{\frac{L}{2},\frac{L}{2}+1}(0)[1-J^2t^2(1+3\lambda^2)/2]$.

Figure 22 compares the longitudinal correlation for $|{\rm PS}\rangle$ and $|{\rm NS}\rangle$ evolving under the integrable and chatic final Hamiltonians. Similarly to what was seen for fidelity, the initial decay of the magnitude of $C^z_{\frac{L}{2},\frac{L}{2}+1}(t)$ for the Néel state is independent of the regime of $\hat{H}_F$, while for $|{\rm PS}\rangle$ it is faster in the chaotic domain. These distinct behaviors, anticipated from Eqs. (68) and (69), emphasize the significance of the initial state also for the dynamics of observables.

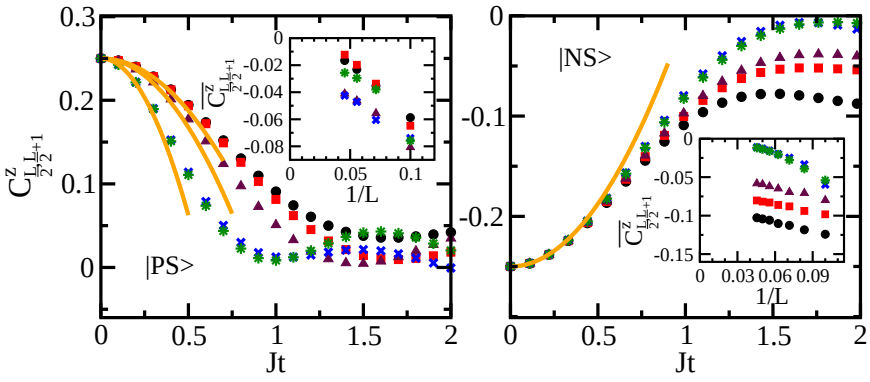

FIG. 22: (Color online) Spin-spin correlation in the z direction between neighboring sites in the middle of the chain. The final Hamiltonians are: $\hat{H}_{\Delta=1,\lambda=0}$ (circle), $\hat{H}_{\Delta=0.5,\lambda=0}$ (square), $\hat{H}_{\Delta=1,\lambda=0.4}$ (triangle), $\hat{H}_{\Delta=1,\lambda=1}$ (cross) and $\hat{H}_{\Delta=0.5,\lambda=1}$ (star). The initial states are indicated. Main panels: $L=16$. Solid curves are the analytical results from Eq. (68) and (69). The insets show the scaling with L of the infinite time average of $C^z_{\frac{L}{2},\frac{L}{2}+1}$, computed in $Jt\in[3000,4000]$.

After a long time, $C^z_{\frac{L}{2},\frac{L}{2}+1}(t)$ fluctuates around the equilibrium value $\overline{C^z}_{\frac{L}{2},\frac{L}{2}+1}$. The saturation value is closest to zero when $E_{\rm ini}$ is closest to the center of the spectrum. This happens for $|{\rm PS}\rangle$ with the integrable Hamiltonians and for $|{\rm NS}\rangle$ with the strongly chaotic Hamiltonians, as can be seen in the insets of Fig. 22.

The insets of Fig. 22 give the scaling of $\overline{C^z}_{\frac{L}{2},\frac{L}{2}+1}$ with system size. For $|\mathrm{NS}\rangle$, the correlations for the strongly chaotic Hamiltonians approach zero as L increases, while the results indicate that integrable and weakly chaotic Hamiltonians may retain memory in the thermodynamic limit. However, we cannot discard the possibility of an acceleration towards zero for L's larger than the ones considered here. The results for $|\mathrm{PS}\rangle$ are less conclusive. For this state, the direction of the spins in the middle of the chain depend on L. This causes the saturation value for small L to oscillate significantly from $\mathrm{mod}(L,4) \neq 0$ to $\mathrm{mod}(L,4) = 0$. To try to delineate a pattern, we show only the results for $\mathrm{mod}(L,4) \neq 0$. The correlations decrease with system size, but more points are necessary for an extrapolation to the thermodynamic limit.

%%%

$\hookrightarrow$ *EXERCISE 20:*

(i) Reproduce Fig. 22.

(ii) Evolve the few-body observables discussed in Sec. VI for a long time. Verify that after a long time, they indeed fluctuate around the infinite-time average.

VERY IMPORTANT EXERCISE!

Fortran code provided.

```
! Project initial state into |ψ_α to get C_α^ini
        call DGEMV('t',dd,dd,1.0d0,VecSite,dd,Initial,1,0.0d0,Calpha,1)
! INSIDE the TIME-LOOP:
        DO tt = tinitial, tfinal
           time = dble(tt)*dt
           Do i = 1, dimTotal
              CosAlpha(i)=Calpha(i)*dcos( time*Eig(i) )
              SinAlpha(i)= - Calpha(i)*dsin( time*Eig(i) )
           Enddo
! Bring the Cos and Sin vectors back to the SITE-BASIS
           call DGEMV('n',dd,dd,1.0d0,VecSite,dd,CosAlpha,1,0.0d0,CosSite1)
           call DGEMV('n',dd,dd,1.0d0,VecSite,dd,SinAlpha,1,0.0d0,SinSite,1)
! Get the observables using the site basis
           call ObservablesTime( )
! write the output files for the observables
        ENDDO

! Example for magnetization of site 3 inside the subroutine ObservablesTime
           Mag(3) = 0.0d0
           Do i = 1, dimTotal
              aux = CosSite(i)**2 + SinSite(i)**2
              Mag(3) = Mag(3) + aux*(-1.0d0)**(1+basis(i,3))
           Enddo
```

%%%

[1] P. Cappellaro, C. Ramanathan, and D. G. Cory, Phys. Rev. Lett. **99**, 250506 (2007).
[2] P. Cappellaro, C. Ramanathan, and D. G. Cory, Phys. Rev. A **76**, 032317 (2007).
[3] C. Hess, Eur. Phys. J. Special Topics **151**, 73 (2007).
[4] S. Trotzky, P. Cheinet, S. Fölling, M. Feld, U. Schnorrberger, A. M. Rey, A. Polkovnikov, E. A. Demler, M. D. Lukin, and I. Bloch, Science **319**, 295 (2008).
[5] J. Simon, W. S. Bakr, R. Ma, M. E. Tai, P. M. Preiss, and M. Greiner, Nature (London) **472**, 307 (2011).
[6] S. Trotzky, Y.-A. Chen, A. Flesch, I. P. McCulloch, U. Schollwöck, J. Eisert, and I. Bloch, Nature Phys. **8**, 325 (2012).
[7] T. Fukuhara, A. Kantian, M. Endres, M. Cheneau, P. Schausz, S. Hild, D. Bellem, U. Schollwöck, T. Giamarchi, C. Gross, et al., Nat. Phys. **9**, 235 (2013).
[8] P. Jordan and E. Wigner, Z. Phys. **47**, 631 (1928).
[9] H. A. Bethe, Z. Phys. **71**, 205 (1931).
[10] K. Joel, D. Kollmar, and L. F. Santos, Am. J. Phys. **81**, 450 (2013).
[11] F. M. Izrailev, Phys. Rep. **196**, 299 (1990).
[12] V. Zelevinsky, B. A. Brown, N. Frazier, and M. Horoi, Phys. Rep. **276**, 85 (1996).
[13] P. Zanardi and N. Paunković, Phys. Rev. E **74**, 031123 (2006), URL http://link.aps.org/doi/10.1103/PhysRevE.74.031123.

[14] E. P. Wigner, Ann. Math. **53**, 36 (1951).
[15] F. Haake, *Quantum Signatures of Chaos* (Springer-Verlag, Berlin, 1991).
[16] T. Guhr, A. Mueller-Gröeling, and H. A. Weidenmüller, Phys. Rep. **299**, 189 (1998).
[17] L. E. Reichl, *The transition to chaos: conservative classical systems and quantum manifestations* (Springer, New York, 2004).
[18] H.-J. Stöckmann, *Quantum Chaos: An Introduction* (Cambridge University Press, Cambridge, 2006).
[19] E. P. Wigner, Ann. Math. **65**, 203 (1957).
[20] E. P. Wigner, in *Statistical theories of spectra: Fluctuations*, edited by C. E. Porter (Academic Press, New York, 1965).
[21] V. Oganesyan and D. A. Huse, Phys. Rev. B **75**, 155111 (2007), URL http://link.aps.org/doi/10.1103/PhysRevB.75.155111.
[22] Y. Y. Atas, E. Bogomolny, O. Giraud, and G. Roux, Phys. Rev. Lett. **110**, 084101 (2013), URL http://link.aps.org/doi/10.1103/PhysRevLett.110.084101.
[23] E. P. Wigner, Ann. Math. **62**, 548 (1955).
[24] J. B. French and S. S. M. Wong, Phys. Lett. B **33**, 449 (1970).
[25] J. Flores, M. Horoi, M. Müller, and T. H. Seligman, Phys. Rev. E **63**, 026204 (2001).
[26] T. A. Brody, J. Flores, J. B. French, P. A. Mello, A. Pandey, and S. S. M. Wong, Rev. Mod. Phys **53**, 385 (1981).
[27] V. K. B. Kota, Phys. Rep. **347**, 223 (2001).
[28] P. R. Zangara, A. D. Dente, E. J. Torres-Herrera, H. M. Pastawski, A. Iucci, and L. F. Santos, Phys. Rev. E **88**, 032913 (2013).
[29] A. Gubin and L. F. Santos, Am. J. Phys. **80**, 246 (2012).
[30] D. A. Rabson, B. N. Narozhny, and A. J. Millis, Phys. Rev. B **69**, 054403 (2004).
[31] L. F. Santos and M. Rigol, Phys. Rev. E **81**, 036206 (2010).
[32] F. C. Alcaraz, M. N. Barber, M. T. Batchelor, R. J. Baxter, and G. R. W. Quispel, J. Phys. A **20**, 6397 (1987).
[33] L. F. Santos, J. Phys. A **37**, 4723 (2004).
[34] P. Jacquod and D. L. Shepelyansky, Phys. Rev. Lett. **79**, 1837 (1997).
[35] J. M. Deutsch, Phys. Rev. A **43**, 2046 (1991).
[36] M. Srednicki, Phys. Rev. E **50**, 888 (1994).
[37] M. Rigol, V. Dunjko, and M. Olshanii, Nature **452**, 854 (2008).
[38] M. Rigol and L. F. Santos, Phys. Rev. A **82**, 011604(R) (2010).
[39] L. F. Santos and M. Rigol, Phys. Rev. E **82**, 031130 (2010).
[40] E. J. Torres-Herrera and L. F. Santos, Phys. Rev. E **89**, 062110 (2014), URL http://link.aps.org/doi/10.1103/PhysRevE.89.062110.
[41] K. He and M. Rigol, Phys. Rev. A **87**, 043615 (2013).
[42] E. J. Torres-Herrera and L. F. Santos, Phys. Rev. E **88**, 042121 (2013), URL http://link.aps.org/doi/10.1103/PhysRevE.88.042121.
[43] J. Ufink, Am. J. Phys. **61**, 935 (1993), URL http://dx.doi.org/10.1119/1.17368.
[44] L. A. Khalfin, Sov. Phys. JETP **6**, 1053 (1958).
[45] L. Fonda, G. C. Ghirardi, and A. Rimini, Rep. Prog. Phys., **41**, 587 (1978).
[46] P. Greenland, Nature **335**, 209 (1988).
[47] C. A. Bertulani and V. G. Zelevinsky, Nuc. Phys. A **568**, 931 (1994); C. H. Lewenkopf and V. G. Zelevinsky, Nucl. Phys. A **569**, 183 (1994); N. Frazier, B. A. Brown, and V. Zelevinsky, Phys. Rev. C **54**, 1665 (1996).
[48] V. V. Flambaum and F. M. Izrailev, Phys. Rev. E **56**, 5144 (1997).
[49] V. V. Flambaum and F. M. Izrailev, Phys. Rev. E **61**, 2539 (2000).
[50] V. V. Flambaum, Aust. J. Phys. **53**, 489 (2000).
[51] V. V. Flambaum and F. M. Izrailev, Phys. Rev. E **64**, 026124 (2001).
[52] V. V. Flambaum and F. M. Izrailev, Phys. Rev. E **64**, 036220 (2001).
[53] V. K. B. Kota and R. Sahu, Phys. Rev. E **64**, 016219 (2001), URL http://link.aps.org/doi/10.1103/PhysRevE.64.016219.
[54] N. Chavda, V. Potbhare, and V. Kota, Physics Letters A **326**, 47 (2004); D. Angom, S. Ghosh, and V. K. B. Kota, Phys. Rev. E **70**, 016209 (2004); V. K. B. Kota, N. D. Chavda, and R. Sahu, Phys. Rev. E **73**, 047203 (2006).
[55] V. K. B. Kota, *Lecture Notes in Physics, vol. 884* (Springer, Heidelberg, 2014).
[56] L. F. Santos, F. Borgonovi, and F. M. Izrailev, Phys. Rev. Lett. **108**, 094102 (2012).
[57] L. F. Santos, F. Borgonovi, and F. M. Izrailev, Phys. Rev. E **85**, 036209 (2012).
[58] E. J. Torres-Herrera and L. F. Santos, Phys. Rev. A **89**, 043620 (2014), URL http://link.aps.org/doi/10.1103/PhysRevA.89.043620.
[59] E. J. Torres-Herrera, M. Vyas, and L. F. Santos, New J. Phys. **16**, 063010 (2014).
[60] E. J. Torres-Herrera, D. Kollmar, and L. F. Santos, arXiv:1403.6481.
[61] P. Reimann, Phys. Rev. Lett. **101**, 190403 (2008).
[62] A. J. Short, New J. Phys. **13**, 053009 (2011).
[63] C. E. Porter, *Statistical Theories of Spectra: Fluctuations* (Academic Press, New York, 1965).
[64] Y. V. Fyodorov, O. A. Chubykalo, F. M. Izrailev, and G. Casati, Phys. Rev. Lett. **76**, 1603 (1996), URL http://link.aps.org/doi/10.1103/PhysRevLett.76.1603.
[65] L. Mandelstam and I. Tamm, J. Phys. USSR **9**, 249 (1945).
[66] I. Ersak, Sov. J. Nucl. Phys. **9**, 263 (1969).
[67] G. N. Fleming, Il Nuovo Cimento **16**, 232 (1973).
[68] K. Bhattacharyya, J. Phys. A **16**, 2993 (1983).

[69] E. A. Gislason, N. H. Sabelli, and J. W. Wood, Phys. Rev. A **31**, 2078 (1985), URL http://link.aps.org/doi/10.1103/PhysRevA.31.2078.
[70] L. Vaidman, Am. J. Phys. **60**, 182 (1992), URL http://dx.doi.org/10.1119/1.16940.
[71] P. Pfeifer, Phys. Rev. Lett. **70**, 3365 (1993).
[72] V. Giovannetti, S. Lloyd, and L. Maccone, Phys. Rev. A **67**, 052109 (2003).
[73] T. B. Boykin, N. Kharche, and G. Klimeck, Eur. J. Phys. **28**, 673 (2007).
[74] L. F. Santos and A. Mitra, Phys. Rev. E **84**, 016206 (2011).
[75] B. Pozgay, J. Stat. Mech. p. 10028 (2013).
[76] B. Pozsgay, arXiv:1309.4593.
[77] D. M. Weld, P. Medley, H. Miyake, D. Hucul, D. E. Pritchard, and W. Ketterle, Phys. Rev. Lett. **103**, 245301 (2009).
[78] A. Koetsier, R. A. Duine, I. Bloch, and H. T. C. Stoof, Phys. Rev. A **77**, 023623 (2008).
[79] C. J. M. Mathy, D. A. Huse, and R. G. Hulet, Phys. Rev. A **86**, 023606 (2012).
[80] *Expokit*, http://www.maths.uq.edu.au/expokit/.
[81] R. B. Sidje, ACM Trans. Math. Softw. **24**, 130 (1998).